R. van der Klauw

A Design Method for Variable Rotational Workspace Extension applied to Telemanipulation Tasks

MSc. Thesis

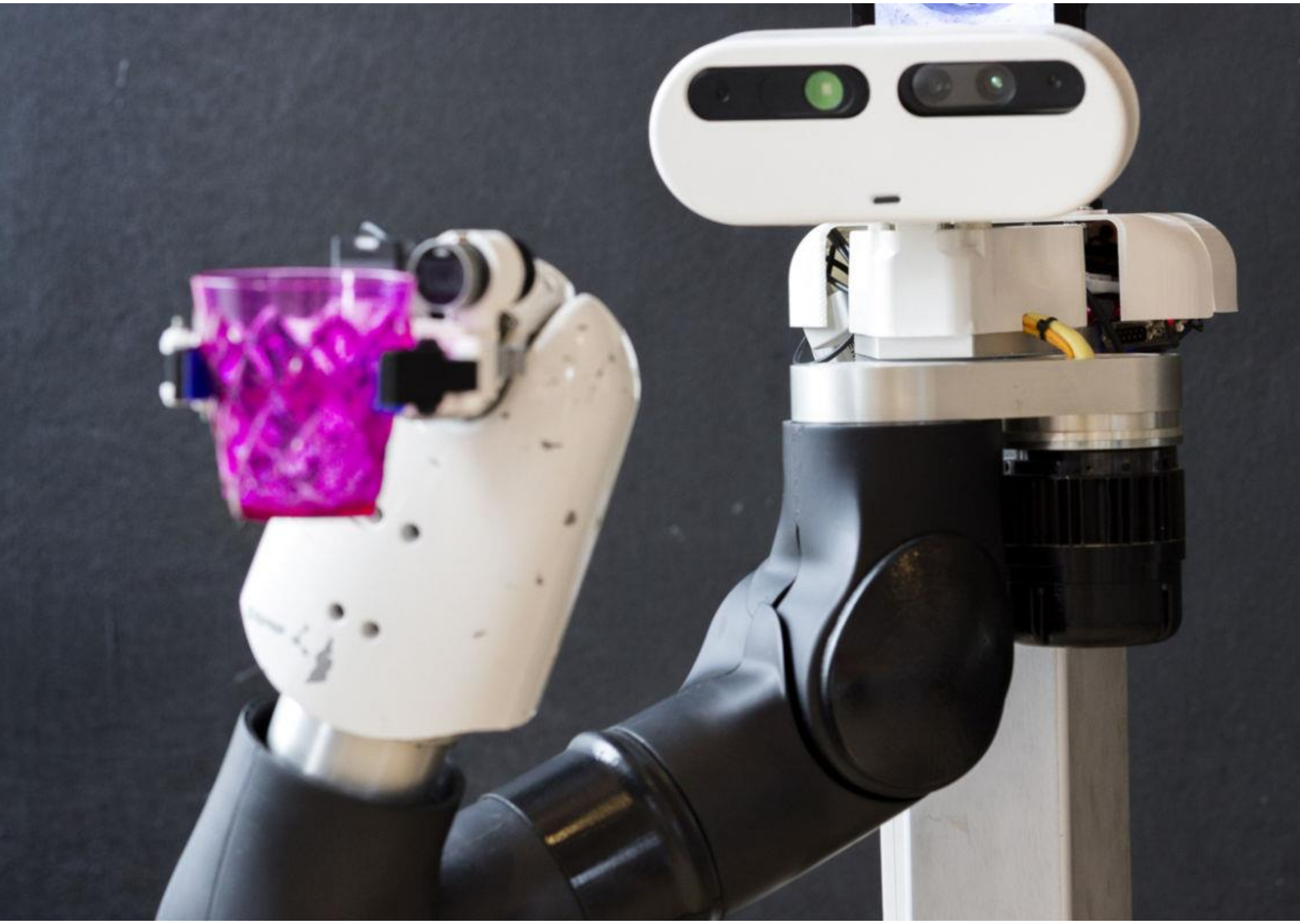

Cover image adopted from:

Elsevier (2017). *http://www.elsevierweekblad.nl/kennis/achtergrond/2017/04/zorgrobot-2-0-geen-klus-te-klein-voor-rose-87002E/*. [image]. Retrieved May 31, 2017.

A Design Method for Variable Rotational Workspace Extension Applied to Telemanipulation Tasks

MSc. Thesis

By

Roel van der Klauw

Student number: 4319087

in partial fulfilment of the requirements for the degree of

Master of Science
in Biomedical Engineering

at the Delft University of Technology,
to be defended publicly on Tuesday June 20, 2017 at 13:00 PM.

Supervisors:	Dr. ir. D.A. Abbink,	TU Delft
	Ir. J.G.W. Wildenbeest,	Heemskerk Innovative Technology B.V.
	Dr. ir. C.J.M. Heemskerk,	Heemskerk Innovative Technology B.V.
Thesis committee:	Dr. ir. D.A. Abbink,	TU Delft
	Dr. ir. J. Kober,	TU Delft
	Dr. ir. C.J.M. Heemskerk,	Heemskerk Innovative Technology B.V.

TUDelft

Preface

This master thesis is the final research for my master in Biomedical Engineering at the TU Delft and is developed in cooperation with Heemskerk Innovative Technology B.V. and the supervision of the Haptics Lab from the technical university of Delft.

The main objective of my research was to propose a new novel methodology to extend the rotational workspace extension during haptic telemanipulations. A variable scaling methodology is proposed, which takes both the task and telemanipulator characteristics into account. A within-subject-haptic-telemanipulation-single-degree-rotational-pointing-experiment was performed in order to evaluate how the variable gain extension method influences the operator task performance while performing a telemanipulation task. The variable scaling design is this study was inspired by a real-life care application.

The first part of this report consists of a scientific paper summarizing the main findings, conclusions and recommendations of my work. The second part consists of appendices which more detailed descriptions of the design methodology and the performed human factors experiment to allow future students and researchers to perform post research on the output of this study.

During my bachelor, Human Movement Sciences and the master Biomedical engineering I created a broad background in the human and in engineering. During this master thesis, it was a challenge to apply the theatrical knowledge about both disciplines into practice. During my graduation, I learned a lot about robotics and got familiar with new hard and software.

I would like to thank everyone who contributed to the finalizing of my Master Thesis. In particular, I want to thank David Abbink and Jeroen Wildenbeest for their enthusiastic and excellent supervision during my graduation. Furthermore, I would like to Cock Heemskerk for providing assistance, work environment and the hardware to perform my experiment. Moreover, I thank all my colleagues at Heemskerk Innovative Technology B.V. for giving excellent feedback during the weekly progress meetings and for the enjoying talks and drinks during the VrijMiBo's. Finally, I thank my parents for their unconditional support during my study.

The entire study is available at http://repository.tudelft.nl/. Further, the raw data, documents, Matlab codes and plots have been submitted to the Biomechanical Engineering depository on a USB stick, which is available on request.

R. van der Klauw
Delft, June 2016

Contents

A Design method for Variable Rotational Workspace Extension applied to Telemanipulation Tasks

Roel van der Klauw, Jeroen G.W. Wildenbeest, Cock J.M. Heemskerk, David A. Abbink

***Abstract*—In telemanipulation commonly master and slave have dissimilar workspaces. Workspace extension methods can overcome this mismatch between master and slave. Literature proposes several workspace extension methods for translations such as scaling and indexing. However, for rotations it is unclear how workspace extension methods should be designed. The present study proposes a methodology to design rotational workspace extension methods with a variable gain. Which is designed based on the speed-accuracy trade-off and several task characteristics, like the distribution of rotational amplitudes during telemanipulation tasks. The effectiveness of the variable gain method is evaluated in terms of task performance and control effort in a within-subject-haptic-telemanipulation-single-degree-rotational-pointing-experiment, based on Fitts' tapping task. The parameters are chosen in accordance with a care robot case study where the rotational workspace of the master device is 45°, but where most tasks require 90° slave rotation, and some even 180°. It is hypothesized that variable gain workspace extension allows improved performance in regions it is customized for (up to 90% of the slave rotations) with respect to a conventional constant scaling, while the operator is able to perform in all regions with similar order of magnitude metrics. To test this hypothesis a variable scaling method, a constant scaling method, and a baseline method (without scaling) are designed. The experimental results show improved performance on fine positioning time and reversal rate for the variable scaling method at the focus region. Furthermore, human operators accept variable scaling and are able to manipulate linear changes of the gain equally smooth as constant gains, while high nonlinear changes of the gain are more difficult to manipulate smoothly. To conclude, this study demonstrates a methodology for designing variable gain workspace extension methods for specific task characteristics which allows improved execution performance compared to the conventional constant scaling method. For applying this methodology in real-life applications, the results need to be scaled for more realistic situations, such as higher degrees of freedom and in-contact tasks.**

***Index Terms*—Telemanipulation, Rotational workspace extension, Variable scaling, Within subject human factors, Fitts' law**

I. Introduction

TELEMANIPULATION enables operators to perform manipulation tasks in remote environments. The environment may not only have different locations but also have different scales, ranging from applications in minimally

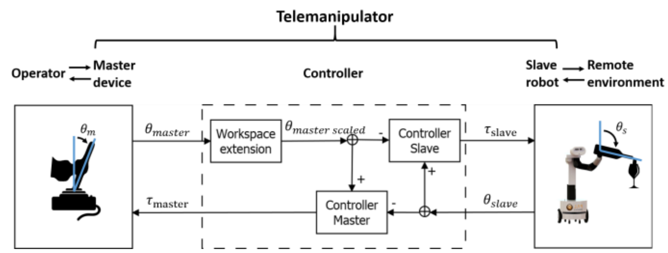

Fig 1: The slave interacts with the remote environment according to (scaled) inputs from the master side, while at the master device force feedback is provided to the operator from the slave side. The controller, consisting of a workspace extension method and a position-position controller architecture [47], manages the information flow, positions (θ) and forces (τ), between master and slave

invasive surgery or micro assembly, to care robot applications [1] or construction cranes [2]. Workspace mapping, extension or reduction, is required to compensate for the varying dimensions between master and slave (Fig 1). In this study the focus is on the extension of the master workspace. Specifically, for rotational workspace extension it is not very well understood how it should be implemented and what the effect on task execution is.

In telemanipulation applications, such as care robot applications [1], nuclear power plant maintenance systems [3] and construction cranes [2], the slave workspace is larger compared to the master workspace (ranging from a factor of 4 to more than 100). The slave's dimensions are matched to the task, while the master's dimensions are matched to human's workspace. Additionally, master devices are often optimized for dynamic performance instead of workspace. For example, a parallel mechanical construction of the master provides a low inertia and a high stiffness, but at the cost of a limited workspace [4]. Workspace extension methods, integrated in the controller (Fig 1), are required to map the limited workspace of the master to the relative large workspace of the slave.

In literature, translational workspace extension is a widely-studied subject (e.g., [5], [6], [7], [8], [9], [10], [11], [12], [13], [14], [15]). Basically, all workspace extension methods are based on position control, velocity control or a combination of both [16]. Position control refers to a control method by which the displacements of the master are directly translated to displacements of the slave. Alternatively, in velocity or rate control the position of the master is translated to a velocity of

R. van der Klauw and J.G.W. Wildenbeest are with the Department of Biomechanical Engineering, Faculty 3mE; Delft University of technology, Mekelweg 2, 2628 CD Delft, The Netherlands, and with Heemskerk Innovative Technology B.V., Mijnbouwstraat 120, 2628 RX Delft, The Netherlands.

D.A. Abbink is with the Department of Biomechanical Engineering, Faculty 3mE; Delft University of technology, Mekelweg 2, 2628 CD Delft, The Netherlands.

C.J.M. Heemskerk is with Heemskerk Innovative Technology B.V., Mijnbouwstraat 120, 2628 RX Delft, The Netherlands.

the slave. Most common used methods in literature within these two control methods are indexing, scaling, ballistic, rate and hybrid control [12] [17]. Indexing is a method where the master displacements are directly mapped to the slave until the master reaches its mechanical limit, then decouples the master from the slave and relocates the master back at its original position. After this relocation, the master and slave are recoupled again and the telemanipulation continues. Scaling refers to a workspace extension method where displacements of the master are multiplied by a gain, constant or variable, and mapped to the slave side. During ballistic control the gain, which maps the displacements of the master to the slave, is a function of both the master position and velocity. In rate control the slave robot moves with a speed proportional to the displacement of the master. Finally, hybrid workspace extension combines both position and velocity control; the workspace is divided into an inner sphere with position control and an outer sphere with velocity control.

Even though rotational telemanipulations are fundamentally different, translations commute while rotations don't, and mentally more demanding for operators than translational telemanipulations [18], there is a lack of literature about rotational workspace extension. Only one study was found about rotational workspace extension [19], in this study Dominjon et al. [20] compared different rotational extension methods, however the accuracy realized in this study was low, with a minimal error of 30°.

The main goal of this study is to introduce a methodology for designing a novel variable rotational workspace extension method, which improves task execution compared to the conventional constant scaling method. This method customizes a variable gain to the task characteristics of an application in order to improve the task execution. A variable rotational workspace extension design, inspired on a real-life care robot application, will be implemented and human in the loop evaluated. It is hypothesized that the variable gain extension method allows improved performance, in terms of fine positioning time, and control effort, in terms of reversal rate, at regions it is optimized for (up to 90% of the slave rotations) with respect to the conventional constant extension method, while the operator is still able to perform in all regions with similar order of magnitude metrics. To test this hypothesis a variable scaling method, a constant scaling method and a baseline method (without scaling) are designed and analyzed in a within-subject-haptic-telemanipulation-single-degree-rotational-pointing-experiment.

II. Design methodology

In this section the introduced design methodology for variable scaling is described more detailed. In section A, the background for the variable scaling method is described. In section B, a general guideline for the design methodology is presented, and in section C, the methodology is applied to a case study inspired on a care robot application.

A. Design background

Rotational telemanipulations are mentally more demanding for operators than translational telemanipulations [18]. By limiting the mental transformations between master and slave reference frames the mental effort reduces and therefore the telemanipulation performance increases [21] [22] [23] [24]. This can be done by preserving nulling compliance, i.e. the property that when the master returns to its initial orientation, the slave also returns to the corresponding initial orientation [21] [25]. Buxton [21] and Poupyrev [25] stated that nulling compliance reduces the required mental transformations during telemanipulations. Workspace extension methods, such as ballistic and hybrid control, shown to be proper methods to extend translational workspaces, however, don't preserve nulling compliance resulting in a continuous varying nulling position of the slave, which decreases the telemanipulation performance. The only workspace extension method which preserves nulling compliance is scaling [26]. So, to realize high performance during rotation workspace extension the proposed methodology is based on scaling:

$$\theta_{slave} = (gain) \cdot \theta_{master} \qquad \text{Eq. 1}$$

In order to design a proper gain, it is important to understand how rotational scaling influences the interaction between operator and telemanipulator. This interaction can be described with Fitts' law (Eq. 2 and Fig 2), a widely-used model to describe the trade-off between speed and accuracy for human movements [27] [28], which we here apply to tele-operated movements. Fitts' law states that the speed accuracy trade-off is dependent on the rotational amplitude of the task (α), referring to gross positioning, and the target width (ω), referring to fine positioning [27] [28]. Gross positioning is getting to the vicinity of the target and fine positioning is the final acquisition of the movement [29].

$$T = a + b \cdot \log_2\left(\frac{\alpha}{\omega} + 1\right) \qquad \text{Eq. 2}$$

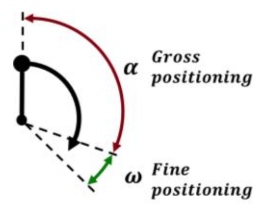

Fig 2: Illustration of the components of Fitts' law applied to a rotational task, with the black arrow denoting the direction of the pointing task. The pointing task can be divided into a gross positioning (α) and a fine positioning (ω) part.

Fitts' model doesn't include a gain, although there is certainly a relationship between the gain and task performance: Jellinek and Card [7] found that plotting the time of a telemanipulation task as a function of the gain resulted in a U-shaped graph [30]. They concluded that by varying the gain a different trade-off occurs between gross and fine positioning, i.e. speed-accuracy trade-off. For gross positioning a high gain is preferred to realize a high speed and for fine positioning a low gain is preferred to realize a high accuracy [29]. Fig 3 illustrates how the U-shaped graph [7] may be used to select an optimal setting

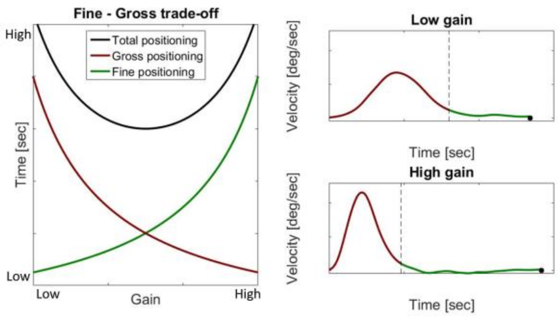

Fig 3: On the left the speed-accuracy trade-off as a function of the gain (adapted from [29]), where the speed-accuracy positioning trade-off is shown. And on the right velocity as a function of time with a low and a high gain, where gross positioning time improves with a high gain, i.e. high velocity, and fine positing time with a low gain, i.e. high accuracy.

for the gain. This can be weighted differently depending on the task requirements, like maximal accuracy, i.e. low gain preferred, or maximal speed, i.e. high gain preferred.

Unfortunately, the constant gain required to cover the mismatch between master and slave workspace does not necessarily represent the optimal solution for specific tasks. This is illustrated by the study of Dominjon [20], where the required gain to map the slave's rotational workspace was not optimal for realizing high accuracy.

In real-life applications, a slave device will be used over a range of varying rotational amplitudes. For example, in many household chores most rotations take place around the initial orientation [3], where most tasks require only small rotations (e.g., small adjustments of objects), while less other require large rotations (e.g., flipping a glass to load a dishwasher). This means that optimal gain is application-dependent and most preferred at rotational amplitude regions where most manipulations occur, which might be adapted by the operator. To avoid continuous adaptations by the operator, we aim to propose a method to determine a single variable gain, based on the distribution of the rotational amplitudes measured during real-world tasks, which maps the whole slave workspace while reaching the optimal gain at preferred rotational amplitude regions.

In summary, telemanipulation performance with scaled rotational workspace extension is influenced by the gain and its influence on the (task-specific) speed-accuracy trade-off. We propose a methodology to tune a single variable gain to accommodate a distribution of rotational task amplitudes, such that the gain allows the full rotational workspace of the slave, while approaching the optimal gain at amplitude regions with most occurring manipulations.

B. Design methodology

In this section a general guideline for designing variable gain workspace extension is presented. The methodology consists of three steps: i) performing an analysis on task and telemanipulator characteristics, ii) defining design constraints, and iii) solving for the parameters of the variable scaling equation.

i) Task and telemanipulator characteristics

Task characteristics

- Probability distribution of rotational amplitudes, to extract the focus region of the workspace and maximal rotational amplitude
- Maximal allowable gain at which the operator is still able to perform the task within a reasonable time, to extract the gain-ranges for the variable scaling design.

Telemanipulator characteristics

- Rotational workspace of the master and slave, to calculate the workspace mismatch ratio.

ii) Design constraints

Based on the gathered information on the task and telemanipulator characteristics it is possible to define the design constraints for the variable scaling method namely the nulling compliance (1), workspace mismatch ratio (2), focus region (2) and maximal allowable gain (4) (Table 1).

Table 1

Design constraints for the variable scaling method

1.	$(\theta_m(\min)\,;\theta_s(\min)) = (0\ ;\ 0)$	Nulling compliance
2.	$\dfrac{\theta_s(max) \vee \theta_{task}(max)}{\theta_m(max)}$	Workspace mismatch ratio
3.	$\%\ of\ frequency\ distribution$	Focus region
4.	$\dfrac{d\theta_m\ (max)}{d\theta_s(max)}$	Maximal allowable gain

iii) Variable scaling parameters

With the design constraints and the scaling workspace extension formula (Eq. 3) it is possible to solve the equation for the unknown parameters, A, B and n, for the variable gain workspace extension method. Where A is the gain at the begin of the workspace, B a constant scaler which ensures the mapping of the whole slave workspace and n the order of the variable gain function.

$$\theta_{slave} = (A + B \cdot \theta_{master}^{n}) \cdot \theta_{master} \qquad \textit{Eq. 3}$$

Case study: Care application

The variable gain workspace extension design in this study is based on a real-life care robot application. The aim of the care robot is to cost-efficiently fill in the increasing gap on the health care labor market, caused by the aging society, by remotely assisting elderly during daily live activities [1] [31]. In this application, precise manipulations are often required since the slave acts in a domestic and vulnerable environment. Hence, accuracy was emphasized over speed, i.e. a low gain is preferred at the region of focus.

i) Task and telemanipulator characteristics

Task characteristics

- Task analysis

Based on the questionnaire performed by Van Hee et al. [32] in healthcare homes a benchmark task was defined. It was found

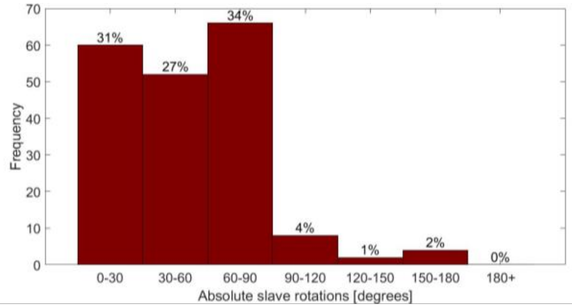

Fig 5: Probability distribution of rotational amplitudes during the meal assistance task of the care application, with their share in percentage on top of the bars. It can be seen that most rotations (92%) occur at the first half of the slave workspace.

that the meal assistance task was a frequent and representative task at which elderly need help. A kinematic task analysis was performed on the meal assistance task, where all absolute rotations of the end-effector were determined and categorized into bins of 30° (Fig 5). A left skewed distribution was detected with a maximal rotational amplitude of 180°. At least 90 percent of all rotations should be included by the region of focus, which means that the focus region is from 0 to 90°.

- Maximal allowable gain

To estimate the maximal allowable gain a small experiment (N=3) was executed, where subjects performed a positioning task which required rotational accuracy of 1°. It was approximated that a gain of 15 was the maximal gain at which the operators could stay within the target width for two seconds.

Telemanipulator characteristics

- Rotational workspace

In the care application, a parallel haptic master is used with a rotational workspace of 45° in all directions. The slave workspace (270°) is larger than the maximal required rotation during the meal assistance task (180°) [33], therefore the workspace mismatch ratio is determined based on the maximal task rotation and the master workspace.

ii) Design constraints

Based on the gathered information about the task and the telemanipulator the design constraints for the care application are defined and shown in Table 2.

Table 2

Design constraints for variable scaling: care application

1.	$(\theta_m(\min)\,;\theta_s(\min)) = (0\ ;\ 0)$	Nulling compliance
2.	$\frac{\theta_{task}(max)}{\theta_m(max)} = \frac{180}{45} = 4$	Workspace mismatch ratio
3.	$90\%\ of\ frequency\ distribution = 90\ degrees$	Focus region
4.	$\frac{d\theta_m\ (max)}{d\theta_s(max)} = 15$	Maximal allowable gain

iii) Variable scaling parameters

Based on the design constraints the unknown parameters of the equation (Eq. 3), A, B and n, are solved (Eq. 4). To evaluate the variable gain workspace extension method, it is compared with a constant scaling method (Eq. 5) and a baseline method (Eq.

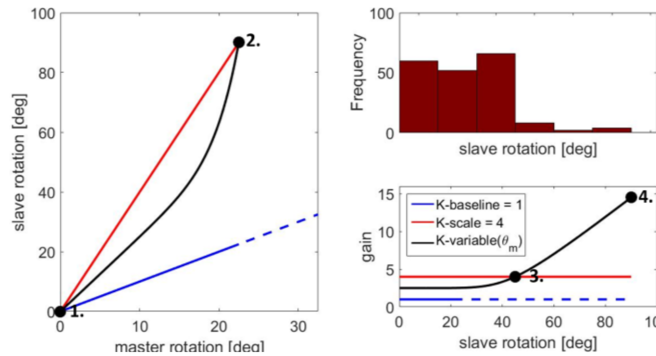

Fig 4: On the left, the slave position as function of the master position for the three workspace extension methods. The dotted line shows a situation where the master workspace has no physical rotational limitations (baseline). On the right the probability distribution of amplitudes during the task on top and the gains for the different workspace extension methods on bottom as a function of the slave rotation. The numbers 1 to 4 represents the design constraints from Table 2. The variable gain at most occurring rotations approaches the optimal gain of 1, i.e. high accuracy, while at the end of the workspace the maximal gain is below 15. Furthermore, the highest non-linearity of the variable gain is at 39°, determined by the area between a linear line and the actual variable gain line for ±5° around each rotation.

6). In Fig 4 the orientation and the gain of the final workspace extension methods are illustrated. For the design in this study, the master and slave workspace are divided by two (master workspace = 22.5°, slave workspace = 90°). This is done in order to realize a master workspace which is physically not limited for the baseline method.

$$\theta_s = (2.5 + (5.1382e^{-10}) \cdot \theta_m^7) \cdot \theta_m \qquad \textit{Eq. 4}$$

$$\theta_s = (4) \cdot \theta_m \qquad \textit{Eq. 5}$$

$$\theta_s = (1) \cdot \theta_m \qquad \textit{Eq. 6}$$

III. Method

A. Participants

Twelve subjects with an age of 21 to 39 years (M=25.2, SD=4.3) voluntarily performed in the experiment. All the participants were right handed and had a normal hand-eye coordination. Two participants had previous telemanipulation experience (4-12 hours training). All participants gave their informed consent. The experiment was approved by the TU Delft Human Research Ethics Committee.

B. Experimental setup

The experimental setup is shown in Fig 7; the participant, i.e. the operator, was shown the remote environment via video feedback from a USB camera. The camera was located straight above the rotating point of the slave. In Fig 8 the visual feedback shown on the cockpit screen is presented, including the slave and the printed map with the rotational tasks.

C. Apparatus

The experiment was performed with the Geomagic touch, developed by 3D systems, as the haptic master, which can realize a maximal force of 3.3N [34]. As a slave, the 7 DoF Ulna robotic arm, developed by PAL Robotics, was used [33]. A

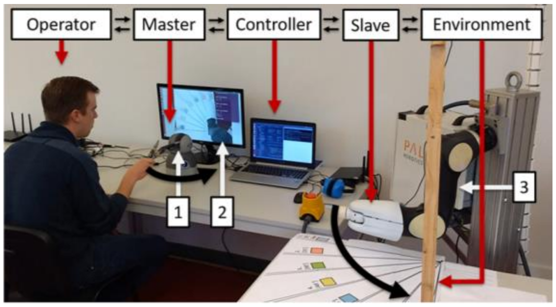

Fig 7: Experimental setup: the operator rotates the slave joint (3) in the remote environment by rotating the master joint (1). The controller manages the information flow between master and slave. The operator receives visual feedback from the remote environment on the cockpit screen (2).

position resolution of 0.1° could be achieved [33] using the master-slave setup.

The controller ran on Ubuntu 14.4 at 1 kHz. As a robotic middleware between the different hardware devices Robot Operating System (ROS) was used [35]. The estimated communication delay between master and slave was 80 msec.

As a controller, a two-channel position-position controller was used (Fig 1) [36]. The master PD controller was used to provide haptic feedback from the slave in the remote environment to the operator. The master PD controller (Eq. 7) was designed to have slightly underdamped ($\zeta = 0.8$) response from master to slave. A cutoff frequency of 50 Hz was chosen in order to tune the PD gains. After tuning a K_p of 144.7245 and K_d of 19.2482 were calculated.

$$C_m\,(s) = (\,Kp \,+\, Kd \cdot s\,) \qquad \textit{Eq. 7}$$

D. Task description

The participants were asked to perform a one degree of freedom rotational pointing task, inspired by Fitts' law translational tapping task [27]. The subject's task was to rotate the robotic arm from start (0°) towards six different targets (15, 20, 30, 45, 65, 90°) by rotating the master device. The targets were visually indicated (Fig 8). The participant received instructions about the desired task via cockpit screen. The target width was 1° for all target rotations. This value was constant to ensure high accurate tasks during the whole experiment. Combining the rotational amplitude (α) and the target width (ω) in Fitts' model (Eq. 2) gives the following IDs: 4.0, 4.4, 5.0, 5.5, 6.0, 6.5 bits.

The time started whenever the participant moved the arm from the start position and stopped whenever the reference point on the robotic arm was within the boundaries of the target for half a second. Whenever the reference point was within the

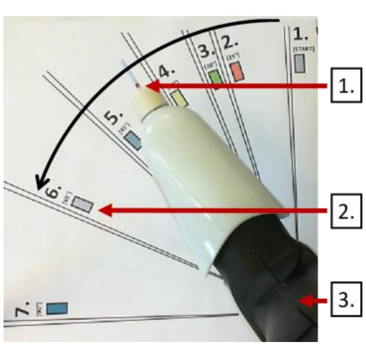

Fig 8: Visual feedback presented on the cockpit screen to the operator while performing the rotational pointing task. With the slave arm, rotating around joint 3, above the map with rotational tasks. The goal was to rotate the reference point (1) within the boundaries of a desired target rotation (2).

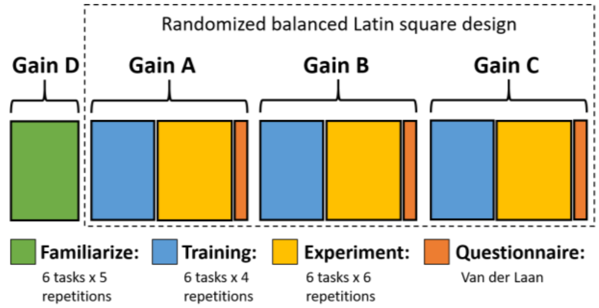

Fig 6: Experimental protocol. Subjects started with familiarization of the setup with Gain D (k=2). This was followed by three blocks in which the three experimental conditions were tested. Each condition started with a training of 4 repetitions, followed by 6 measured repetitions and the Van der Laan questionnaire. The order in which the conditions were presented was randomized by means of a balanced Latin square.

boundaries a progress bar started filling to indicate the status of the task, if the reference point moved out of the boundaries the progress bar was putted to zero again. After the task was completed the participant was guided, with haptic feedback, towards the start position. Whenever the operator was for half a second at the start position the next target was presented on the screen. This process continued till all repetitions were performed.

The task instruction, provided to the participants, was to perform the task as fast as possible, while emphasizing accuracy rather than speed. Which is similar to the task instructions provided by Fitts' original experiment [27].

E. Experimental design

A within subject human in the loop telemanipulation experiment was performed. The three experimental conditions were randomized according the balanced Latin square principle among the participants. The experiment started with an informed consent and a short introduction about the experimental setup. This was followed by a familiarization session to practice with the system and get familiar with the telemanipulation concept. The familiarization was done with a constant gain of 2. The familiarization was followed by the real experiment. Each experimental condition started with four training trails directly followed with six trials recorded for the experiment. After each experimental condition a Van der Laan questionnaire was taken. In Fig 6 the generic protocol for the experiment is shown.

F. Data acquisition

The orientations of the master and slave were recorded at 1 kHz. Before analyzing the data, the raw data of the master and slave were resampled at 200 Hz. Furthermore, the signals were filtered using positive anti-causal filtering with a second order low pas Butterworth and a cut-off frequency of 10 Hz.

G. Metrics

To determine the task performance the following metrics were defined; time [sec] and Fitts' index of performance (IP) [bits/sec]. The time metric was divided into total positioning time, gross positioning time and fine positioning time (Fig 9).

- Total positioning time is the time in seconds it requires the participant to complete the whole task.

- Gross positioning time is the time in seconds it requires the participant to complete the task from start to target rotation minus five degrees.
- Fine positioning time is the time in seconds it requires the participant to complete the last five degrees of the task.
- The Index of Performance (Eq. 8) is used as a measure of human performance. This metric was calculated by using the adapted model of Fitts' law (Eq. 2) to determine the coefficient b experimentally with the use of linear regression [37].

$$IP = 1/b \qquad \textit{Eq. 8}$$

To determine control performance the following metrics were defined; mean absolute jerk normalized by peak speed $[deg/sec^2]$ and reversal rate [-].

- Jerk, the time-derivative of acceleration, is used as a metric which shows the smoothness of a movement. Smoothness is a hallmark for skilled and coordinated human movements. In this study the smoothness of the movement is measured by the mean absolute jerk (Eq. 9) [38]. This metrics is normalized by peak speed, such that the metric is a measure of smoothness only and not confound with changes in overall movement speed.

$$\frac{1}{\dot{x}_{\text{peak}}} \int |\dddot{x}(\text{t})|\text{dt} \qquad \textit{Eq. 9}$$

- The reversal rate is the amount of reversals of the operator during the task at the master side. The amount of reversals is an estimation of the control effort of the operator [39]. The reversal rate was calculated by counting the amount of zero crossings of the master velocity (Fig 9).

Finally, the subjective Van der Laan questionnaire was used as a metric for the acceptance of the three workspace extension methods. This questionnaire consists of nine questions and accesses the acceptance on two dimensions; usefulness and satisfying [40].

H. Statistical analysis

Before performing the interferential statistics, the major outliers were detected and excluded (18 trials in total). Tukey's method was used to exclude the major outliers based on the total positioning time [41]. The outliers were removed, since they were caused by uninteresting reasons. For example; the concentration might have lapsed on that trial, or the participant hesitated because momentarily forgot the target rotation.

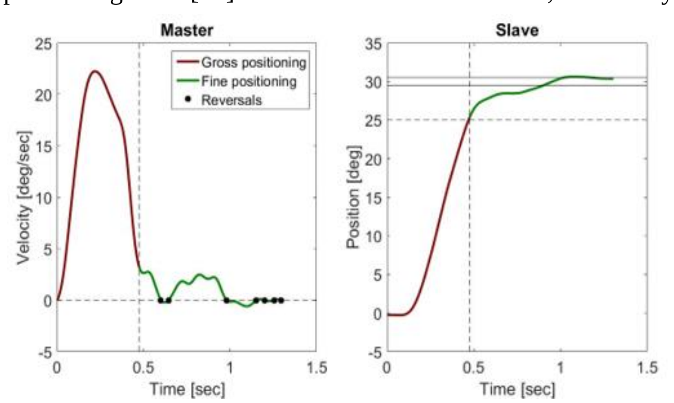

Fig 9: Typical trial with the constant scaling method. On the left the master input velocity as function of time, where gross positioning requires a relative high velocity and fine positioning a low velocity. The black dots showing the reversals. On the right the slave output orientation as a function of time, where the gross positioning ends and the fine positioning starts at 5° before the target rotation (30°)

The calculated metrics were averaged over the repetitions per participant, for each of the conditions. The comparison between the experimental conditions was made on basis of population, assuming a normal distribution. To analyze the effect of the different scaling methods a one-way repeated-measures analysis of variance (ANOVA) was performed. The assumption of sphericity, equality of variance of the differences between the scaling methods, was tested with Mauchlys Sphericity Test. Whenever the sphericity is violated a Greenhouse-Geisser correction was performed.

A summary of the parameters of current experiment are presented in Table 3.

Table 3

Summary of the experimental design

Task	Fitts based 1 DoF rotational pointing task
Amplitude (α)	15, 20, 30, 45, 65, 90°
Target width (ω)	1°
Index of Difficulty	4.0, 4.4, 5.0, 5.5, 6.0, 6.5 bits
Conditions	Constant scaling, baseline scaling and variable scaling
Instruction	As fast as possible, while emphasizing accuracy rather than speed
Metrics	Time (total, gross, fine) [sec], Fitts Index of performance [bits/sec], reversal rate [#], mean absolute jerk normalized by peak speed $[\text{deg}/\text{sec}^2]$, Van der Laan questionnaire [-]
Group size	12 participants
Repetitions	4 repetitions per task for training and 6 repetitions per task for data analysis
Design	Within subject balanced Latin square design

IV. Results

The figures in this section show the mean and the 95 percent confidence interval (CI) of the metrics of all 12 participants.

In this result section, only the post hoc comparisons with the variable scaling are shown in order to enhance clarity of the results. Results with a p-value below 0.05 were considered as significant (α = 0.05). Fig 10 shows the trials of a typical participant performing the experiment with the three different workspace extension methods.

A. Task performance

- Time

The mean values and 95% of CI of the three workspace extension methods for all the tasks for fine -, gross - and total positioning time are presented in Table 4. The interferential statistics for the time metrics are shown in Table 5 and Fig 11.

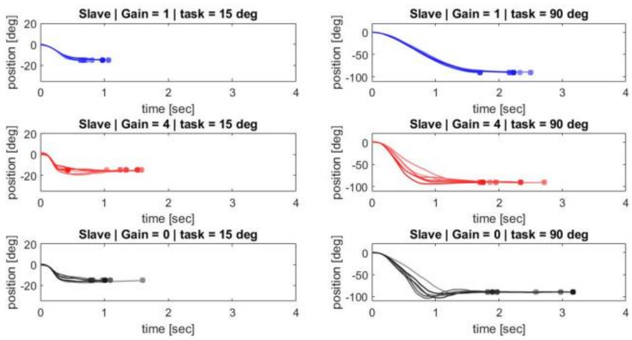

Fig 10: On the left a typical slave output of a small rotational task (15 deg) and on the right a large rotational task (90°) for the three different scaling methods; baseline (blue), constant scaling (red) and variable scaling (black). The darkness of the lines increases with each trial. The different approaching strategies can be seen for the three methods.

<u>Gross positioning time</u>

A significant main effect was found for all the rotational tasks (F≥26.9, p<0.001). After performing post hoc tests between variable and constant scaling it was founded that the constant scaling performed significant faster for all rotations (p<0.001), except for 90° where no differences were detected (p=0.6597). Post hoc comparisons between the variable and baseline scaling indicated that the mean gross positioning time of variable scaling was significantly lower (p<0.01) than the baseline scaling for all rotations, except for 45° (p=0.4014).

<u>Fine positioning time</u>

A main effect was found between the different workspace extension methods for all the rotations (F≥18.3, p<0.001). Post hoc tests revealed significant improved time for the variable scaling method compared to the constant method (p<0.05) for tasks up to 30°. No differences were found between the constant and the variable scaling method for 45 and 65° rotation (p=0.6465 and p=0.0963 respectively). Finally, for the task of 90° a significant improved performance of constant scaling (p<0.001) was found with respect to the variable scaling. Regarding the baseline scaling significant improved performance were found for all the rotations (p<0.05).
Furthermore, there was a positive correlation between the gain and fine positioning time (r=0.99, p<0.001).

Table 4: **Time - Descriptive statistics: Mean (95% CI)**

Task (deg)	**Gross positioning time [sec]**			**Fine positioning time [sec]**			**Total positioning time [sec]**		
	Baseline	**Constant**	**Variable**	**Baseline**	**Constant**	**Variable**	**Baseline**	**Constant**	**Variable**
15	0,42 (0.06)	0,10 (0.02)	0,22 (0.05)	0,47 (0.06)	0,92 (0.09)	0,64 (0.09)	0,89 (0.09)	1,02 (0.10)	0,87 (0.11)
20	0,43 (0.07)	0,21 (0.04)	0,31 (0.06)	0,48 (0.09)	0,83 (0.10)	0,69 (0.08)	0,91 (0.10)	1,04 (0.11)	1,00 (0.09)
30	0,70 (0.09)	0,35 (0.05)	0,54 (0.09)	0,52 (0.09)	0,88 (0.12)	0,68 (0.06)	1,22 (0.11)	1,23 (0.13)	1,22 (0.11)
45	0,87 (0.07)	0,53 (0.07)	0,83 (0.10)	0,53 (0.10)	0,89 (0.07)	0,92 (0.11)	1,41 (0.11)	1,42 (0.10)	1,75 (0.18)
65	1,17 (0.11)	0,71 (0.11)	0,94 (0.10)	0,39 (0.06)	1,02 (0.14)	1,34 (0.28)	1,56 (0.09)	1,74 (0.15)	2,25 (0.30)
90	1,44 (0.16)	0,91 (0.14)	0,89 (0.12)	0,55 (0.12)	1,03 (0.16)	2,23 (0.44)	1,99 (0.15)	1,94 (0.14)	3,12 (0.43)

Table 5: **Time: Interferential statistics: One way repeated measures ANOVA**

Task (deg)	**Gross positioning time**			**Fine positioning time**			**Total positioning time**		
	Main effect	**Post hoc Variable to**		**Main effect**	**Post hoc Variable to**		**Main effect**	**Post hoc Variable to**	
		Baseline	**Constant**		**Baseline**	**Constant**		**Baseline**	**Constant**
15	F(2,22)=144.0, p<0.001	p<0.001	p<0.001	F(2,22)=48.5, p<0.001	p<0.001	p<0.001	F(2,22)=4.6, p<0.05	p=0.7470	p<0.001
20	F(2,22)=53.1, p<0.001	p<0.001	p<0.001	F(2,22)=19.8, p<0.001	p<0.001	p<0.05	F(2,22)=2.9, p=0.0766	-	-
30	F(2,22)=67.9, p<0.001	p<0.001	p<0.001	F(2,22)=11.8, p<0.001	p<0.05	p<0.05	F(2,22)=0.0, p=0.9975	-	-
45	F(2,22)=35.7, p<0.001	p=0.4014	p<0.001	F(2,22)=18.3, p<0.001	p<0.001	p=0.6465	F(2,22)=12.6, p<0.001	p<0.01	p<0.01
65	F(1.3,13.9)=34.5, p<0.001	p<0.01	p<0.001	F(1.3,14.7)=26.2, p<0.001	p<0.001	p=0.0963	F(1.3,14.7)=11.3, p<0.01	p<0.01	p<0.05
90	F(1.3,14.3)=26.9, p<0.001	p<0.001	p=0.6597	F(2,22)=47.4, p<0.001	p<0.001	p<0.001	F(1.2,13.4)=25.2 , P<0.001	p<0.001	p<0.001

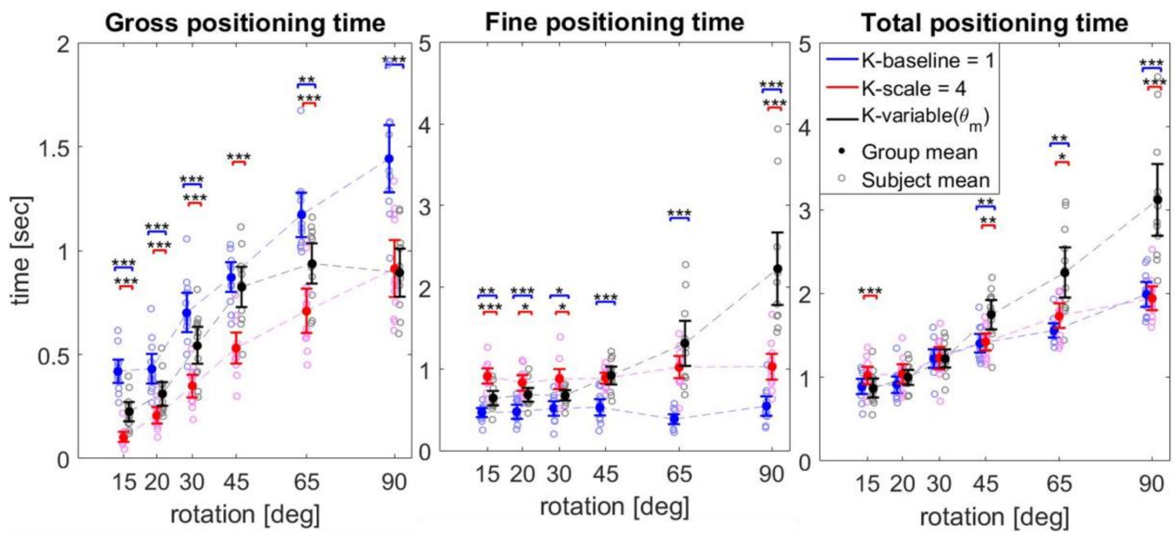

*Fig 11: The time metrics plotted against the rotation. On the left the gross positioning time can be seen, where the variable scaling is faster than the baseline but slower compared to the constant scaling. At the final rotation the variable and constant scaling are similar. In the middle the fine positioning time is presented, where the baseline is faster than the constant scaling and both methods are constant over the rotations. Further, the variable scaling is faster than the constant scaling for rotations below 45°, after this rotation it is the other way around. Finally, on the right the total positioning time, where for 15° the variable scaling is faster than the constant scaling, for 20° till 45° no differences are detected and for rotations of 45° and higher the variable scaling is slower compared to the constant and baseline scaling. Differences are shown with *** for p ≤ 0.001, ** for p ≤ 0.01 and * for p ≤ 0.05, further a red bar represents difference between the variable and constant method and a blue bar between variable and baseline.*

Total positioning time

For total positioning time, significant main effects were found for 15, 45, 65 and 90° ($F \geq 4.6$, $p<0.05$). So, no differences were found between the workspace extension methods for 20 and 30° rotation. Post hoc comparison between variable scaling and constant scaling shows a significant improved performance for variable scaling on the 15° ($p<0.001$). Furthermore, significant decreased performance is detected for 45, 65 and 90° ($p<0.01$, $p<0.05$ and $p<0.001$ respectively). The post hoc comparisons between the variable scaling and baseline scaling indicate improved performance of the variable scaling for the last three tasks ($p<0.01$, $p<0.01$ and $p<0.001$ respectively). Furthermore, no differences were found for the smaller rotations (<45°).

- Fitts law

A linear regression was calculated to predict completion time based on the index of difficulty ($T = a + b \cdot ID$). Respectively for baseline scaling, constant scaling and variable scaling were the following a and b values found: a = -0.88 (0.27), -0.61 (0.32) and -2.81 (0.76) and b = 0.42 (0.05), 0.38 (0.06) and 0.86 (0.17). A significant regression equation was found for all three workspace extension methods ($F(1,4)=82.6$, $p<0.001$, $R2=0.95$, $F(1,4)=104.8$, $p<0.001$, $R2=0.96$ and $F(1,4)=50.0$, $p<0.01$, $R2=0.93$ for baseline, constant and variable respectively).

Regarding the index of performance (Fig 13), a main effect was found ($F(2,22)=26.8$, $p<0.001$). After performing a post hoc test differences were found between the variable scaling (M=1.28 (0.22)) and baseline scaling (M=2.46 (0.30), $p<0.001$) and constant scaling (M=2.79 (0.42), $p<0.001$).

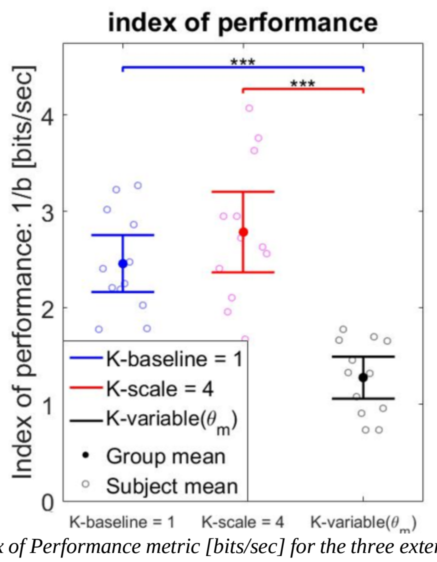

*Fig 13: Index of Performance metric [bits/sec] for the three extension methods. Differences are seen between the variable scaling method and the other two extension methods. differences are shown with *** for p ≤ 0.001, ** for p ≤ 0.01 and * for p ≤ 0.05, further a red bar represents difference between the variable and constant method and a blue bar between variable and baseline.*

B. Control performance

- Jerk

The descriptive statistics and the interferential statistics for mean absolute jerk, normalize by peak speed at the master and slave side are shown in Table 6, Table 7 and Fig 2.

No significance main effects were found for the master between the conditions for the rotations 15, 20, 65 and 90° ($p=0.7188$, $p=0.0955$, $p=0.1803$ and $p=0.5232$ respectively). For the rotation of 30° a significant main effect was found ($F(1.3,14.4)=7.6$, $p<0.05$), with post hoc tests indicating decreased smoothness for the variable scaling compared to the baseline scaling ($p<0.05$) and the constant scaling ($p<0.05$). Furthermore, for the rotation of 45° a significant main effect was found ($F(1.4,15.1)=10.6$, $p<0.01$), with post hoc tests indicating decreased smoothness for the variable scaling compared to the baseline scaling ($p<0.01$) and the constant scaling ($p<0.01$).

For the slave jerk no significance main effects were found between the conditions for the rotations 15, 20, 65 and 90° ($p=0.8497$, $p=0.0969$, $p=0.0552$ and $p=0.6581$ respectively). At the slave side the effects were found at the same rotations, namely 30 and 45° ($F(2,22)=5.4$, $p<0.05$ and $F(1.3,14.4)=14.7$, $p<0.001$ respectively). For 30° Posthoc tests indicate less smoothness for the variable scaling compared to the constant scaling ($p<0.05$) and to the baseline scaling ($p<0.05$). For 45° post hoc test show less smoothness for the variable scaling compared to the constant scaling ($p<0.01$) and to the baseline scaling ($p<0.01$).

Table 6: Jerk master: Descriptive statistics: Mean (95% CI)

Task (deg)	Baseline	Constant	Variable
15	0.39 (0.14) e+16	0.47 (0.22) e+16	0.47 (0.34) e+16
20	0.17 (0.13) e+16	0.42 (0.27) e+16	0.54 (0.34) e+16
30	0.46 (0.26) e+16	0.56 (0.22) e+16	1.07 (0.45) e+16
45	0.71 (0.23) e+16	1.03 (0.41) e+16	2.14 (0.88) e+16
65	1.15 (0.43) e+16	1.82 (0.67) e+16	2.32 (1.30) e+16
90	2.69 (1.05) e+16	3.30 (1.28) e+16	2.32 (1.56) e+16

Table 7: Jerk slave: Descriptive statistics: Mean (95% CI)

Task (deg)	Baseline	Constant	Variable
15	0.24 (0.08) e+16	0.21 (0.09) e+16	0.22 (0.14) e+16
20	0.10 (0.07) e+16	0.20 (0.12) e+16	0.26 (0.14) e+16
30	0.26 (0.16) e+16	0.27 (0.09) e+16	0.48 (0.17) e+16
45	0.38 (0.12) e+16	0.46 (0.17) e+16	1.13 (0.42) e+16
65	0.54 (0.20) e+16	0.78 (0.25) e+16	1.43 (0.73) e+16
90	1.26 (0.48) e+16	1.34 (0.45) e+16	1.61 (1.14) e+16

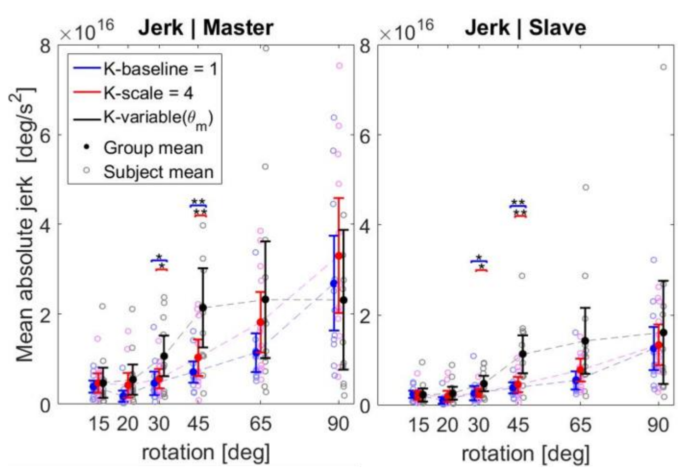

*Fig 12: Mean absolute jerk normalized by peak speed. On the left the jerk of the master and on the right the jerk of the slave versus the rotational amplitude. At both graphs the variable scaling has higher jerk compared to the baseline and constant method at 30° and 45°, for the other rotations no differences were detected. Differences are shown with *** for p ≤ 0.001, ** for p ≤ 0.01 and * for p ≤ 0.05, further a red bar represents difference between the variable and constant method and a blue bar between variable and baseline.*

- Reversal rate

The descriptive statistics and the interferential statistics for reversal rate are shown in Table 8, Table 9 and in Fig 14. A main effect was found between the different workspace extension methods for all the rotations (F≥7.1, p<0.01). Post hoc tests revealed less reversals for the variable scaling method compared to the constant method (p<0.05 and p<0.01) for tasks 15 and 30° respectively. No differences were found between the constant and the variable scaling method for 30 and 45° rotation (p=0.7889 and p=0.1921 respectively). Finally, for the task of 65 and 90° a significant improved performance of constant scaling (p<0.05 and p<0.001 respectively) was found with respect to variable scaling. Regarding the baseline scaling improved performance was found for all the rotations (p<0.05), except for 15 and 30° (p=0.0546 and p=0.7823 respectively).

Table 8: **Descriptive statistics: Mean (95% CI)**

Task (deg)	**Reversal rate**		
	Baseline	**Constant**	**Variable**
15	1,52 (0.36)	2,92 (0.54)	2,14 (0.53)
20	1,16 (0.40)	2,53 (0.58)	2,43 (0.81)
30	1,67 (0.78)	3,18 (0.81)	1,54 (0.63)
45	1,31 (0.61)	2,83 (1.03)	3,70 (1.20)
65	0,72 (0.32)	3,72 (1.08)	8,26 (2.93)
90	1,06 (0.65)	4,29 (1.63)	16,45 (4.44)

Table 9: **Interferential statistics: One way repeated measures ANOVA**

Task (deg)	**Reversal rate**		
	Main effect	**Post hoc Variable to**	
		Constant	**Baseline**
15	F(2,22)=10.2, p<0.001	p=0.0546	p<0.05
20	F(2,22)=7.6, p<0.01	p<0.05	p=0.7889
30	F(2,22)=7.1, p<0.01	p=0.7823	p<0.01
45	F(2,22)=7.3, p<0.01	p<0.01	p=0.1921
65	F(1.2,13.0)=16.1, p<0.01	p<0.001	p<0.05
90	F(1.3,14.5)=40.9 , p<0.001	p<0.001	p<0.001

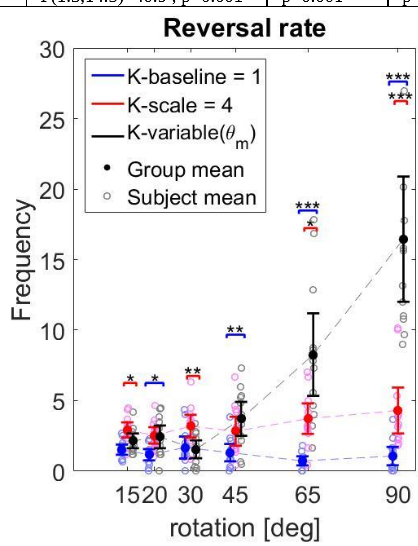

*Fig 14: Reversal rate versus the rotations. For lower rotations (15, 30°) reversal rate is less for variable scaling compared to constant scaling. For larger rotations (>45°) more reversals are detected for the variable scaling with respect to constant and baseline scaling. Differences are shown with *** for p ≤ 0.001, ** for p ≤ 0.01 and * for p ≤ 0.05, further a red bar represents difference between the variable and constant method and a blue bar between variable and baseline.*

C. Acceptance scale

- Van der Laan questionnaire

All means are positive for the three workspace extension methods on both dimension (Fig 15). For usefulness, the following means were found M=0.40 (0.26), M=0.77 (0.40) and M=0.65 (0.24) for baseline, constant and variable respectively. And for satisfying M=0.73 (0.19), M=0.42 (0.43) and M=0.04 (0.36) for baseline, constant and variable respectively. This suggest that all three scaling methods are accepted by the participants. Furthermore, no main effect was found for usefulness (F(2,22)=1.9, p=0.1803). On satisfying level a main effect was found (F(2,22)=3.8, p<0.05), after post hoc analysis a difference was detected between variable scaling and baseline scaling (p<0.01).

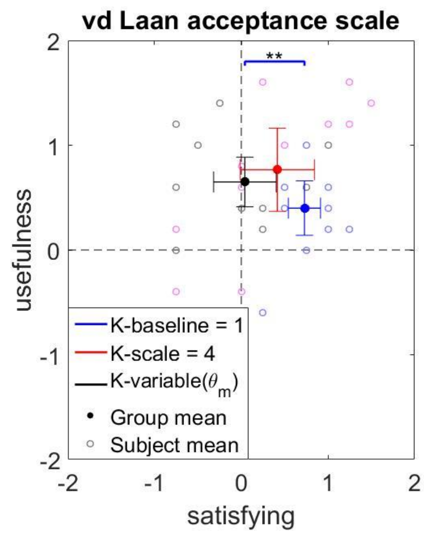

*Fig 15: Van der Laan acceptance scale; on the horizontal axis the satisfying dimension and on the vertical axis the usefulness dimension. No differences between the methods on the usefulness dimension are detected. On the satisfying dimension differences between variable and baseline method are detected. Further, all mean values are at the top right plan, i.e. positive scores on both dimensions. Differences are shown with *** for p ≤ 0.001, ** for p ≤ 0.01 and * for p ≤ 0.05, further a red bar represents difference between the variable and constant method and a blue bar between variable and baseline.*

V. Discussion

The primary goal of this study was to present and evaluate a methodology for designing variable rotational scaling method. It was expected that the variable rotational workspace extension design improves the task performance at most occurring rotations. A care robot application was taken as a case study.

The experiment showed improved performance (fine positioning time up to 30% faster) and control effort (up to 51% less reversals) with the variable scaling at the focus regions (up to 45°) compared to the constant scaling. On the other hand decreased performance was found at regions not focused on. These results suggest that subjects were able to successfully control a scaling method with a variable gain while improving the performance at most occurring tasks, i.e. the focus region.

For more depth understanding of the variable rotational workspace extension method all the metrics are analyzed separately in the following section.

Effect on metrics

- Time

Variable scaling showed improved performance at the smallest rotational task (15°) for the total positioning time compared to the constant scaling. Furthermore, variable scaling showed decreased performance at large rotational tasks (≥45°). This suggest that the variable scaling method is no improvement for rotations higher than 15° on total positioning time compared to the conventional constant scaling method. However, looking more closely to the variable scaling method, improved performance on the fine positioning time was found at the focus region. According to literature a lower gain should improve translational fine positioning [7] [29]. The results of this study confirm the findings for rotational tasks, where a positive relationship was found between the gain and fine positioning time. Although, gross positioning time increased for the focus region. This can be explained with the U-shaped gain influence on the speed-accuracy trade-off suggested by MacKenzie [29]. The design methodology focused on maximal accuracy, i.e. the focus lied on fine positioning rather than gross positioning.

In terms of time, this study demonstrates that with variable gains it is possible to play with the speed-accuracy trade-off and manipulate it at predefined regions, and thereby improve the performance in terms of time compared to constant scaling.

- Fitts' law

For Fitts' law significant linear relationships were found, between the completion time of the three scaling methods and the Index of Difficulty, with regression coefficients of 0.93 and up. These results show that for all the workspace extension methods Fitts' law relationship can be used to explain and predict outcomes for telemanipulated rotational scaling tasks, both for constant and variable scaling. This means that the movement strategies, i.e. speed-accuracy trade-off, of translational pointing movements are similar to scaled rotational pointing movements.

Furthermore, the variable scaling method showed decreased performance on the Index of Performance metric compared to the constant and baseline scaling. This suggest that the variable scaling method has decreased human performance during rotational telemanipulations compared to the constant and baseline scaling. However, the Index of Performance is one value representing the whole range of index of difficulties, i.e. it doesn't distinguish between focus and non-focus regions of the variable scaling method. Therefore, the Index of Performance metric is a proper model to analyze constant scaling methods, however for variable scaling methods it does not describe the trade-off between focus and non-focus regions of the variable gain, and therefore underestimates the performance of the variable scaling method at focus regions.

Altogether, it is possible to predict and extrapolate outcomes with the model of Fitts, for both constant and variable scaling methods. Furthermore, the Index of Difficulty is not a good metric to describe the task performance of the variable scaling method, since it doesn't distinguish between focus and non-focus regions.

- Mean absolute jerk

Comparing the mean values of the mean absolute jerk of all the extension methods for the master and slave it can be seen that the jerk of the slave is lower with respect to the master. This suggest that the operator tries to manipulate the slave as smooth as possible instead of their own arm movements at the master side; the operator is able to integrate the telemanipulator into their intern model. Furthermore, variable scaling showed no differences on the mean absolute jerk metric for small (<30°) and large rotational tasks (>65°) compared to constant scaling at both the master and slave side. However, for rotations at 30 and 45° significant higher jerk was detected for the variable scaling method compared to the constant and baseline scaling method. This higher jerk suggests that the movements with the variable scaling method are less smooth and therefore less skilled and coordinated [38], compared to the constant and baseline method. The high jerk can be explained regarding the gain graph (Fig 4), where the highest non-linear changes of the gain occur around 39°. This suggests that human operators are able to manipulate linear changes of the gain equally smooth as constant gains, however nonlinear changes of the gain are more difficult to manipulate smoothly. In future research the smoothness of the telemanipulation can be considered in the methodology for variable scaling design.

In conclusion, the operator integrates the telemanipulator system into their intern model, in order to manipulate the slave as smooth as possible. Differences in smoothness were found between variable and constant scaling at non-linear changes of the gain, while for the most rotations the manipulation was equally smooth.

- Reversal rate

For the variable scaling method, an improvement on reversal rate was found for the focus region (up to 45°) compared to the constant scaling. On the contrary, at non-focus regions the reversal rate increased for the variable scaling with respect to the constant scaling method. The results show that the control effort for the variable gain extension method improves for focus regions and decreases for non-focus regions, compared to the constant scaling method. This increase in control effort can be explained by the increasing gain of the variable scaling at higher rotations, which is according to literature, where improved control performance were found for lower gains [7] [42] [25]. Looking more detailed to a single trial all reversals were found at the end of the task, i.e. during fine positioning. This means that fine positioning has a higher control effort compared to gross positioning.

In short, the variable scaling method realizes low control effort at the focus region compared to the constant scaling method.

- Acceptance scale

For the variable scaling method no differences were found on the subjective acceptance scale compared to the constant scaling method. This suggest that the operator has no clear preference for the constant or variable scaling method. Furthermore, all three methods were in the top right plane of the Van der Laan acceptance plot (Fig 15) which suggest that all the scaling methods are considered useful and satisfying.

Overall, the variable scaling method is equally accepted, and considered as useful and satisfying, as the constant scaling method.

- Conclusion metrics

The experimental results show improved performance on fine positioning time and reversal rate for the variable scaling method at the focus regions compared to constant scaling. Furthermore, human operators accept variable scaling equally as constant scaling and are able to manipulate linear changes of the gain equally smooth as constant gains; however nonlinear changes of the gain are more difficult to manipulate smoothly. Based on the linear regression applied to Fitts' model, the speed-accuracy trade-off is similar for translational and rotational tasks, which provides better insight in rotational telemanipulations and makes it possible to extrapolate the results found in this research.

Limitations and future work

The results found in this study are gathered in an experimental setup which is an abstract representation of the real world.

First of all, the results are dependent on the task characteristics, such as rotational amplitudes and target widths. For example, the variable scaling method would have improved performance at the end of the workspace whenever the target widths are larger, due to the (task-specific) speed-accuracy trade-off. In this study the target width was kept constant (1°) and rotational amplitudes up to 90° were tested. However, this is not the case in real applications, such as the care robot application where rotations up to 180° were found. Furthermore, the accuracy is not constant for all the subtasks. By expanding the task characteristics, the design of the variable scaling method changes as well, due to the changing design constraints. The principle of the proposed design methodology stays the same, and is therefore applicable for varying task characteristics.

Furthermore, only free air tasks were performed with the slave. According to Wildenbeest et al. [44] a telemanipulation task can be categorized into four fundamental subtasks, namely: free air, contact transition, translational contact and rotational contact. In order to realize better understanding of the performance of variable scaling during real life tasks, all the fundamental subtasks need to be implemented in the experimental setup. During the proposed variable scaling method, directional compliance is not always preserved, which could negatively influence the haptic feedback performance during in-contact tasks [25]. Furthermore, the haptic feedback needs to be scaled according to the variable gain in order to realize realistic forces to the operator over the whole workspace. Therefore, smart solutions need to be defined in future research in order to provide high quality haptic feedback during all fundamental subtasks.

Moreover, an abstract one DoF rotational task was chosen as the experimental task to minimize the noise caused by known and unknown variables. However, a one DoF task is not realistic since real-life tasks often take place in six DoF. It is expected that the variable scaling method is applicable for higher DoF tasks, since Dominjon [20] showed that humans are able to perform a higher DoF task with constant rotational scaling method.

By extending the variable scaling method to higher DoF tasks another question arises about the applicability of the variable scaling method for translational tasks. It is expected that the variable gain extension method is applicable and useful for translational tasks. Since it is expected that the probability distribution of the amplitudes are also skewed for translational tasks, as in the care robot application. However, variable scaling may not be the best method for extending translational workspaces, due to the fact that the proposed method is designed for rotational tasks, i.e. high priority given to nulling compliance. This nulling compliance is only preserved by scaling, and therefore all the other extension methods were excluded in this study. However, nulling compliance is less important during translations, since these tasks are mentally les demanding [18]. According to literature hybrid control is an excellent method for extending translational workspace [5] [7] [12] [13] [14] [15], compared to the other existing workspace extension methods. An interesting area for future research is to investigate what the effect is on the task – and control performance with different extension methods for translations and rotations within the same telemanipulator.

Finally, in this research the variable scaling method was applied in order to extend the workspace of the master. However, as mentioned in the introduction, the workspace mismatch between master and slave can also be the other way around, i.e. workspace reduction, such as minimally invasive surgery and micro assembly. It is expected that the methodology of variable scaling is applicable for reducing the master workspace. By downscaling of the master workspace an increased accuracy can be realized at regions were most precise manipulations take place, which improves the telemanipulation performance in applications such as minimally invasive surgeries where accuracy is highly relevant. Besides, higher gains can be integrated in the variable gain at regions where high velocity is required. In short, during workspace reduction, the same as for workspace extension, the variable gain can be tuned based on the task characteristics, like rotational amplitude distribution, in order to improve telemanipulation performance.

To conclude, this results of this study show that the presented methodology, based on the influence of the gain on the speed-accuracy trade-off, for designing variable rotational workspace extension methods allow improved execution performance in regions it is optimized for compared to conventional constant scaling. However, future research is essential to test the variable gain workspace extension method in more realistic experimental setups, such as higher DoF and in-contact tasks.

Conclusion

Due to lack of literature about rotational workspace extension the goal of this research was to propose and evaluate a methodology for designing variable scaling workspace extension. The effect of variable scaling on teleoperated task performance and control performance was analyzed for an accurate 1DoF pointing task inspired by a care robot application.

For the experimental conditions studied, we conclude that:

- the variable scaling improves telemanipulation execution performance in terms of fine positioning and reversal rate at the focus region compared to the constant method.
- subjects are able to manipulate the variable gain equally smooth as constant gain, indicating skilled and coordinated manipulations, while high nonlinear changes of the gain are more difficult to manipulate smoothly.
- for all the workspace extension methods Fitts' law relationship can be used to explain and predict outcomes for telemanipulated rotational scaling tasks.

Altogether, this study demonstrated that with variable gains it is possible to play with the speed accuracy trade-off and manipulate it at predefined regions of the slave workspace. The introduced methodology for designing variable rotational workspace extension methods allows improved task performance compared to the state-of-the-art conventional constant scaling method at the focus regions, as in the care application where the focus region includes more than 90% of all tasks.

ACKNOWLEDGEMENTS

This research was supported by Heemskerk Innovative Technology B.V., Delft, and the Haptics lab from the TU Delft. I also thank the participants for their time and constructive attitude during the experiment.

REFERENCES

[1] Technology Heemskerk Innovative (HIT), "Semi Autonomous Care Robot (SACRO)," [Online]. Available: http://www.heemskerk-innovative.nl/?project=semi-autonomous-care-robot-sacro. [Accessed 28 March 2017].

[2] A. Barrow and W. Harwin, "Design and analysis of a haptic device desgin for large and fast movements," *Machines,* vol. 8, no. 4, 2016.

[3] E. Versteeg, "Requirements analysis of 7-DOF parallel haptic master device and experimental comparison of two workspace extension techniques for teleoperation in a real life task," TU Twente, Twente, 2016.

[4] P. Lambert, "Parallel robots with configurable platforms; Precision and microsystems engineering," TU Delft, Delft, 2013.

[5] J. Barrio, M. Ferre, F. Suarez-Ruiz and R. Aracil, "A Remote Handling Rate-Position Controller for Telemanipulating in a Large workspace," *Fusion Engineering and Design,* vol. 89, no. 1, pp. 25-28, 2013.

[6] J. Barrio, F. Suarez-Ruiz, M. Ferre and R. Aracil, "A rate position haptic controller for large telemanipulation workspaces," *IEEE/RSJ INternational conference on intelligent robots and systems,* pp. 58-63, 2012.

[7] G. Casiez, D. Vogel, Q. Pan and C. Chailou, "RubberEdge Reducing Clutching by Combining position and rate control with elastic feedback," *Proceedings of the 20th annual ACM symposium on User interface software and technology,* pp. 129-138, 2007.

[8] F. Conti and O. Khatib, "Spanning large workspaces using small haptic devices," *Eurohaptics Conference,* pp. 183-188, 2005.

[9] A. Das, A. Jaju and P. Pal, "Evaluation of Motion Mapping from a Haptic device to an industrial robot for effective master slave manipulation," *International Journal of Robotics and Automation,* vol. 28, no. 1, pp. 206-3657, 2013.

[10] L. Dominjon, J. Perret and A. Lecuyer, "Novel devices and interaction techniques for human-scale haptics," *The visual computer,* vol. 23, no. 4, pp. 257-266, 2007.

[11] L. Liu, G. Liu, Y. Zhang and D. Wang, "A Modified Motion Mapping Method for Haptic Device based Space teleoperation," *Robot and human interactive communication,* pp. 449-453, 2014.

[12] M. Mamdouh, A. Ramadan and A. Abo-Ismael, "Evaluation of a proposed workspace spanning technique for small haptic device based manipulator teleoperation," *Intelligent robotics and applications,* pp. 161-170, 2012.

[13] F. Ruiz, "Human robot interaction for telemanipulation in large workspaces," CSIC - Centro de Automática y Robótica (CAR), Madrid, 2014.

[14] M. Radi, Workspace scaling and haptic feedback for industrial telepresence and teleaction systems with heavy-duty teleoperators, Munchen: Herbert Utz Verslag, 2012.

[15] M. Voskuil, "Human-centered control method with optimal task execution for master-slave systems with infinite virtual workspace of the slave," Delft University of Technology, Delft, 2015.

[16] D. McRuer and H. Jex, "A Review of Quasi-Linear Pilot Models," *Transactions on human factors in electronics,* vol. 8, no. 3, 1967.

[17] A. Perez and J. Rosell, "An assisted re-synchronization method for robotic teleoperated tasks," *IEEE International Conference on Robotics and Automation,* pp. 886-891, 2011.

[18] K. Hinckley, J. Tullio, R. Pausch, D. Proffitt and N. Kassell, "Usability analysis of 3D rotation techniques," *UIST ACM,* vol. 17, pp. 1-10, 1997.

[19] R. van der Klauw, "Workspace extension method for parallel haptic master devices: Application teleoperation with a care robot," TU Delft, Delft, 2016.

[20] L. Dominjon, A. Lecuyer, J. Brukhardt and S. Richir, "Haptic hybrid rotations: Overcoming hardware angular limitations of force feedback devices," *Virtual reality conference,* pp. 167-174, 2006.

[21] W. Buxton, in *There's More to Interaction than Meets the Eye: Some Issues in Manual Input*, Hillsdale, New Jersey, Lawrence Erlbaum Associates, 1986, pp. 319-337.

[22] D. Bowman, E. Kruijff, J. LaViola and I. Poupyrev, 3D user interfaces; theory and practice, Boston: Pearson Education, Inc., 2011.

[23] B. DeJong, E. Colgate and M. Peshkin, "Improving teleoperation: reducing mental rotations and translations," *International conference on robotics and automation,* pp. 3708-3714, 2004.

[24] M. Menchaca-Brandan, A. Liu, C. Oman and A. Natapoff, "Influence of perspective taking and mental rotation abilities in space teleoperation," *international conference on Human-robot interaction* , vol. 12, pp. 271-278, 2007.

[25] I. Poupyrev, S. Weghorst and S. Fels, "Non-Isomorphic 3D Rotational Techniques," *Human factors in computing systems*, pp. 240-547, 2000.

[26] S. Zhai, "Human Performance in Six Degree of Freedom Input Control," University of Toronto, Toronto, 1995.

[27] P. Fitts, "The information capacity of the human motor system in controlling the amplitude of movment," *Journal of experimental psychology*, vol. 47, pp. 381-391, 1954.

[28] M. Stoelen and D. Akin, "Assessment of Fitts' Law for Quantifying Combined Rotational and Translational Movements," *Human factors,* vol. 52, no. 1, pp. 63-77, 2010.

[29] I. MacKenzie, "Input devices and interaction techniques for advanced computing," *Virtual environment and advanced interface design,* pp. 437-470, 1995.

[30] H. Jellinek and S. Card, "Powermice and user performance," in *ACM Conference on Human Factors in Computing Systems*, 1990.

[31] Rijksinstituut voor Volksgezondheid en Milieu (RIVM), "Toekomstverkenning RIVM: Een gezonder Nederland met meer chronisch zieken," 20 October 2016. [Online]. Available: http://www.rivm.nl/Documenten_en_publicaties/Algemeen_Actueel/Nieuwsberichten/2014/Toekomstverkenning_RIVM_Een_gezonder_Nederland_met_meer_chronisch_zieken. [Accessed 28 March 2017].

[32] K. Hee, M. Osch and E. Veerdonk, "Meerwaarde van robotica in de zorg," *Rose robots for care,* 2015.

[33] PAL robotics, ULNA handbook, Barcelona, 2014.

[34] 3D Systems, Geomagic touch device guide, Morrisville, 2013.

[35] http://wiki.ros.org/ROS/, "ROS wiki," Robotic operating system (ROS), [Online]. Available: wiki.ros.org/ROS/. [Accessed 28 March 2017].

[36] G. Christiansson, "Hard Master, Soft Slave Haptic," TU Delft, Delft, 2007.

[37] I. MacKenzie, "Fitts law as a research and design tool in human computer interaction," *Human computer interaction,* vol. 7, no. 1, pp. 91-139, 1992.

[38] B. Rohrer, S. Fasoli, H. Krebs, R. Hughes, B. Volpe, W. Frontera, J. Stein and N. Hogan, "Movement smoothness changes during stroke recovery," *The journal of neuroscience,* vol. 22, no. 18, pp. 8297-8304, 2002.

[39] W. MacDonald and E. Hoffmann, "Review of relationships between steering wheel reversal rate and drive task demand," *Human factors,* vol. 22, no. 6, pp. 733-739, 1980.

[40] J. van der Laan, A. Heino and D. Waard, "A simple procedure for the assessment of acceptance of advanced transport telematics," *Transportation research,* vol. 5, no. 1, pp. 1-10, 1997.

[41] J. Tukey, Exploratory data analysis, 1997.

[42] J. Accot and S. Zhai, "Scale effects in steering law tasks: Do device size and different motor joints matter?," in *CHI'2001*, 2001.

[43] J. Arnaut and J. Grenstein, "Is display/control gain a useful metric for optimizing an interface," *Human factors,* vol. 32, no. 6, pp. 651-663, 1990.

[44] J. Wildenbeest, A. Abbink, C. Heemskerk, F. van der Helm and H. Boessenkool, "The impact of haptic feedback quality on the performance of teleoperated assembly tasks," *IEEE transactions on haptics*, vol. 6, no. 2, pp. 242-252, 2013.

[45] D. Ryu, S. Kang, M. Kim and J. Song, "Multi-modal user interface for teleoperation of ROBHAZ-DT2 field robot system," *Intelligent robots and systems,* pp. 168-173, 2004.

[46] T. Brooks, "Telerobotic Response Requirements," *IEEE international conference sysetms, man and cybernetics,* pp. 113-120, 1990.

[47] B. Hannaford, L. Wood, D. McAffee and H. Zak, "Performance evaluation of a six-axis generalized force-reflecting teleoperator," *IEEE trans. systems, man and cybernetics,* vol. 3, no. 21, pp. 620-633, 1991.

Appendix 1: Design methodology

Workspace extension methods

During haptic telemanipulations, the workspace of the master is often smaller compared to the workspace of the slave. This mismatch is caused by physical limitations of the workspace of the human operator (human arm dimensions) or by physical limitations of the workspace of the haptic master, with respect to the slave workspace.

To overcome the mismatch between master and slave, workspace extension methods are inevitable. Workspace extension methods are integrated in the controller of the telemanipulator and determine how the workspace of the master is mapped to the workspace of the slave. A human operator is only able to stably control a zero - or a first order teleoperated system (McRuer & Jex, 1967). Therefore, the available workspace extension methods in literature are all based on two main fundamental principles; 1) position control (zero order) and 2) velocity control (first order) (Fig 16). Position control refers to a control method by which the displacements of the master are directly translated to displacements of the slave. Velocity control refers to a control method by which the position of the master is translated to a velocity of the slave. This control method is commonly called rate control (Zhai, 1995).

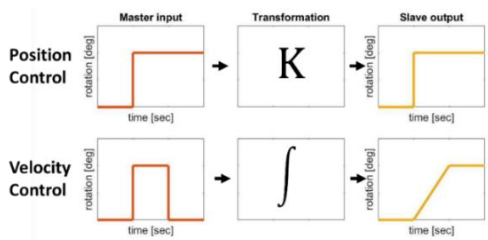

Fig 16: On top the position control with the master input directly mapped to the slave output. And below the velocity control with the master input integrated and mapped to the slave output (adapted from Zhai, 1995).

Five common workspace extension methods are available in literature to overcome the workspace mismatch between a relative small master and large slave, namely indexing, scaling, ballistic, rate and hybrid control (Fig 17). In the following sections, all methods are described shortly. Further, the extension methods are explained with a 1DoF example task. In the example task a target rotations (at 2 degrees) needs to be reached with the slave by controlling a master with a workspace of 1 degree using the different extension methods. Whenever the target is reached the master moves back towards its initial position, in order to test if the methods preserve the nulling compliance, which ensures that when the master returns to its initial orientation the slave also returns to the corresponding initial orientation (Buxton, 1986). Which is a major benefit during mentally demanding rotational telemanipulations in terms of task performances (Buxton, 1986, Poupyrev, 2000, Dejong et al., 2004 and Menchaca-Brandon et al., 2007).

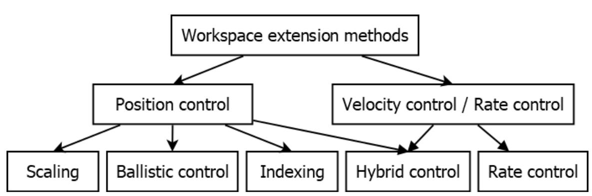

Fig 17: The available workspace extension methods found in literature. All methods are based on position – and/or velocity control. Within position control; scaling, ballistic and indexing control can be found. Further, within velocity control the rate control can be found. Finally, hybrid control is a combination of both position and velocity control.

Indexing

This workspace extension method is also called clutching or re-synchronization. During indexing the end-effector of the slave is position controlled. Whenever reaching the mechanical limit of the physical workspace of the master, the operator decouples the master from the slave and relocates the end-effector of the master back to its original position (without moving the slave robot), referred to as an index action in Fig 18. After this relocation, the master and the slave are recoupled again (Mamdouh et al., 2012 and Perez & Rosell, 2011). In Fig 18 it can be seen that the master and slave are out of sync at the end of the task when the master is at its initial position. This means that indexing does not preserve nulling compliance. An everyday example of indexing is the computer mouse jump. Computer mouse jumps are used whenever reaching the edge of the mouse mat and replacing it back in the middle of the mat. Mathematically rotational indexing method can be expressed as follows: $\theta_{slave} = \theta_{master} + \theta_{slave\ memory}$.

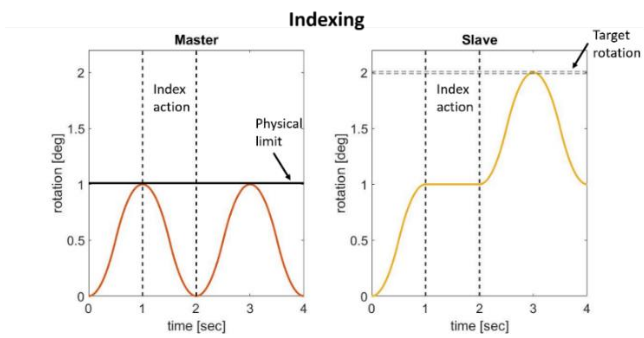

Fig 18: Indexing control with the master on the left with the physical limit of the workspace at 1 degree and the slave on the right with the target rotation at 2 degrees. The master control the slave directly, until the mechanical limit is reached, at that point the index action takes place (between the vertical dotted lines), where the master is moving and the slave is not moving. After this the master and slave are recoupled and the task is completed. At the end of the task no nulling compliance is preserved.

Scaling

During scaling control the slave is position controlled by the master. The scaling workspace extension method refers to the method where the displacements of the master is multiplied by a gain and then mapped to the slave side (Fig 19). From Fig 19 it can be concluded that the scaling method preserves nulling compliance, since the master and slave are at their initial orientation at the end of the task. The gain during this extension method can be constant or variable. Mathematically the rotational scaling method can be expressed as follows: $\theta_{slave} = k_p * \theta_{master}$.

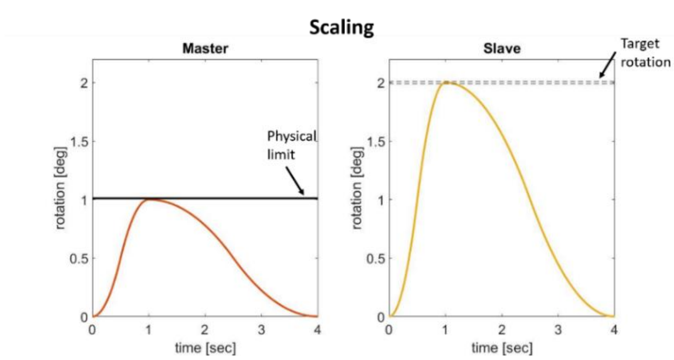

Fig 19: Scaling control with the master on the left with the physical limit of the workspace at 1 degree and the slave on the right with the target rotation at 2 degrees. The master controls the slave with a gain of 2. At the end of the task the nulling compliance is preserves.

Ballistic

Ballistic control is similar to scaling control, however during ballistic control the gain is dependent on the speed of the master end-effector. If the end-effector of the master has a low speed the gain will be low. And if the master device moves quickly there is a high gain (Fig 20). This means that at slow movements of the master the workspace is small with a relatively high accuracy. And at quick movements of the master the workspace is large with a relatively low accuracy (Perez & Rosell, 2011). In Fig 20 the movement towards the target is much faster, i.e. high gain, compared to the movement towards the initial position of the master, i.e. lower gain. Due to the different gains, caused by the varying velocities, the nulling compliance is not preserved. An example of this method is a computer mouse, where the gain is function of both the position and velocity of the master. Mathematically the rotational ballistic control can be expressed as follows: $\theta_{slave} = k_p * \theta_{master}$ with the gain $k_p = k_v * \dot{\theta}_{master}$.

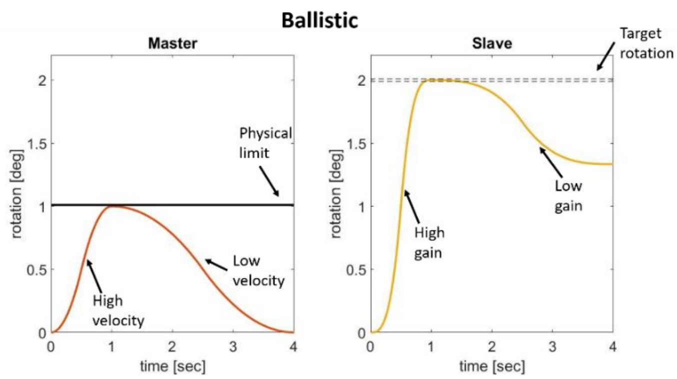

Fig 20: Ballistic control with the master on the left with the physical limit of the workspace at 1 degree and the slave on the right with the target rotation at 2 degrees. The task starts with a relative high velocity, i.e. a high gain, and ends with a low velocity, i.e. low gain, therefore the nulling compliance is not preserved at the end of the task.

Rate

During rate control the slave moves with a speed proportional to the displacement of the master (Fig 21) (Mamdouh et al., 2012 and Perez & Rosell, 2011). Rate control does not preserve nulling compliance, as can be seen in Fig 21. An example for an application where rate control is commonly used is in industrial cranes. Mathematically rotational rate control can be expressed as follows: $\dot{\theta}_{slave} = k_v * \theta_m$.

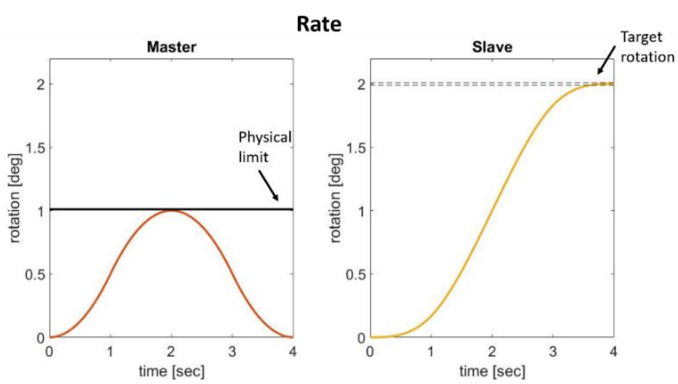

Fig 21: Rate control with the master on the left with the physical limit of the workspace at 1 degree and the slave on the right with the target rotation at 2 degrees. The orientations of the master are integrated and mapped to the slave. At the end of the task the nulling compliance is not preserved.

Hybrid
Within the hybrid workspace extension method, position and velocity control are combined. The workspace is divided into an inner zone with position control, also called position zone, and an outer zone with velocity control, also called velocity zone (Mamdouh et al., 2012 and Perez & Rosell, 2011). The switching between the workspace extension methods occurs whenever the end-effector of the master passes the border between both zones. By holding the end-effector of the master in the inner zone the operator can control the slave under position control. Whenever the end-effector is moved into the outer zone the operator can control the slave under velocity control (Fig 22). This control method does not preserve nulling compliance due to the velocity control part. Mathematically the rotational hybrid method can be expressed as follows:

$$\theta_{slave} = k_p * \theta_{master} \quad if\ \theta_{master}\ is\ within\ inner\ zone$$
$$\dot{\theta}_{slave} = k_v * \theta_{master} \quad if\ \theta_{master}\ is\ within\ outer\ zone$$

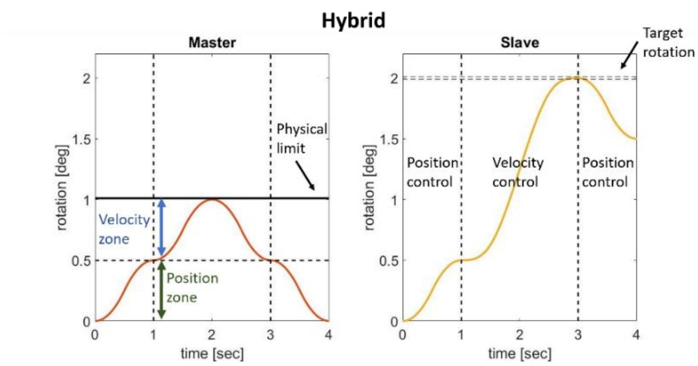

Fig 22: Hybrid control with the master on the left with the physical limit of the workspace at 1 degree, further the control switch border is at 0.5 degrees of the master workspace. And the slave on the right with the different control modes separated with the vertical dotted lines and the target rotation at 2 degrees. The task starts with position control until the master enters the outer zone from that moment the slave is velocity controlled. At the end of the task the master moves back to its initial position in the inner zone. The nulling compliance is not preserved.

Scientific gap

Regarding the available literature about workspace extension methods with a relative small master several studies were found on translational workspace extension. However, only one study about rotational workspace extension, performed by Dominjon et al. (2006), was found (Fig 23) (Klauw, 2016). Due to the lack of literate on rotational workspace extension it is unclear to what extend the workspace extension methods can and should be applied for rotations.

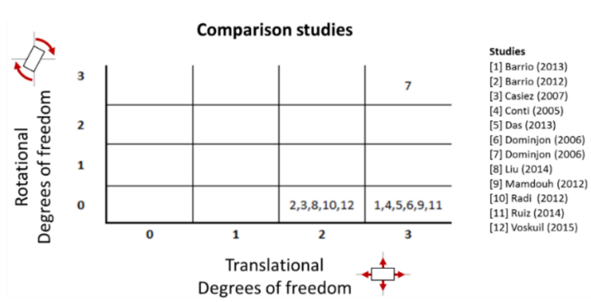

Fig 23: The results of the comparison study performed by Klauw (2016). On the vertical axis, the rotational DoF of the experimental setup and the horizontal axis the translational DoF of the experimental setup of the studied extension methods. Many studies can be found in the bottom row, i.e. translational extension method. However, only one study at the top right, i.e. rotational workspace extension.

Dominjon et al. (2006)

Dominjon et al. (2006) performed an experiment about rotational workspace extension and compared a hybrid rotational method, a constant rotational scaling method and a rotational indexing method. In this experiment 15 participants were asked to build a pyramid of cubes in a virtual environment. The participants were asked to perform the task as precise as possible. Task performances were measured in terms of completion time (sec) and accuracy (error in degrees). A serial Haption Virtuose 6D was used as the haptic master and the Novodex SDK was used as the virtual slave. The workspace of the master was four times smaller than the slave workspace. From the results of this experiment, it was found that on completion time hybrid control (131 sec) was significant faster than indexing (216 sec) and scaling control (285 sec). For accuracy, no significant differences were found, however the absolute values on accuracy were quite low, namely scaling performed best (error of 31 degrees), followed by hybrid (error of 41 degrees) and indexing (error of 44 degrees).

Variable rotational scaling methodology

Nulling compliance

In order to realize high performance during, mentally demanding, rotational telemanipulation tasks the focus in this research lies on rotational scaling, since scaling is the only workspace extension method which preserves nulling compliance. This can be seen in the figures in the previous sections (Fig 18, Fig 19, Fig 20, Fig 21 and Fig 22), where only with scaling the master and slave are at their initial positions at the end of the task, i.e. preserve nulling compliance. Buxton (1986) and Poupyrev (2000) stated that nulling compliance reduces the required mental transformations during telemanipulations. By reducing the mental transformations during telemanipulations the operator performances increases, in terms of errors, completion time and learning time.

Fitts' law

Fitts' law is used to understand the human machine interaction between the operator and the telemanipulator while rotational scaling. This is a widely-used model to study in and output values of a haptic interface (Samur, 2012). The model of Fitts describes the trade-off between accuracy and speed for rapid human movements, based on the human motor system information capacity (Fitts, 1954). Fitts' original model was designed for translational movements, in this study an adapted model is used to describe rotational movements:

$$T = a + b \cdot ID$$

$$ID = \log_2\left(\frac{\alpha}{\omega} + 1\right)$$

The speed accuracy trade-off is described in the concept of Index of difficulty (ID). The ID, which is measured in bits, is consisting of a logarithmic function including on the rotational amplitude of the task (α), referring to gross positioning, and the target width (ω), referring to fine positioning. Further, T is the completion time of the task. The coefficients a and b are dependent of the system, describing factors of the system like clicking buttons, input delays etc. The coefficients are experimentally determined by linear regression.

Gain

There is no term for the gain of the rotational scaling in the model of Fitts. This is logic since Fitts originally tried to describe direct human movements, i.e. gain of one. However, this does not mean that Fitts law is independent of gains. Jellinek and Card (1990) found that the gain has a U-shaped relation with the completion time (Fig 24). They stated that varying the gain evokes a trade-off between gross and fine positioning time. This means that for fine positioning a low gain is optimal and for gross positioning a high gain is optimal. The total time is the sum of the fine and gross positioning time. The U-shaped graph suggests that the optimal setting is the gain which minimizes the total time. However, this is not necessarily the optimal gain due to the fact that accuracy is sometimes more important than gross positioning or the other way around, i.e. the optimal gain is dependent on the task requirements.

Based on the speed accuracy trade-off described by Fitts (1954) and the influence of the gain on this trade-off (Jellinek & Card, 1990) it is possible to determine the optimal gain for a specific task for the scaling method. The optimal gain is often not the equal to the gain required as the constant gain for the workspace extension to map the master workspace to the whole larger slave workspace. This is also the case in the study of Dominjon (2006), where the required gain to map the slave workspace (k=4) was not the optimal gain for realizing high accuracy, causing low performance on accuracy.

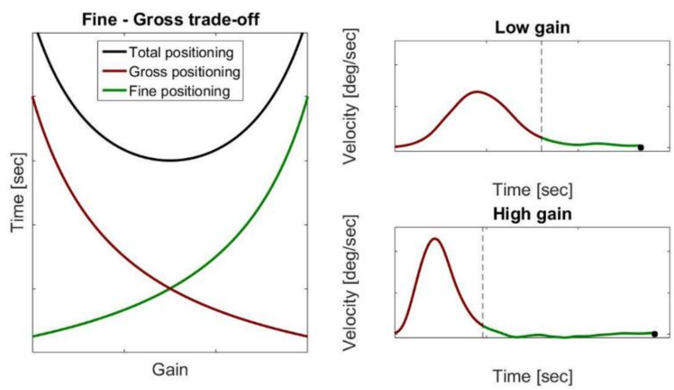

Fig 24: The U-shaped relation between the gain and the completion time on the left. In this graph it can be seen that fine positioning performs best with a low gain and gross positioning with a high gain. And their influence on the speed-accuracy tradeoff on the right, where a low gain realizes a relative low speed by high accuracy and the high gain a high speed but low accuracy.

Distribution

The distribution of the rotations in the slave workspace is often variable. For example, in many household chores most rotations take place around the initial orientation (Versteeg, 2016). The best performances are most preferred at the begin of the workspace, i.e. where most manipulations take place. The methodology introduced in this study conveniently uses this variable distribution of rotational amplitudes during tasks by a variable gain. With the variable gain, it is possible to approach the optimal gain at the most frequent occurring rotations, while the whole slave workspace is mapped. For less frequent used rotations the gain will be less optimal. Altogether, this will increase the overall performance. An example is shown in Fig 25 where a low gain is preferred. It can be seen that the variable controller has a lower gain for the most used rotations compared to the conventional constant scaling.

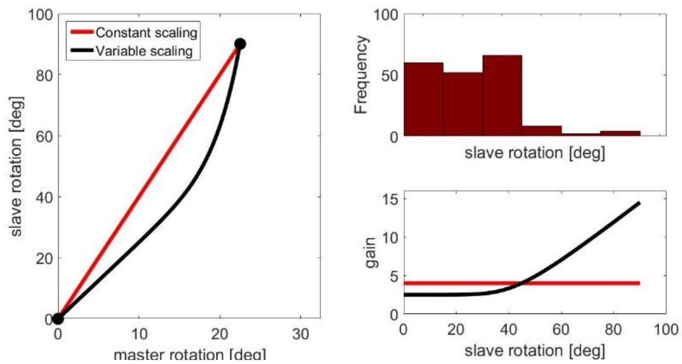

Fig 25: On the left a constant and a variable controller presented as slave rotations as a function of the master rotations. And on the top right the rotational task distribution and on the bottom right the gain of the different scaling methods. In the graph it can be seen that relative low gains are realized at most occurring rotations for the variable controller compared to the constant controller.

Design methodology for variable rotational scaling

In this section a methodology is described for designing variable gain workspace extension methods. The aim of this methodology is to adjust the variable gain and the task characteristics to each other, such that the gain approaches the optimal gain at preferred regions of the slave workspace.

Three steps are required in order to design the variable scaling method:

i) Analysis on task and telemanipulator characteristics
ii) Defining design constraints
iii) Solve variable scaling equation

i) Task and telemanipulator characteristics

Task characteristics

- Task analysis to determine the probability distribution of rotational amplitudes. This is required to define the region at which the workspace extension method should perform best and to determine the maximal rotational amplitude.
- Maximal allowable gain at which the operator is able to perform the all tasks. To define the gain-ranges for the design requirements.

Telemanipulator characteristics

- Rotational workspace of master and slave to calculate the master-slave ratio.

ii) Design constraints

Based on the gathered information on the task and telemanipulator it is possible to define the design constraints for the variable scaling method (Table 1). With the nulling compliance, which ensures that when the master is at its initial position the slave is at the same initial position. Further, the workspace mismatch ratio requirement makes sure that the whole slave workspace is mapped by the master workspace. This is defined based on the master workspace divided by the slave workspace or the maximal rotational task; using on the lowest value of both, i.e. worse case scenario. The focus region stands for the region where the optimal gain needs to be approached by the variable gain, which is based on the task distribution. Finally, the maximal allowable gain is the maximal gain which the extension method can contain, i.e. gain-ranges for the variable gain design.

Table 10

Design constraints for the variable scaling method

1.	$(\theta_m(\min)\,;\theta_s(\min)) = (0\ ;\ 0)$	Nulling compliance
2.	$\frac{\theta_s(max) \vee \theta_{task}(max)}{\theta_m(max)}$	Workspace mismatch ratio
3.	$\%\ of\ frequency\ distribution$	Focus region
4.	$\frac{d\theta_m\ (max)}{d\theta_s(max)}$	Maximal allowable gain

iii) Variable scaling parameters

In this study a power function is chosen as the gain of the variable method, although other options are possible such as polynomial or exponential.

$$\theta_{slave} = (A + B \cdot \theta_{master}^{n})\theta_{master}$$

With the design constraints (Table 1) and the scaling workspace extension formula the parameters A, B and n can be calculated for the variable gain workspace extension method. Where A stands for the gain at the begin of the workspace. B stands for the constant scaling factor, such that the whole slave workspace is mapped. And n stands for the order of the variable gain function.

The fit function is used to determine the possible solutions of the scaling method which meet the design constraints. Input parameters are the maximal slave rotation (slave_max), the maximal master rotation (master_max), the maximal allowable gain (max_allowable_gain) and the region of focus (focus_region). The focus region is the highest rotation of the focus region. Finally, margins define the allowable deviations from the design constraints. Based on these parameters the fit function determines the possible parameters for A, B and n. Whenever more solutions are possible it is up to the designer to decide which solution is most suitable for the application.

```
for n = [1:.1:99]

    for A = [1:.1:99]

        B       = (slave_max/(master_max^n)) - (master_max/(master_max^n))*A;
        Y       = A.*X + B.*X.^n;
        dY      = diff(Y);
        dX      = diff(X);
        gain    = dY./dX;

        if  (   gain(focus_region)     < slave_max/master_max + margin       ,...
             && gain(focus_region)     > slave_max/master_max - margin       ,...
             && gain(slave_max)        < max_allowable_gain                  ,...
             && gain(slave_max)        > max_allowable_gain - max_gain_margin )

                A_value(end+1)= A;
                B_value(end+1)= B;
                n_value(end+1)= n;
         end
    end
```

Case study: Care robot application

In order to explain and evaluate the methodology for variable rotational scaling design a case study is performed about a care robot application.

Due to the aging population in the Netherlands a two-sided societal problem occurs; on one side a growing need for health care and on the other side a reduced labor force capable of providing the care needed; i.e. shortage in the labor market. To fill the gap on the labor market a teleoperated assistive care robot can be used. An example of an assistive care robot is the Semi-Autonomous Care Robot (SACRo). The SACRo remotely assists elderly during daily live activities. Heemskerk Innovative Technology (HIT) in cooperation with PAL robotics is developing the SACRo. Elderly have problems with performing ADL's on their own due to the physical limitations caused by the aging process. With the assistance of the care robot elderly can live independently for a longer period and increase therefore their quality of their daily living. The main goal of the SACRo project is therefore to assist elderly with their activities in daily life (ADL), such as setting the table (Heemskerk Innovative Technology, 2017).

The care robot assists elderly at their home semi-autonomously from a remote care center (Fig 26). This means that the slave is controlled using haptic telemanipulations in combination with autonomy, i.e., the robot acts autonomous while the human operator is still involving during hard tasks by taking over control. Due to this structure the operator is able to manipulate several slaves at different locations from one remote care center. Hereby the shortage on the labor market issue can be solved cost-efficiently.

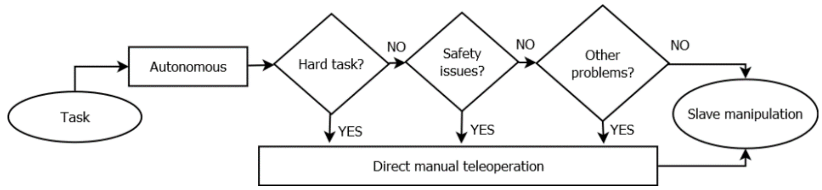

Fig 26: A flow chart of the principle of the semi-autonomous control for the care robot. Where can be seen that the slave performs autonomously if the task is not too hard and no safety or other issues occur. Whenever, one of those points can be answered with yes an operator takes over control by direct manual teleoperation.

i) Task and telemanipulator characteristics

Task characteristics

The care robot needs to assist patients in a high variety of assistance tasks, from setting the table to assisting elderly to the toilet. During telemanipulations in the care robot application it is essential that the manipulations are performed accurately, since the robot acts in a domestic and vulnerable environment. Therefore, the accuracy is a primary requirement and speed is a secondary requirement during the care application.

For further analysis on the task characteristics a typical and representative benchmark task was determined to be analyzed more detailed. The study of Van Hee et al. (2015) was used to determine a typical and representative task. Van Hee et al. (2015) performed a questionnaire in healthcare homes to determine the ADLs by which elderly needs assistance. The meal task appeared to be a frequent and representative task for assistance of the care robot.

For determining the probability distribution of rotational amplitudes, a kinematic task analysis was performed on the meal assistance task. A general test scene was chosen based on real settings in real-life health care homes, based on Thebe (Breda) and Siza (Arnhem). In Fig 32 the used gripper, furniture and objects are shown on which the kinematic analysis was performed. The meal assistance task was categorized in four subtasks:

- setting the table
- preparing drinks
- preparing food
- cleaning the table

All absolute rotations of the end-effector were determined during the meal assistance task and categorized into bins of 30 degrees. In Table 12 the results of the kinematic task analysis are shown. In Fig 27 the distribution of the rotational amplitudes during the meal assistance task is shown. A left skewed distribution was detected with a maximal rotational amplitude of 180 degrees. As focus region, at least 90 percent of all rotations should be included, which means that the focus region is from 0 to 90 degrees.

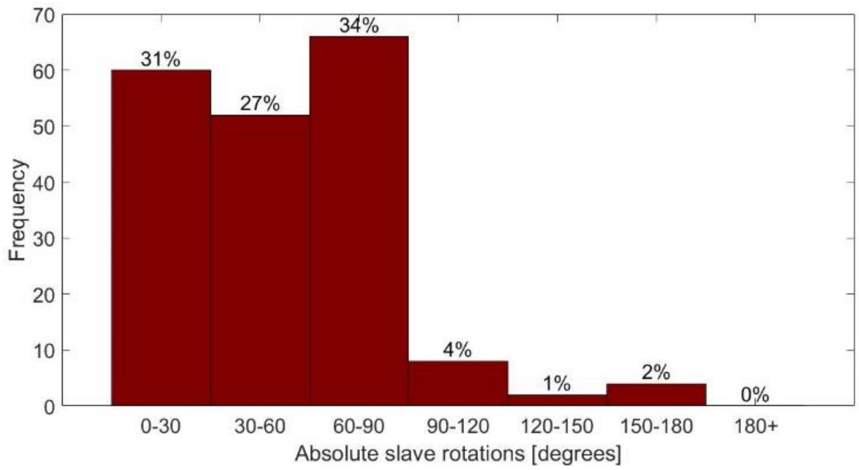

Fig 27: The probability distribution of the rotational amplitudes during the meal assistance task. It can be seen that most rotations take place at the first half of the master workspace (92%).

Further, a small experiment (N=3) was performed to determine the maximal allowable gain while performing an accurate task. A rotational target width of 1 degree was chosen in this study as an accurate task. The experimental setup was similar to the setup of the real experiment, described more detailed in appendix 2. The instruction was to keep the end-effector within the target boundaries for two seconds. During this experiment the constant gain was increased by steps of 1, starting with a constant gain of 4. Whenever the operator was able to perform the task the gain was increased by 1. This was continued until the operator was not able to perform the task. All participants were able to succeed the task with a gain of 15, however with a higher gain than 15 only one participant was able to succeed the task (maximal gain of 16). Therefore, it was concluded that a gain of 15 is the maximal allowable gain at which the operator can perform accurate tasks in this specific setup.

Telemanipulator characteristics

In the care application, the Saptic, developed by TU Delft and HIT, was used as the haptic master device (Lambert, 2013). The Saptic is a 7 DoF parallel haptic master with a rotational workspace of 45 degrees in all directions (Fig 28).

The Take It And Go (Tiago) robot, developed by PAL Robotics, is used as the mobile manipulator service robot. The Ulna arm is mounted on the spine of the care robot (PAL Robotics, 2014). The Ulna arm is a 7 DoF robotic arm and used as the slave in the care application (Fig 29). The rotational workspace of the Ulna robotic arm (270 degrees) is larger than the maximal required rotation during the task (180 degrees) (Fig 27) (PAL Robotics, 2014). Therefore, the workspace mismatch ratio is determined based on the maximal task rotation and not on the slave workspace.

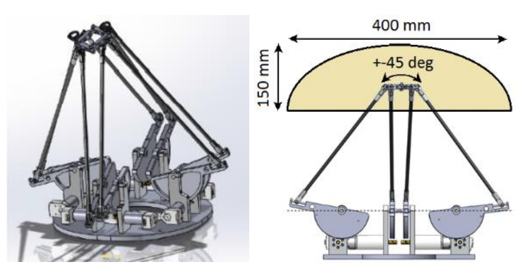

Fig 28: The Saptic parallel haptic master, with a limited workspace (45 degrees)

Fig 29: On the left and the TIAGO service slave robot. And on the right the ulna arm with a workspace of 270 degrees.

ii) Design constraints

Based on the gathered information the design constraints are defined. A complete overview of the design constraints for the care application are shown in Table 2, with a workspace mismatch ratio of 4, the focus region between 0 and 90 degrees, and the maximal allowable gain of 15.

Table 11

Design constraints care application

1.	$(\theta_m(\min)\,;\theta_s(\min)) = (0\ ;\ 0)$	Nulling compliance
2.	$\frac{\theta_{task}(max)}{\theta_m(max)} = \frac{180}{45} = 4$	Workspace mismatch ratio
3.	$90\%\ of\ frequency\ distribution = 90\ degrees$	Focus region
4.	$\frac{d\theta_m\ (max)}{d\theta_s(max)} = 15$	Maximal allowable gain

iii) Variable scaling parameters

For the design in this study, the master and slave workspace are divided by two (master workspace = 22.5°, slave workspace = 90°). This is done in order to realize a master workspace which is physically not limited for the baseline method. Based on the design constraints the unknown parameters, A, B and n, of the variable gain workspace extension equation for the care application was solved with the fit function:

$$\theta_s = (2.5 + (5.1382e^{-10}) \cdot \theta_m^7) \cdot \theta_m$$

To evaluate the variable gain workspace extension method, it is compared with a baseline method:

$$\theta_s = (1) \cdot \theta_m$$

and a constant scaling method:

$$\theta_s = (4) \cdot \theta_m$$

In Fig 30 the rotations and the gains three different workspace extension methods are shown. Further, the distribution and the design constraints are illustrated.

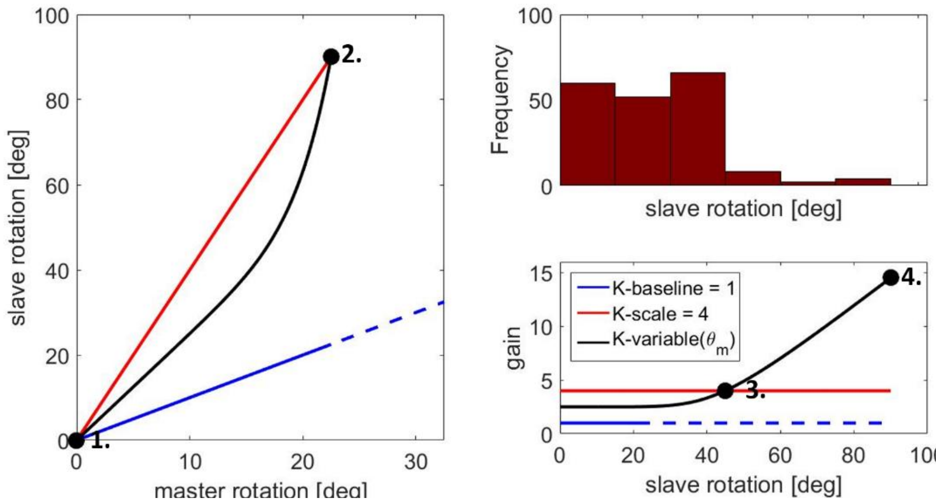

Fig 30: On the left, the slave position as function of the master position for the workspace extension methods. The dotted line shows a situation where the master workspace has no physical rotational limitations (baseline). On the right the probability distribution of amplitudes during the task on top and the gains for the different workspace extension methods on bottom as a function of the slave rotation. The numbers 1 to 4 represents the design constraints from Table 2; 1 = nulling compliance, 2 = master-slave ratio, 3 = edge of focus region, 4 = maximal allowable gain. It is possible to see that the variable gain at most occurring rotations is lower compared to the constant gain

Linearity of the variable gain

The non-linearity of the gain was calculated by the area between a linear line and the actual non-linear gain. The linear line is calculated for 5 degrees before and 5 degrees after the target rotation (Fig 31). In Fig 31 the non-linearity of the variable gain is shown, where the largest non-linearity takes place at 39 degrees. Furthermore, at small (<20 degrees) and large (>65 degrees) the variable gain approaches a linear function.

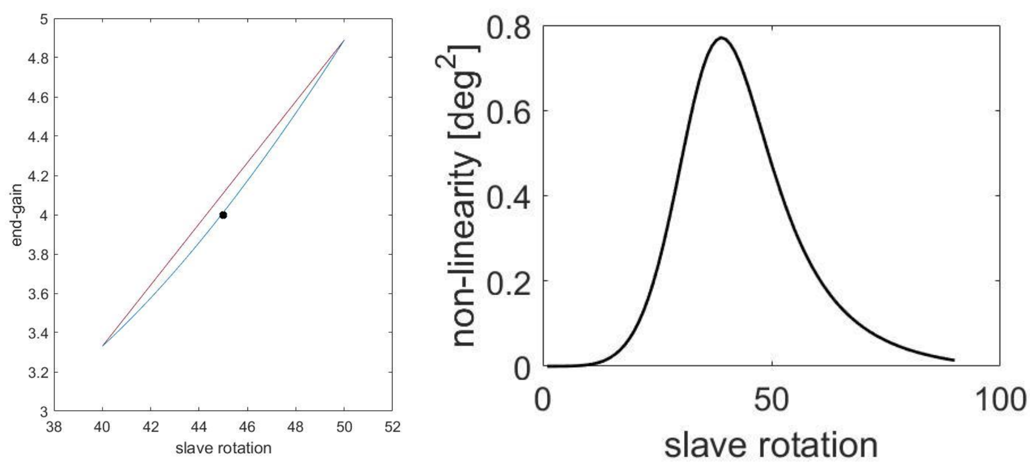

Fig 31: On the left an example of the calculation of the non-linearity, where the area is calculated between the linear red line and the non-linear blue line of the variable gain. This is done for 5 degrees before and after the task. And on the right the non-linearity of the variable scaling method. The non-linearity's are shown for all the rotations, where can be seen that the highest non-linearity's is at 40 degrees.

Kinematic task analysis

Fig 32: The used gripper, furniture and objects in the task analysis. Top left the end-effector and the initial orientation during the analysis. Further on the top the furniture in the care home is shown. And on the bottom line the objects which required manipulations during the meal assistance task are show.

Table 12: Kinematic task analysis					
		PITCH	**ROLL**	**YAW**	
		Rx	**Ry**	**Rz**	**Description**
Setting the table					
	Open kitchen cabinet	0	0	90	Grasp handle
		0	0	120	Open door
		0	0	-120	Back to initial position
	Pick placemat from kitchen cabinet	60	90	0	Pick placemat
		-60	0	0	Hold placemat during navigation
	Place placemat on table	60	0	0	Place placemat
		-60	-90	0	Back to initial position
	Pick plate from kitchen cabinet	30	90	0	Pick plate
		-30	0	0	Hold plate during navigation
	Place plate on placemat	30	0	0	Place plate
		-30	-90	0	Back to initial position
	Pick cup from kitchen cabinet	0	0	60	Pick cup
		0	0	-60	Hold cup during navigation
	Place cup on table above plate	0	180	30	Place cup
		0	-180	-30	Back to initial position
	Pick bread sack from kitchen cabinet	60	0	0	Pick bread
		-60	0	0	Hold bread during navigation

	Place bread sack on table	60	0	0	Place bread
		-60	0	0	Back to initial position
	Pick sprinkles package from kitchen cabinet	30	0	60	Pick sprinkles package
		-30	0	-60	Hold sprinkles package during navigation
	Place sprinkles package on table	30	0	0	Place sprinkles package
		-30	0	0	Back to initial position
	Close kitchen cabinet	0	0	90	Grasp handle
		0	0	-90	Close door
	Open drawer	90	90	0	Grasp handle
		-90	-90	0	Back to initial position
	Pick fork from drawer	90	0	0	Pick fork
		-90	0	0	Hold fork during navigation
	Place fork on the left of the plate	90	0	0	Place fork
		-90	0	0	Back to initial position
	Pick knife from drawer	90	0	0	Pick knife
		-90	0	0	Hold knife during navigation
	Place knife on the right of the plate	90	0	0	Place knife
		-90	0	0	Back to initial position
	Pick spoon from drawer	90	0	0	Pick spoon
		-90	0	0	Hold spoon during navigation
	Place spoon on top of the plate	90	90	0	Place spoon
		-90	-90	0	Back to initial position
	Close drawer	0	0	0	Push drawer
	Open fridge	0	0	90	Grasp handle
		0	150	0	Open door
		0	-150	0	Back to initial position
	Pick cheese package from fridge	30	0	60	Pick cheese package
		-30	0	-60	Hold cheese package during navigation
	Place cheese package on table	30	0	0	Place cheese package
		-30	0	0	Back to initial position
	Pick drink package from fridge	30	0	60	Pick drink package
		-30	0	-60	Hold drink package during navigation
	Place drink package on table	30	0	0	Place drink package
		-30	0	0	Back to initial position

	Close fridge	0	0	90	Grasp handle
		0	0	-90	Close door
Preparing drinks					
	Pick drink package from table	30	0	0	Pick drink package
		-30	0	60	Rotate to cup
	Pour cup (amount 1)	0	30	0	Pouring task (amount 1)
		0	-30	-60	Back to rest position
	Pour cup (amount 2)	0	60	0	Pouring task (amount 2)
		0	-60	-60	Back to rest position
	Pour cup (amount 3)	0	90	0	Pouring task (amount 3)
		0	-90	-60	Back to rest position
	Place drink package on table	-30	0	0	Place drink package
		30	0	0	Back to initial position
Preparing food					
	Open bread sack	60	0	0	Open bread sack
		-60	0	0	Back to initial position
	Pick slice of bread from bread sack	60	90	0	Pick slice of bread
		-60	0	0	Hold slice of bread during navigation
	Place bread on plate	60	0	0	Place slice of bread
		-60	-90	0	Back to initial position
	Close bread sack	60	0	0	Close bread sack
		-60	0	0	Back to initial position
	Pick sprinkles package from table	30	0	0	Pick sprinkles package
		-30	0	60	Rotate to plate
	Put sprinkles on bread (amount 1)	0	30	0	Pouring task (amount 1)
		0	-30	-60	Back to rest position
	Put sprinkles on bread (amount 2)	0	60	0	Pouring task (amount 2)
		0	-60	-60	Back to rest position
	Put sprinkles on bread (amount 3)	0	90	0	Pouring task (amount 3)
		0	-90	-60	Back to rest position
	Place sprinkles package on table	-30	0	0	Place sprinkles package
		30	0	0	Back to initial position
	Open cheese package	0	60	0	Pick package
		0	0	90	Open package

		0	-60	-90	Back to initial position
	Pick slice of cheese	30	60	0	Pick slice of cheese
		-30	0	0	Hold slice of cheese for navigation
	Put slice of cheese on bread	60	0	0	Place slice of cheese
		-60	-60	0	Back to initial position
	Close cheese package	0	90	90	Pick package
		0	0	-90	Close package
		0	-90	0	Back to initial position
Cleaning table					
	Open kitchen cabinet	0	0	90	Grasp handle
		0	0	-90	Open door
		0	0	0	Back to initial position
	Pick placemat from table	30	90	0	Pick placemat
		-30	0	0	Hold placemat during navigation
	Place placemat in kitchen cabinet	60	0	0	Place placemat
		-60	-90	0	Back to initial position
	Pick bread from table	60	0	0	Pick bread
		-60	0	0	Hold bread during navigation
	Place bread in kitchen cabinet	60	0	0	Place bread
		-60	0	0	Back to initial position
	Pick sprinkles package from table	30	0	0	Pick sprinkles package
		-30	0	0	Hold sprinkles package during navigation
	Place sprinkles package in kitchen cabinet	30	0	-60	Place sprinkles package
		-30	0	60	Back to initial position
	Close kitchen cabinet	0	0	90	Grasp handle
		0	0	-90	Close door
	Open fridge	0	0	90	Grasp handle
		0	0	120	Open door
		0	0	-120	Back to initial position
	Pick cheese package from table	30	0	0	Pick cheese package
		-30	0	0	Hold cheese package during navigation
	Place cheese package in fridge	30	0	120	Place cheese package
		-30	0	-120	Back to initial position
	Pick drink package from table	30	0	0	Pick drink package

		-30	0	0	Hold drink package during navigation
	Place drink package in fridge	30	0	60	Place drink package
		-30	0	-60	Back to initial position
	Close fridge	0	0	90	Grasp handle
		0	0	-90	Close door
	Open dishwasher	90	90	0	Grasp handle
		-90	0	0	Open door
		0	-90	0	Back to initial position
	Pick plate from table	30	90	0	Pick plate
		-30	0	0	Hold plate during navigation
	Place plate in dishwasher	-30	-120	30	Place plate in dishwasher
		30	120	-30	Back to initial position
	Pick fork from table	90	0	0	Pick fork
		-90	0	0	Hold fork during navigation
	Place fork in dishwasher	30	0	0	Place fork
		-30	0	0	Back to initial position
	Pick knife from table	90	0	0	Pick knife
		-90	0	0	Hold knife during navigation
	Place knife in dishwasher	30	0	0	Place knife
		-30	0	0	Back to initial position
	Pick spoon from table	90	90	0	Pick spoon
		-90	-90	0	Hold spoon during navigation
	Place spoon in dishwasher	30	0	0	Place spoon
		-30	0	0	Back to initial position
	Pick cup from table	0	0	30	Pick cup
		0	0	-30	Hold cup during navigation
	Place cup in dishwasher	0	180	0	Place cup
		0	-180	0	Back to initial position
	Close dishwasher	0	90	0	Grasp handle
		90	0	0	Close door
		-90	-90	0	Back to initial position

Appendix 2: Experimental setup

In the majority of the experiments about workspace extension during telemanipulations the task is performed in a virtual environment, such as in Casiez et al. (2007), Conti & Khatib (2005), Voskuil (2015), Dominjon et al. (2006) and Accot & Zhai (2001). The use of a virtual environment reduces the noise of the measurements. However, in virtual environments there are made assumptions and simplifications to describe the real world, which makes the experimental results more difficult to apply in real applications. Therefore, this study is conducted with a real slave robot such that the results of this study can be extrapolated to real applications more easily.

The telemanipulation systems used in the experiment consists of five components, namely the operator, the master, the controller, the slave and the remote environment (Fig 33 and Fig 34). The slave manipulates the remote environment according to (scaled) commands of the operator to the master. And the master applies haptic feedback to the operator from the remote environment. The controller manages the bilateral information flow, positions and forces, between master and the slave. The controller consisted of a position-position control architecture. The participant, i.e. the operator, was located without direct visuals on the slave. The operator had contact with the slave and the remote environment via video and force feedback. The camera was located straight above the rotating point of the slave. With the camera images the operator was able to see the end-effector and the targets in the remote environment on the cockpit screen (Fig 40). The remote environment, in which the slave performed its free air motions, existed of a printed map with different rotational tasks on it. The map was located directly below the slave. The experiment was performed with The Geomagic touch as the master and the 7 DoF Ulna robotic arm was used as the slave (PAL robotics, 2014).

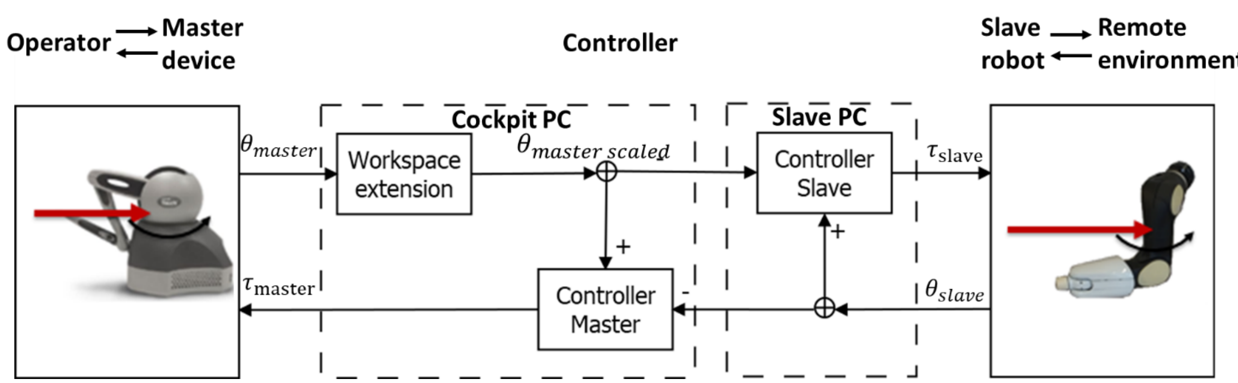

Fig 33: The five components of a telemanipulation system. The slave interacts with the remote environment according to (scaled) inputs of the master side, while the master device force feedback to the operator from the slave side. The controller manages the information flow and consists of a workspace extension method and a position-position controller architecture. In this experiment the controller and the workspace extension method at the cockpit pc were modified. The symbols θ and τ refer to the rotations and torques respectively.

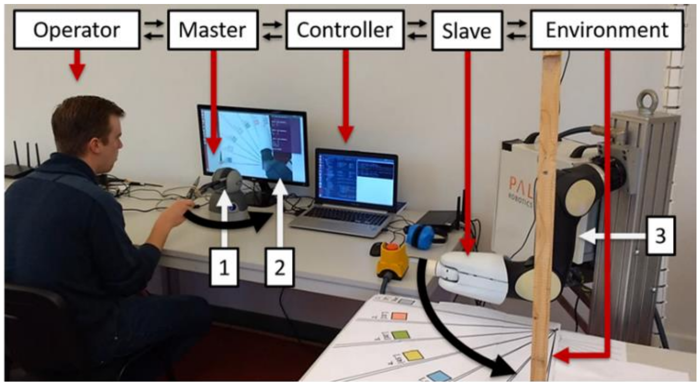

Fig 34: Experimental setup. The operator rotates the slave joint (3) in the remote environment by rotating the master joint (1). The controller manages the information flow between master and slave. The operator receives visual feedback from the remote environment on the cockpit screen (2).

As a robotics middleware, between the different hardware devices, Robot Operating System (ROS) was used. ROS is a collection of software frameworks which provides libraries and tools for robot applications (Giang, 2017). The controller ran on an Ubuntu 14.4 PC. In Fig 35 it is possible to see the different nodes communicating together during the experiment. Central in this this figure is the controller node. This node manages and manipulates the in- and outcoming signals from the master and slave device. Further the feedback - and the camera node provide input to the graphical user interface (GUI) node in order to provide visual task feedback to the operator on the cockpit screen. Finally, the recorder node is used to record the data during the experiment for post experimental analysis. In the following sections the hard and software are described more detailed.

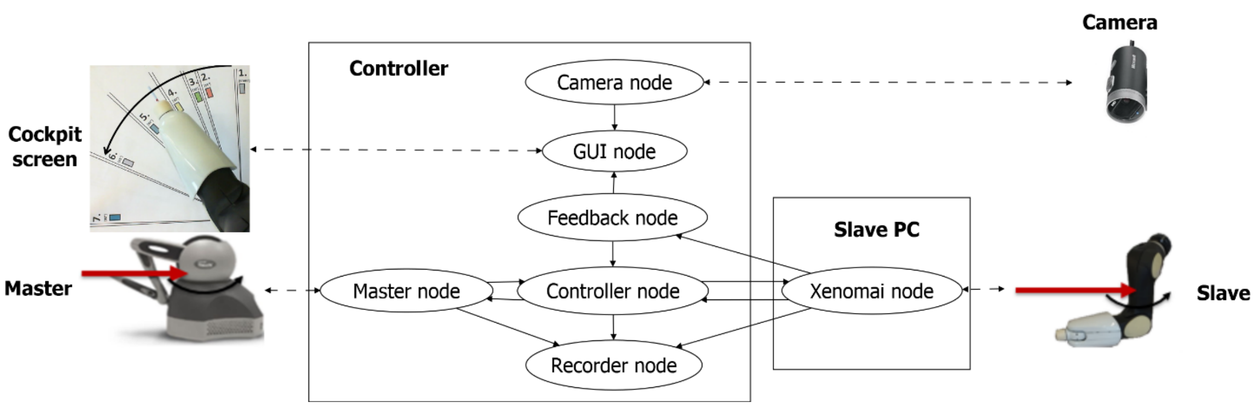

Fig 35: Hardware and software structure of the experimental setup. The master nodes receive orientations from the master and sends force towards the master. Further, the controller node manages the information flow between master and slave and includes the PD-controller for force feedback and the workspace extension method. The Xenomai node manages the in- and outcoming signals of the slave. Further, the feedback node, GUI node and Camera node are providing the operator from feedback. Finally, the recorder node records the required data for post experiment analysis.

Master

The Geomagic touch, developed by 3D systems, is used as the master device (3D systems, 2013). The Geomagic touch is a midrange professional haptic device (Fig 36). It is a motorized device that applies force feedback to the operators' hand, allowing to feel dynamics of the slave in the remote environment. This device can provide force feedback up to 3 Newton in all translational degrees of freedom. Since 1 DoF task was performed in the experiment only one joint of the master device was used, namely the so-called ball joint. The workspace of this joint is 110 degrees.

Fig 36: The Geomagic touch master device. The hand indicates the position of grip of the operator. The red arrow indicates the used ball joint and the black arrow indicates the rotational direction.

Slave

The 7 DoF Ulna robotic arm, developed at Pal robotics, was used as the slave during the experiment (PAL robotics, 2014). Joint 3 with a workspace of 195 degrees was controlled by the master ball joint (Fig 37). On the slave pc, there were running software controllers which were connected to the controller boards on the robotic arm. On top of the software controllers there were running hardware controllers on dedicated controller boards connected to the motor modules. At the slave side, no software adjustments were applied to the controllers, since this was proprietary of PAL Robotics: the slave was (only) connected with the controller PC with the use of ROS.

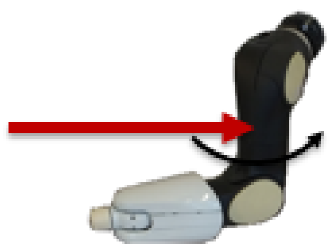

Fig 37: The ULNA robotic slave arm, with the red arrow indicating the used joint and the black arrow indicating the rotational direction.

Connectivity

The connection between controller pc and the master and slave was via an Ethernet cable. This configuration was chosen to limit the delay between the master and the slave. The input delay between master and slave was about 0.08 seconds. The system position precision is based on the specifications of the master and slave devices. The slave device had the lowest precision of 0.1 degree, and therefore the precision of the master slave system. This value is high enough to perform the experimental task (1 degree).

Controller

The controller node manages the information flow between the master and the slave (Fig 38). From the master node the controller node received the orientations of the master. The controller node transforms these master orientations according to the workspace extension method towards scaled master orientations and sent those values towards the slave (xenomai node). The workspace extension methods are described more detailed in appendix 1.

Furthermore, a position-position two channel controller architecture was used in order to provide haptic feedback. This controller uses both the position of the master and the slave, which were measured by servos. The controller uses both measured positions to calculate the difference (error) between the master and the slave. The master controller used a PD controller to minimize the difference in position between the master and the slave. The PD controller was such designed that it was a little bit underdamped in order to keep stability ($\zeta = 0.8$). On the basis of the human's physiological properties, Brooks 1990 stated that a force feedback signal should have a minimal bandwidth of 20-30 Hz for "meaningful perception". To be sure that this bandwidth was realized a theoretical cutoff frequency of 50 Hz was chosen. This value is chosen, however not critical since only free air motions are performed during the experiment. For designing the PD controller, a mass-spring system, was used to describe the master (3D systems, 2013). The PD gains were tuned with the closed loop transfer function, first order characteristic polynomial formula, the relative damping and cutoff-frequency (Astrom, 2002). For tuning the PD controller, the pidTuner function in Matlab was used. After tuning the PD gains a K_p of 144.7245 and K_d of 19.2482 were found (Fig 39). This values are multiplied by 3 in order to realize the right amplitude of the force, up to 2N. Further there was a force guiding the operator back to the initial start positon whenever the task was succeeded. This was realized with a simple PD controller towards the start position.

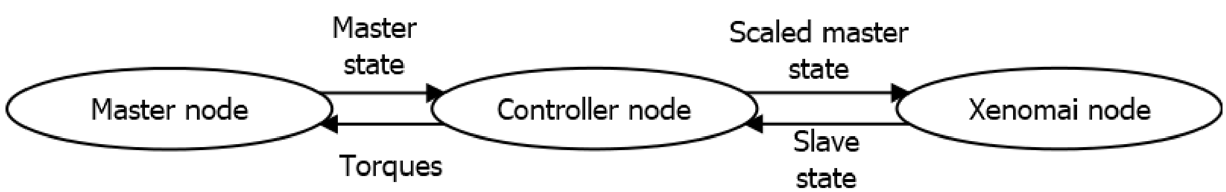

Fig 38: The information flow between the different nodes between the master and slave. The controller node sends information about the force feedback towards the master node and desired position of the slave to the Xenomai node. Further, the controller node receives information from the master about the commanded rotations and from the slave it receives information about the current state of the slave.

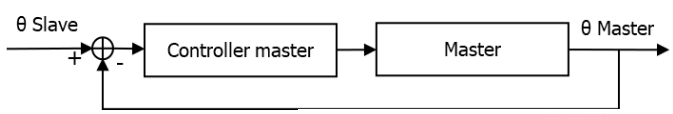

$$Master = \frac{1}{0.45s^2 + 3s}$$

$$Controller\ master = Kp + Kd\ s$$

$$\frac{X_m}{X_s} = \frac{Controller_{master} * Master}{1 + Controller_{master} * master}$$

$$\zeta = 0.8$$

$$Kd = 2 * \zeta * \sqrt{Kp}$$

$$Cut\ off\ frequency = 50\ Hz$$

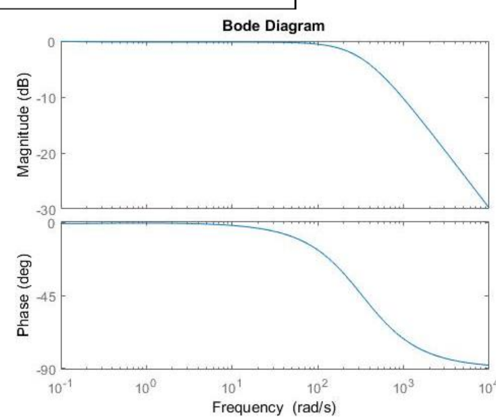

Fig 39: The feedback closed loop block diagram, with the master PD controller, the master, and the master and slave rotations. Further, the used formulas and the mass spring system to calculate the Kp and Kd values of the PD controller. Finally, the bode diagram after fine tuning the controller. In this diagram it can be seen that the theoretical cut off frequency lies at 50 Hz.

Task feedback

The task feedback provided to the operator by the cockpit screen consisted of visual feedback and the task state (Fig 40). The graphical user interface (GUI) node realizes the visual feedback by using the images of the USB camera from the camera node and the task state information from the feedback node.

The visual feedback was provided by a USB camera (Microsoft life cam cinema) located at the remote environment. The camera was located straight above the rotating point of the slave. The visual feedback showed the slave end-effector moving in the remote environment above the task map. The delay of the USB camera towards the cockpit screen was about 0.1 seconds. Besides the visual feedback of the USB camera the task state was showed on the cockpit screen. The task state consisted of the desired task and a progress bar. The desired task indicated the target rotations and were based on predefined random generated target sequences. The progress bar indicated the progress of the task; whenever the slave end-effector was within the target boundaries of the desired task the progress bar started filling. Whenever the task was completed the controller node received information that the task was finished and commanded the master to guide the operator back towards the start position with the use of force feedback. The task state information was provided by the feedback node which on its turn used the actual orientations of the slave from the xenomai node and the predefined desired task sequences (Fig 41).

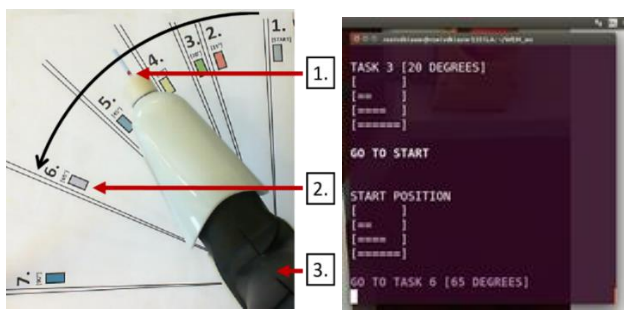

Fig 40: Visual feedback presented on the cockpit screen to the operator while performing the rotational pointing task on the left. With the slave arm, rotating around 3, above the map with rotational tasks. The goal was to rotate the reference point (1) within the boundaries of a desired target rotation (2). On the right the progress bar is shown, where it is possible to see the progress bar filling and the desired task is indicated (task 6, 65 degrees).

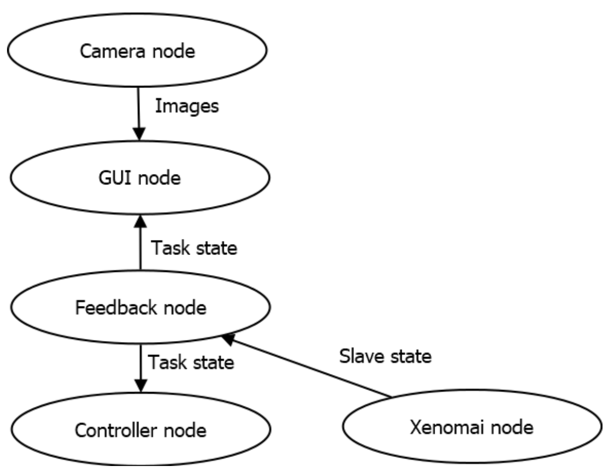

Fig 41: The information flow between the different nodes for the task feedback. The GUI node receives information about the task state from the feedback node and images from the camera node from the remote environment. The feedback node defines the task state by gathering information from the Xenomai node.

Recorder

The data was recorded at 1 kHz. The recording was done with the use of the ROS bag function (ROS, 2015). This is a set of tools for recording and playing back ROS topics. The recorder node uses information from the master node, controller node and the xenomai node (Fig 42).

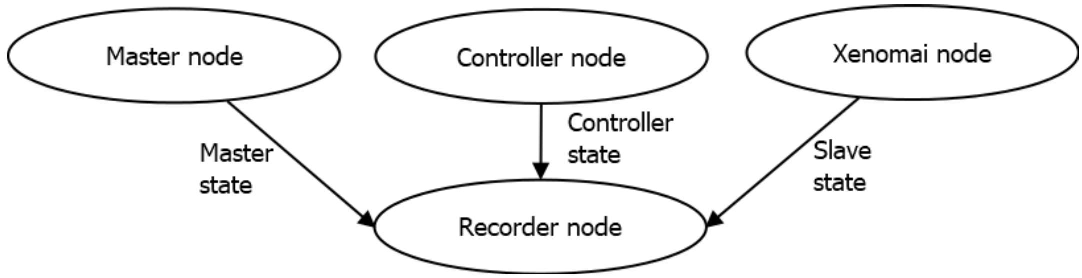

Fig 42: The information flow between the different nodes for the recorder node. The recorder node records topics from the master node, controller node and the xenomai node in order to analyze the data after the experiment.

Short guideline to run setup

In order to run the setup, the following steps must be fulfilled.

Setup PCs and hardware

1) Connect the Geomagic touch and the Robot PC to the Controller PC with Ethernet cables
2) Connect the USB camera with the Controller PC via the USB port.
3) Turn on the Controller PC, the Robot PC and the Geomagic touch master device

Connect with master

1) Open terminal (press alt+ctr+t)
2) Go to Geomagic Touch folder ($cd /opt/geomagic_touch_device_drivers)
3) Run Geomagic Touch setup ($./Geomagic_Touch_Setup)
4) Pair the Master and the Controller PC (click on the pairing button)
5) Pair the Master and the Controller PC (press the Pair button at the back of the Geomagic Touch device)

Master verification and calibration

1) Open terminal (press alt+ctr+t)
2) Go to Geomagic Touch folder ($cd /opt /geomagic_touch_device_drivers)
3) Run Geomagic Touch diagnostics ($./Geomagic_Touch_Diagnostics)
4) The Geomagic touch diagnostic application will open and the verification and calibration starts

Connect with slave

1) Connect to ROSE-WIFI
2) Open internet browser
3) Go to web interface (/anaconda-2c:8080)
4) Check if booted correctly (1. Dianostics tab)
5) Go to control modes (7. Control modes tab)
6) Change to position control (Change to Position control tab)

Launch file

1) Open terminal (press alt+ctr+t)
2) Go to launch file folder ($cd /home/WEM_ws/src/scaling_marco_arm/launch)
3) Open launch file ($gedit experiment_jc.launch*)*
4) Change setting of the setup

- seq_number – Randomized sequence
  (0 = Training sequence, 1-3 = experimental sequences)
- gain – The different workspace extension methods
  (0 = variable, 1 = baseline, 2 = training, 4 = constant)

Launch setup

1) Open terminal 1 (press alt+ctr+t)
2) Launch setup ($roslaunch scaling_marco_arm experiment_jc.launch)
3) Open terminal 2 (press alt+ctr+t)
4) Run task feedback node ($rosrun scaling_marco_arm listener_task_jc)
5) Couple/decouple master and slave (Press light gray button on the Geomagic Touch)
6) Activate/deactivate force feedback (Press dark gray button on the Geomagic Touch)

Close setup

1) Deactivate force feedback (Press dark gray button on the Geomagic Touch)
2) Decouple master and slave (Press light gray button on the Geomagic Touch)
3) Shutdown Geomagic touch and Robot PC

Appendix 3: Pilot studies, protocol and metrics

Before performing the real experiment two pilot studies were performed. The goal of the pilot studies was to test the feasibly of the experiment and to improve were necessary. This was done based on the data and the feedback from the participants. In the following sections, short descriptions, plots, conclusions and recommendations of the two pilot studies are presented. No interferential statistics were performed with the collected data, since it is hard to draw conclusions form a small number of participants. Instead the data was analyzed by eye. The instructions for the pointing task were the same for the real experiment as for the two pilot studies, namely to move towards a target presented at the cockpit screen as fast as possible while emphasizing accuracy rather than speed. A more detailed description of the instructions is provided in appendix 5. The experimental setup used in the pilot studies was also the same as in the real experiment for the two pilots and described more detailed in appendix 2. Furthermore, the metrics and protocol are described in full detail in the following sections.

Pilot study one

The main goal of the first pilot study was to test if the human operators were able to perform and understand the experimental task and setup. Further the goal was to see how the human operators perform with a simple linear variable scaling method. Finally, with the data of this pilot study the metrics and the protocol were defined. A summary of the first pilot study is shown in Table 13 and Fig 43.

Table 13

Summary pilot study one

Master	Geomagic touch (ball joint)
Slave	Ulna (joint 3)
Teleoperation	Bilateral
Task	Fitts based 1 DoF rotational pointing task
Amplitude (α)	15, 20, 30, 45, 65, 90 degrees
Target width (ω)	1 degrees
Index of Difficulty	4.0, 4.4, 5.0, 5.5, 6.0, 6.5 bits
Conditions	Constant scaling (1, 4) and linear variable scaling
Variable scaling	$\theta_{slave} = (1 + (0.1333)\theta_{master})\theta_{master}$
Instruction	As fast as possible, while emphasizing accuracy rather than speed
Metrics	Time [sec], Reversal rate, Overshoot, Van der Laan questionnaire
Group size	4 participants
Repetitions	10 repetitions per task

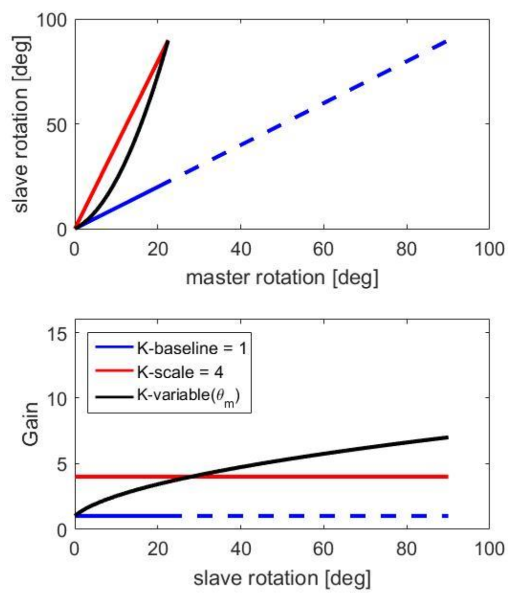

Fig 43: The used scaling methods, baseline, constant and simple variable scaling method. On top the slave rotation versus the master rotation. The dotted line shows a situation where the master workspace has no physical rotational limitations (baseline). And on the bottom the gain versus the slave rotation. Here can be seen that the baseline and constant scaling have a constant gain, while the variable scaling method varies over the rotations.

Raw data

In Fig 44 and Fig 45 samples of the raw data are shown from the first pilot study. In Fig 44 the orientations of the master and slave are shown while performing the experiment with a constant scaling method (k=4). Further, in Fig 45 the time traces of separate trials are shown for one participant for the three different extension methods for small rotations (15 degrees) and large rotations (90 degrees).

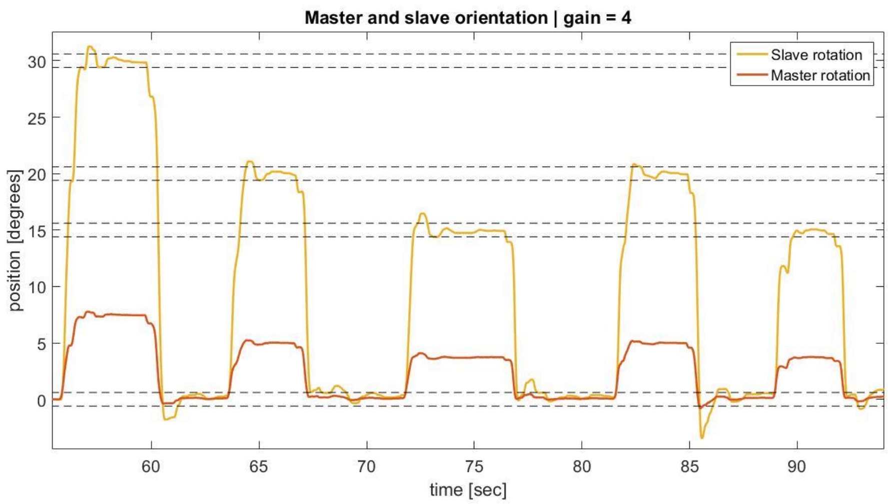

Fig 44: Master and slave orientation in the same graph for a small-time sample, while performing the pilot study with a constant scaling factor of four. In this graph the influence of the gain can be seen clearly, where the master makes smaller rotations than the slave.

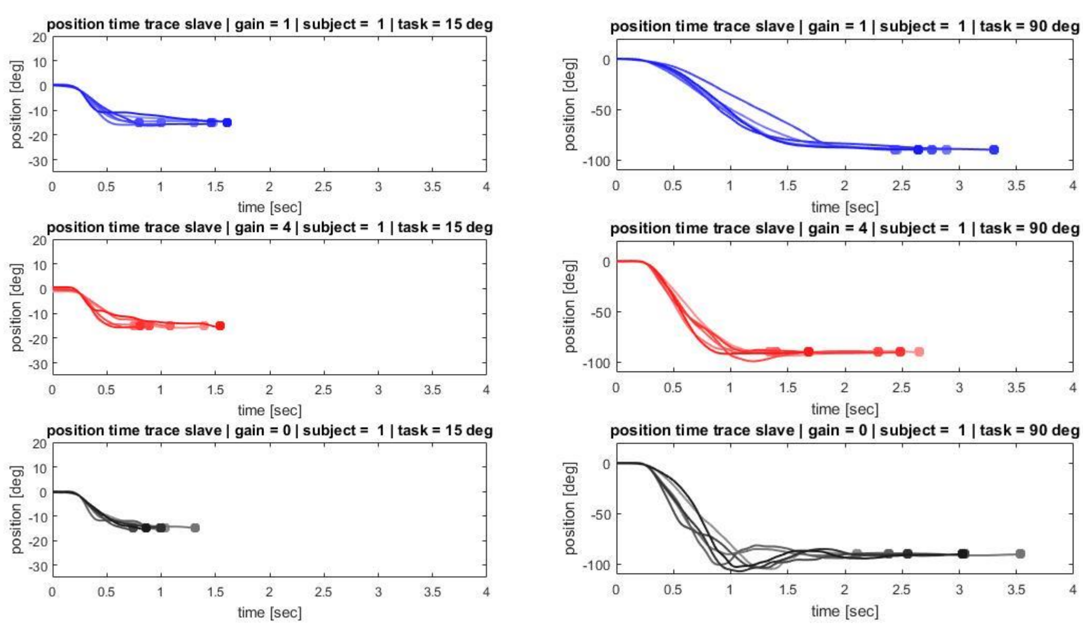

Fig 45: On the left a typical slave output of a small rotational task (15 deg) and on the right a large rotational task (90°) for the three different scaling methods; baseline (blue), constant scaling (red) and variable scaling (black). The darkness of the lines increases with each trial. The different approaching strategies can be seen for the three methods.

Protocol

For defining the protocol, it is required to determine the learning curve for the different scaling methods. For determining the learning curve of the different extension methods the mean time of the trials are exponentially fitted ($y = a + b\ e^{-x}$). Based on the fitted learning curve (Fig 46) it can be concluded that four trials are required to reach the steady state of the learning curve for all the workspace extension methods. Although, it needs to be mentioned that the variable scaling design is not at the same form as used in the real experiment. Based on these results the protocol starts with four training trials followed by six trials for measurements. For the familiarization session five trials are chosen in order to be sure that all participants were trained enough (Fig 47).

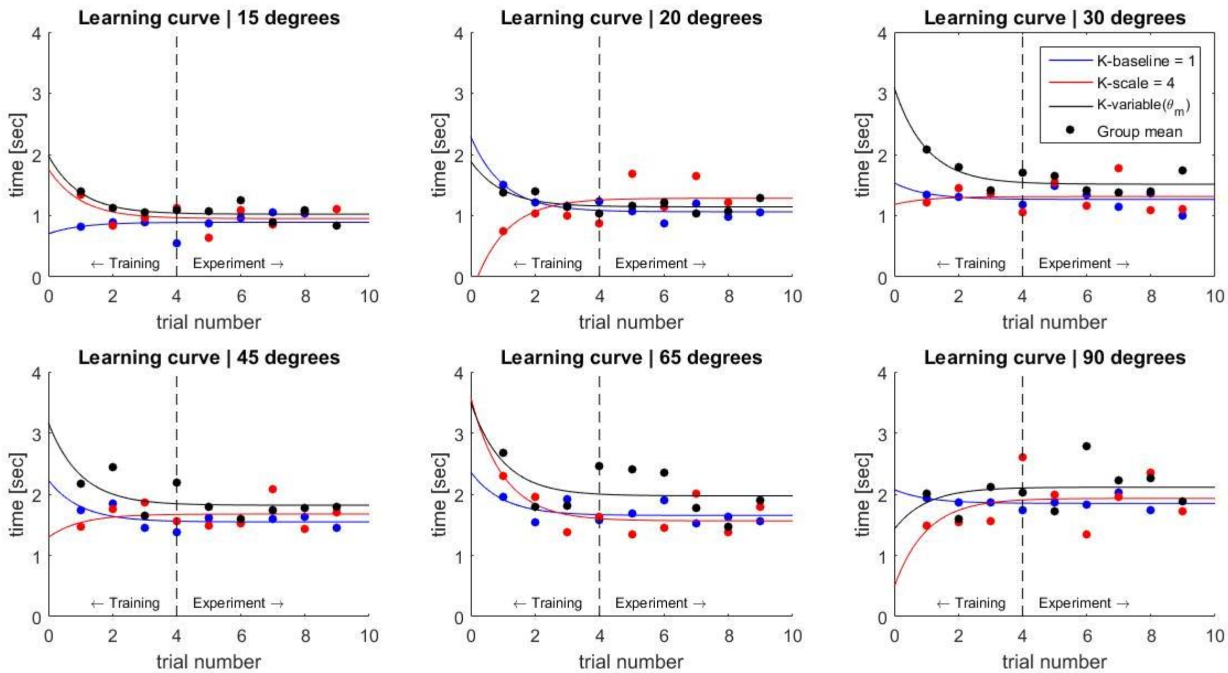

Fig 46: Fitted learning plots for the different workspace extension methods for all the tasks. In the graphs it can be seen that for all the methods and for all the rotations the learning curve reaches its steady state after four repetitions, which is presented in the graphs as a dotted line.

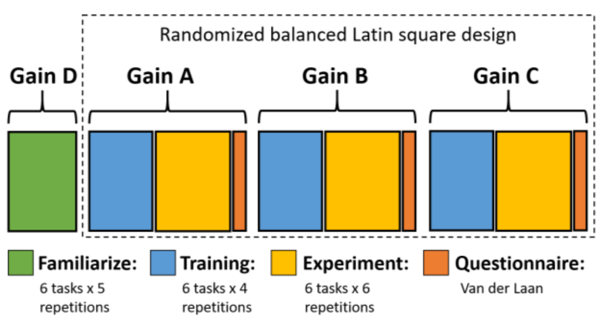

Fig 47: Protocol of the experiment for one participant. Starting with familiarization of the setup with Gain D (k=2). Followed by the experiment with the three-experimental condition (randomized). Each condition started with a training of 4 repetitions, followed by 6 measured repetitions and the Van der Laan questionnaire.

Metrics

Overshoot

The positioning task can be divided into two subtasks, namely gross positioning and fine positioning (MacKenzie, 1995). Gross positioning is getting to the vicinity of the target and fine positioning is the final acquisition of the movement. There are different strategies to complete a pointing task in terms of overshoot (Casiez et al., 2007). The optimal strategy is gross positioning without under- or overshoot. This strategy is optimal but not realistic, because there is always some over- or undershoot. The second strategy is gross positioning with undershoot. And the final strategy is gross positioning with overshoot (Fig 48).

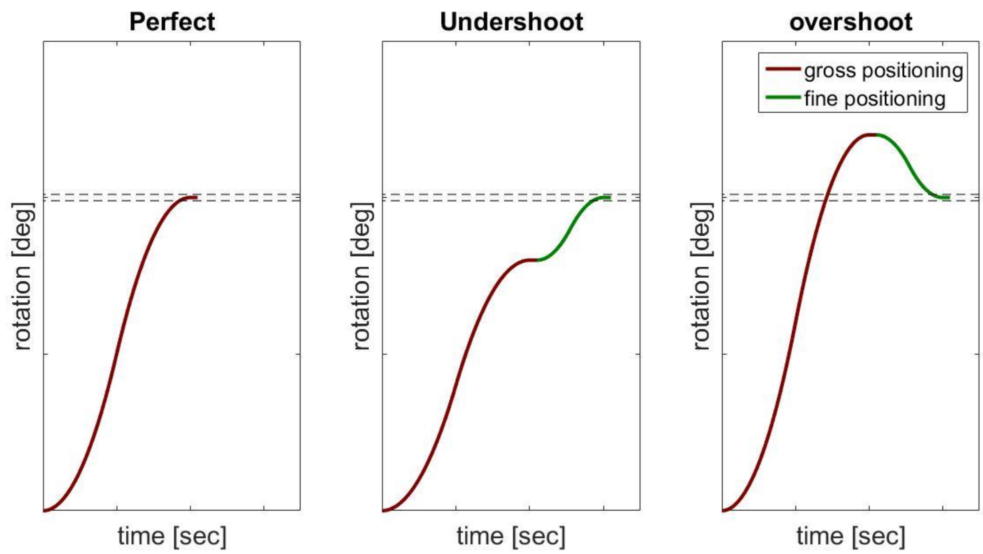

Fig 48: Different strategies to perform ballistic movements (adapted from Meyer et al., 1988). With the corrective phases, or in this study called the overshoot phases. In the left graph a perfect situation is shown, i.e. no overshoot, in the middle graph a situation with undershoot and in the right graph a situation with overshoot. The last to graphs require corrective movements.

To determine the overshoot during the pilot study the slave rotations beyond than the desired target rotation of the slave were measured. This was determined with the use of the following code:

```
overshoot_task = ((target_task_deg) - (actual_slave_deg));
if(overshoot_task > 0)
    overshoot_task = 0;
else
    overshoot_task = overshoot_task;
end
```

The results of the pilot study are shown in Fig 49. In these plots, it can be seen that the mean overshoot is limited (< 3 degrees). Based on the raw data the overshoot mostly occurred during the last final acquisition. Further, no large differences were found between the different workspace extension methods. The data suggest that the strategy with undershoot is used by the operators. This suggestion can be confirmed regarding the data of the time traces. This means that (the majority) of the tasks is performed with the undershoot strategy. Which is important to know for defining the metrics for fine and gross positioning.

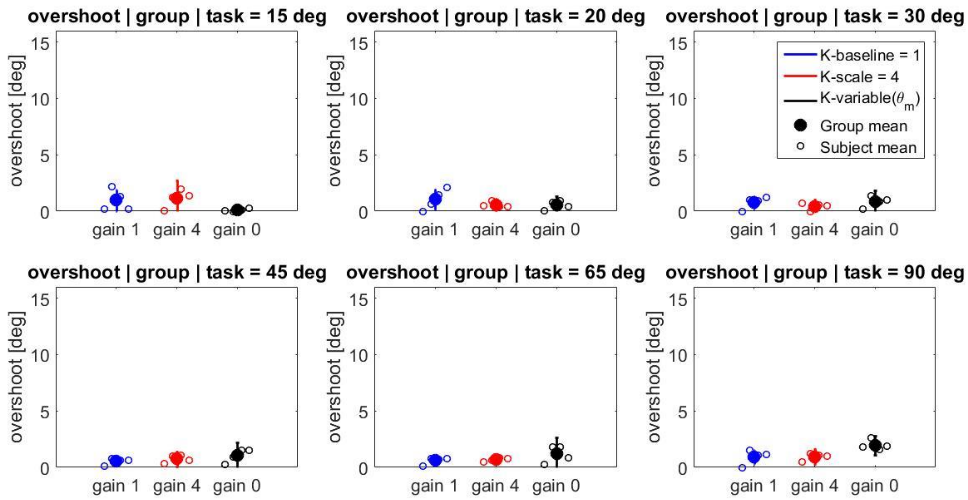

Fig 49: Mean overshoot plot for the different workspace extension methods for the different rotational tasks. In these graphs it can be seen that there is little overshoot during the tasks, further no large differences were detected between the control methods. This suggest that the operator uses an undershoot approach.

Positioning time

In order to define the fine and gross positioning metrics it is important to determine which strategy (undershoot or overshoot) is used during the experiment. Based on the results of the overshoot metric is was concluded that the majority of the tasks is performed with the undershoot strategy. Based on this the fine positioning metric is defined as the last 5 degrees before the target rotation. The value of 5 degrees was subjectively chosen based on the raw time traces (positions and velocities). So, whenever the slave end-effector crosses the target rotation minus 5 degrees the fine positioning starts and the gross positioning stops (Fig 50). This was determined with the use of the following code:

```
if (actual_slave_deg < (target_task_deg - 5));
    gross_positioning_time = actual_time - start_time;
end

fine_positioning_time = total_positioning_time - gross_positioning_time;
```

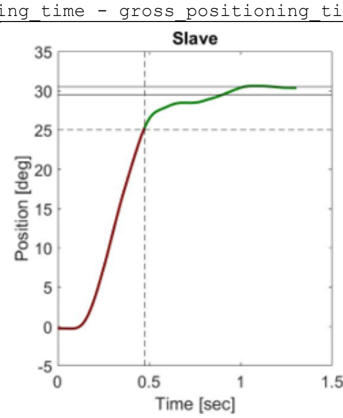

Fig 50: Gross and fine positioning shown for a typical trial. the slave output orientation as a function of time, where the gross positioning ends and the fine positioning starts at 5° before the target rotation (30°). The vertical and horizontal dotted line separate the fine and gross positioning. Further, is shown between the horizontal black lines.

When applying the positioning time metrics to the pilot study data the plots in Fig 52 for fine, gross and total positioning time can be found. The shapes of the plots are as expected according to the model of Fitts (Fitts, 1954):

$$T = a + b \cdot ID$$

$$ID = \log_2\left(\frac{\alpha}{\omega} + 1\right)$$

During the experiment the alpha (rotational task) varied and the omega (target width) was constant. Based on Fitts' formula a logarithmic shape for the total and gross positioning task was expected. Furthermore, a constant flat shape for the fine positioning was expected (Fig 51). The expectations can be confirmed with the data of the constant gain (Fig 52). Regarding the influence of the gain it was expected that a high gain causes improved performance for gross positioning and decreased performance for fine positioning. And a low gain causes improved performance for fine positioning and decreased performance for gross positioning (Jellinek & Card, 1990). The results in Fig 52 confirm these expectations. The pilot results suggest that the metrics for fine and gross positioning time were chosen correctly.

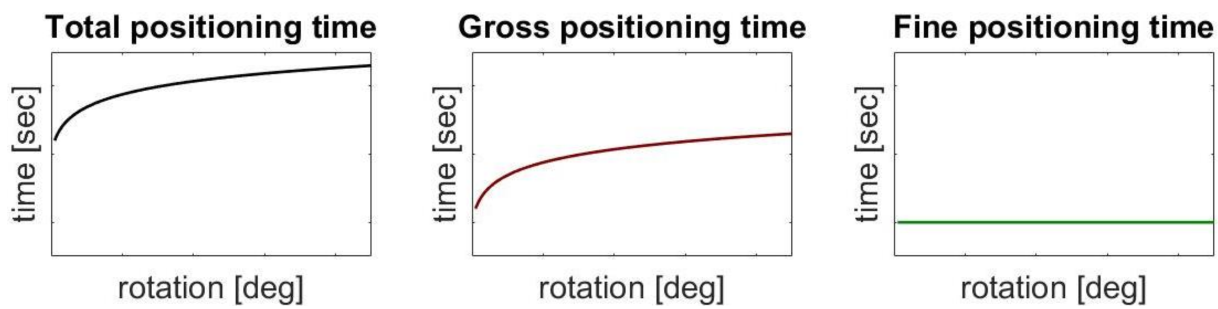

Fig 51: Predictions of the fine, gross and total positioning task according to Fitts' law. Based on the formula of Fitts and the task descriptions a logarithmic shape is expected for the total and gross positioning time and for fine positioning time a flat line is expected.

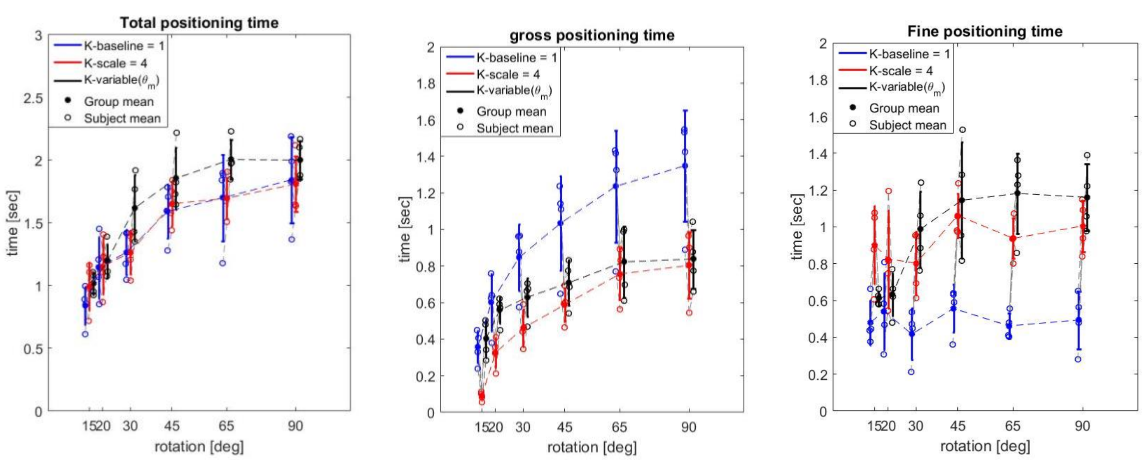

Fig 52: Total, gross and fine positioning time as a function of the different rotational tasks for all the different extension methods. For total positioning time similar results can be seen between the baseline and constant scaling, further the variable scaling has a higher total time. For gross positioning, it can be seen that the baseline method has a higher time compared to the constant and variable scaling method. Finally, for fine positioning the baseline method performs best in terms of time compared to the constant and variable scaling method.

Reversal rate

The reversal rate is the amount of reversals of the operator during the task at the master side. Based on literature the amount of reversals is an estimation of the control effort of the operator (MacDonald & Hoffmann, 1980). The reversal rate was calculated by counting the amount of zero crossings of the master velocity (Fig 53). This was determined with the use of the following code:

```
if (actual_master_vel>0 && previous_master_vel<0) || (actual_master_vel<0 && previous_master_vel>0)
      reversal_rate = reversal_rate + 1;
end
```

In Fig 53 a typical trial is shown with the reversals at the end of the task. And in Fig 54 the results of the reversal rate during the pilot study is shown.

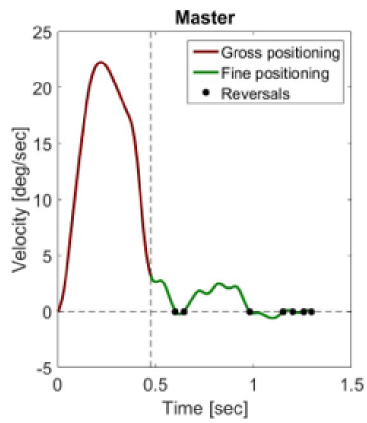

Fig 53: Master velocity during a typical trial. The master input velocity as function of time, where gross positioning requires a relative high velocity and fine positioning a low velocity. The black dots showing the reversals. The vertical dotted line represents the null velocity line, for counting the reversals. And the vertical dotted line separates the fine and gross positioning task.

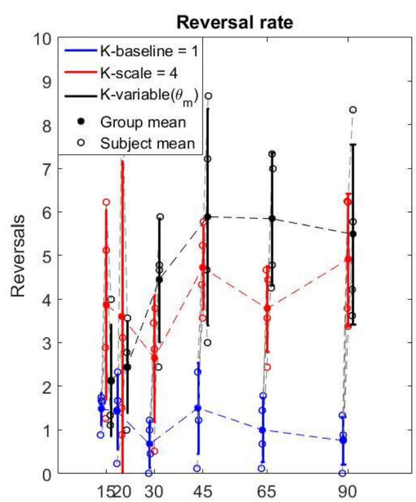

Fig 54: Reversal rate for the different extension methods as a function of the rotational amplitudes. In this plot it can be seen that a low gain, i.e. baseline scaling, has the lowest amount of reversals compared to higher gains, i.e. constant and variable. Further, the variable increases for higher rotations, i.e. higher gains.

Van der Laan questionnaire

The van der Laan questionnaire, used as a subjective scale to measure the acceptance for the different workspace extension methods, was experienced by the participants as a good questionnaire. This questionnaire is showed in appendix 6. The data from the questionnaire was not analyzed in detail in this pilot study, since the data of four subjects will not say much.

Main recommendations and conclusions

Based on the first pilot study it can be concluded that human operators were able to understand and perform the pointing task with the provided setup and feedback at the cockpit screen. Besides, the task descriptions were clear to the operators in order to perform the task. Further, human operators were able to operate with a simple linear variable scaling method.

The exact definitions of the positioning metrics, fine and gross, were defined based on the pilot data. The results from this pilot study suggest that the metric definitions are valid, since the outcome are according to literature. Further, the reversal rate metric and the van der Laan questionnaire are looking valid for analyzing the control effort and acceptance respectively. The overshoot metric will not be used in following studies, since almost no overshoot took place while performing the experiment, caused by the undershoot strategy of the operators.

The results from this pilot study look positive. In the next pilot study a non-linear variable scaling design for the care application (see, appendix 1) will be implemented and tested. Further, in the next pilot study the robustness of the setup is tested.

Pilot study two

Main goal of the second pilot study was to evaluate the variable extension method designed according to the methodology presented in this study for the care application (appendix 1). One participant performed the experiment. A summary of the second pilot study is shown in Table 14 and Fig 55.

Table 14

Summary pilot study two

Master	Geomagic touch (ball joint)
Slave	Ulna (joint 3)
Teleoperation	Bilateral
Task	Fitts based 1 DoF rotational pointing task
Amplitude (α)	15, 20, 30, 45, 65, 90 degrees
Target width (ω)	1 degrees
Index of Difficulty	4.0, 4.4, 5.0, 5.5, 6.0, 6.5 bits
Conditions	Constant scaling 1, 4, non-linear variable scaling
Variable scaling	$\theta_{slave} = (2.5 + (5.1382e - 10)\theta_{master})\theta_{master}$
Instruction	As fast as possible, while emphasizing accuracy rather than speed
Metrics	Time (total, gross, fine) [sec], Reversal rate, Van der Laan questionnaire
Group size	1 participants
Repetitions	10 repetitions per task: 4 training and 6 for measurement

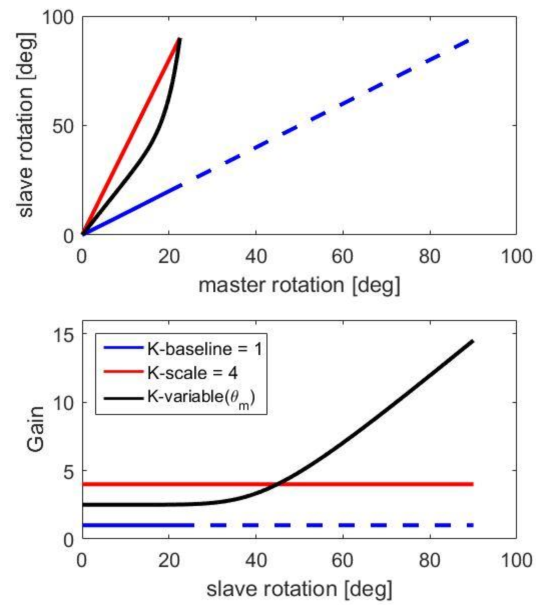

Fig 55: The used scaling methods, baseline, constant and designed variable scaling method for the care application. On top the slave rotation versus the master rotation. The dotted line shows a situation where the master workspace has no physical rotational limitations (baseline). And on the bottom the gain versus the slave rotation. Here can be seen that the baseline and constant scaling have a constant gain, while the variable scaling method varies over the rotations.

The time metrics and reversal rate metric are shown in Fig 56 and Fig 57. Based on the results of pilot study two it can be concluded that a human operator is able to perform the tasks with the designed variable workspace extension method, since all tasks were performed within a reasonable amount of time. The variable scaling method showed improved performance for the one participant on the smaller rotations for the variable scaling method compared to the constant scaling (Fig 56). This was expected since the variable extension method was designed to improve performance at small rotations (up to 45 degrees, see appendix 1). Similar results were found for both the pilot studies for the constant scaling methods, this means that the setup of the experiment is robust over time and over participants.

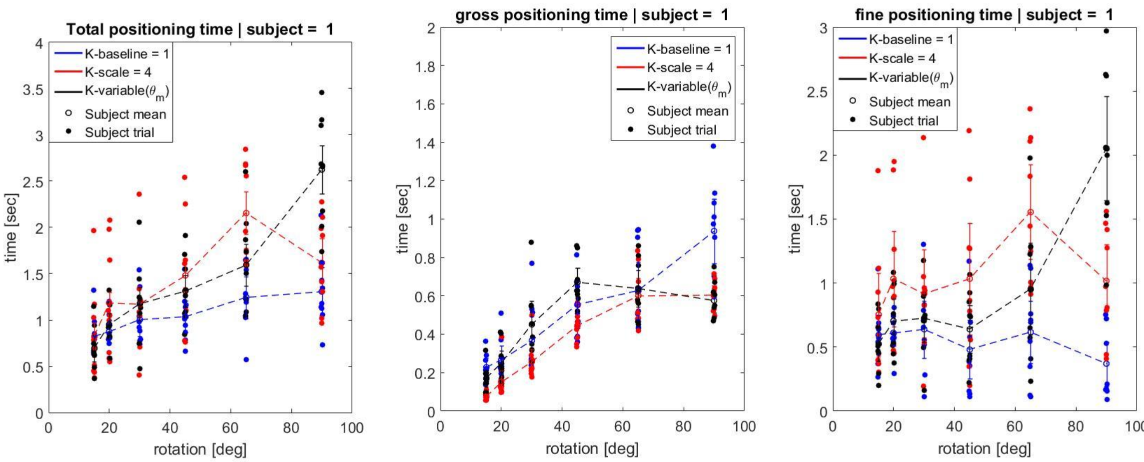

Fig 56: Total, gross and fine positioning time as a function of the different rotational tasks for all the different extension methods. For total positioning time similar results can be seen between the baseline has a lower time compared to the constant and variable scaling. For gross positioning, it can be seen that the baseline method has a higher time compared to the constant and variable scaling method. Finally, for fine positioning the baseline method performs best in terms of time compared to the constant and variable scaling method. The main conclusion from these graphs is the that human operator is able to manipulate variable scaling within a reasonable amount of time.

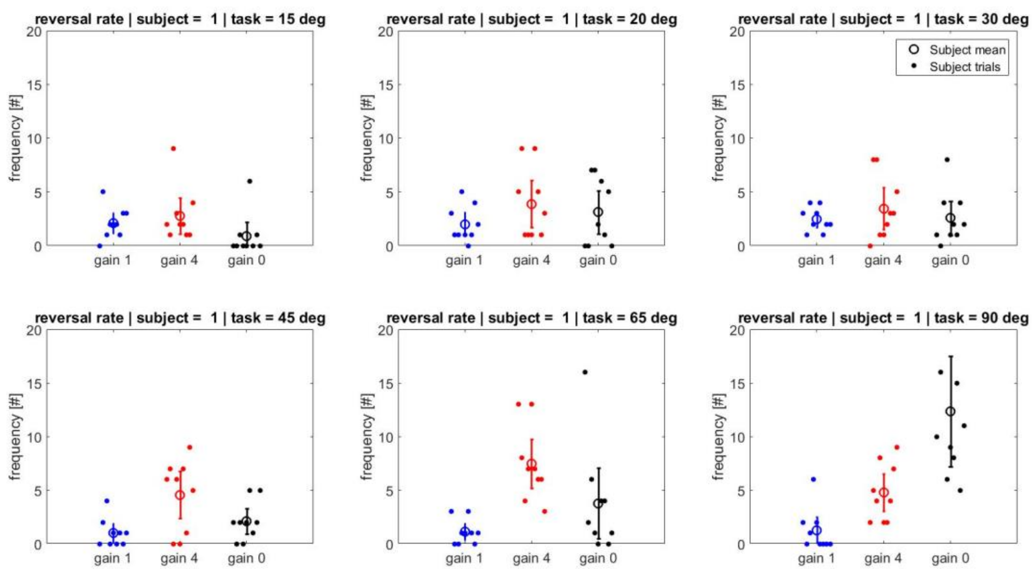

Fig 57: Reversal rate of the different extension methods for the different rotational tasks. The baseline controller, i.e. lowest gain, has less reversals for all rotations compared to constant and variable scaling. Further, the amount of reversal increases for the variable scaling while the gain increases.

Appendix 4: Results experiment

Data acquisition

The orientations of the master and slave were recorded at 1 kHz. Before analyzing the data, the raw data of the master and slave were resampled at 200 Hz. Furthermore, the signals were filtered using positive anti-causal filtering. Average human movements can be described with a frequency of 5 Hz (Brooks, 1990), to make sure that all the human movements were analyzed a second order low pas Butterworth was used with a cut-off frequency of 10 Hz.

Raw data

Training curve

In the pilot study is was detected that the learning curve reached its steady state after four trials. The results of the real experiment confirm these findings (Fig 58), also for the, different variable scaling design.

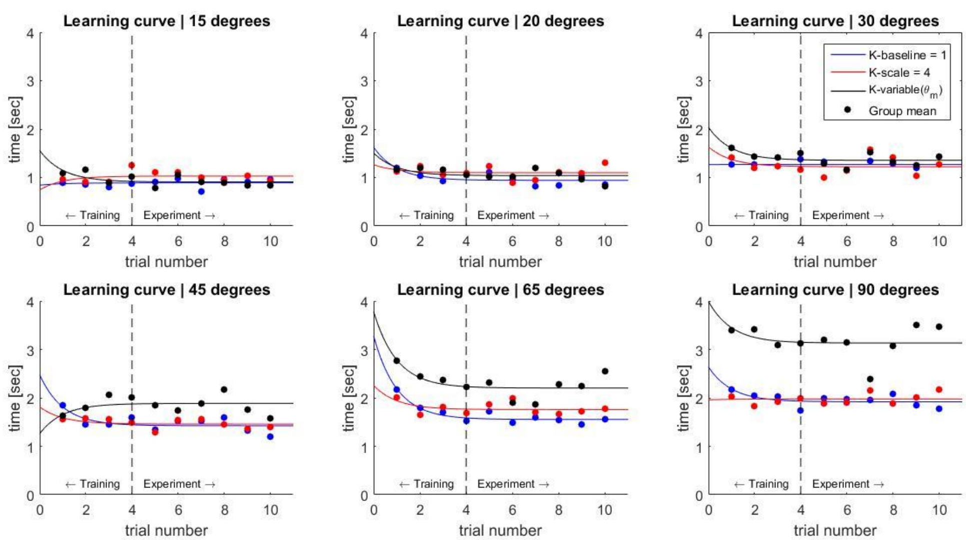

Fig 58: Learning curve for the real experiment for the different extension methods and the different tasks. In the graphs it can be seen that for all the methods and for all the rotations the learning curve reaches its steady state after four repetitions, which is presented in the graphs as a dotted line.

Typical participant

In this section the time traces, of the positions (Fig 59) and velocities (Fig 60), for a typical participant (subject number 12) are shown for the last six trials. On the left the master input time traces and on the right the slave output time traces, for each task (15, 20, 30, 45, 65 and 90 degrees) for the three different workspace extension methods are shown, namely baseline (blue), constant (red) and variable (black) scaling. The shapes of the graphs are typical for human rapid pointing movements (Fitts, 1954 and Casiez et al., 2007). In the velocity-graphs bell-shaped curves are detected, which stands for smooth movements (Rohrer et al., 2002).

Position time traces

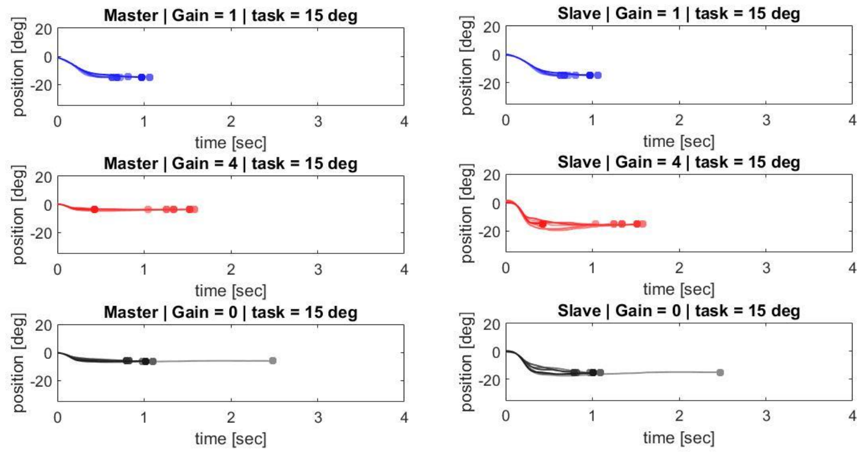

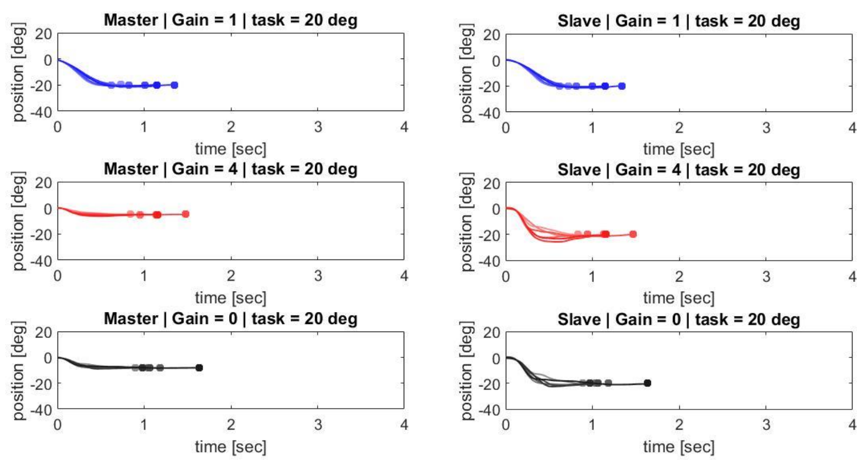

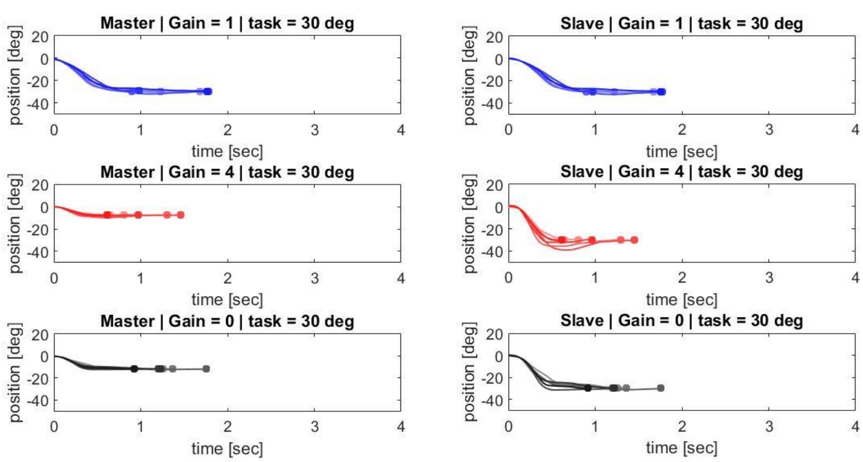

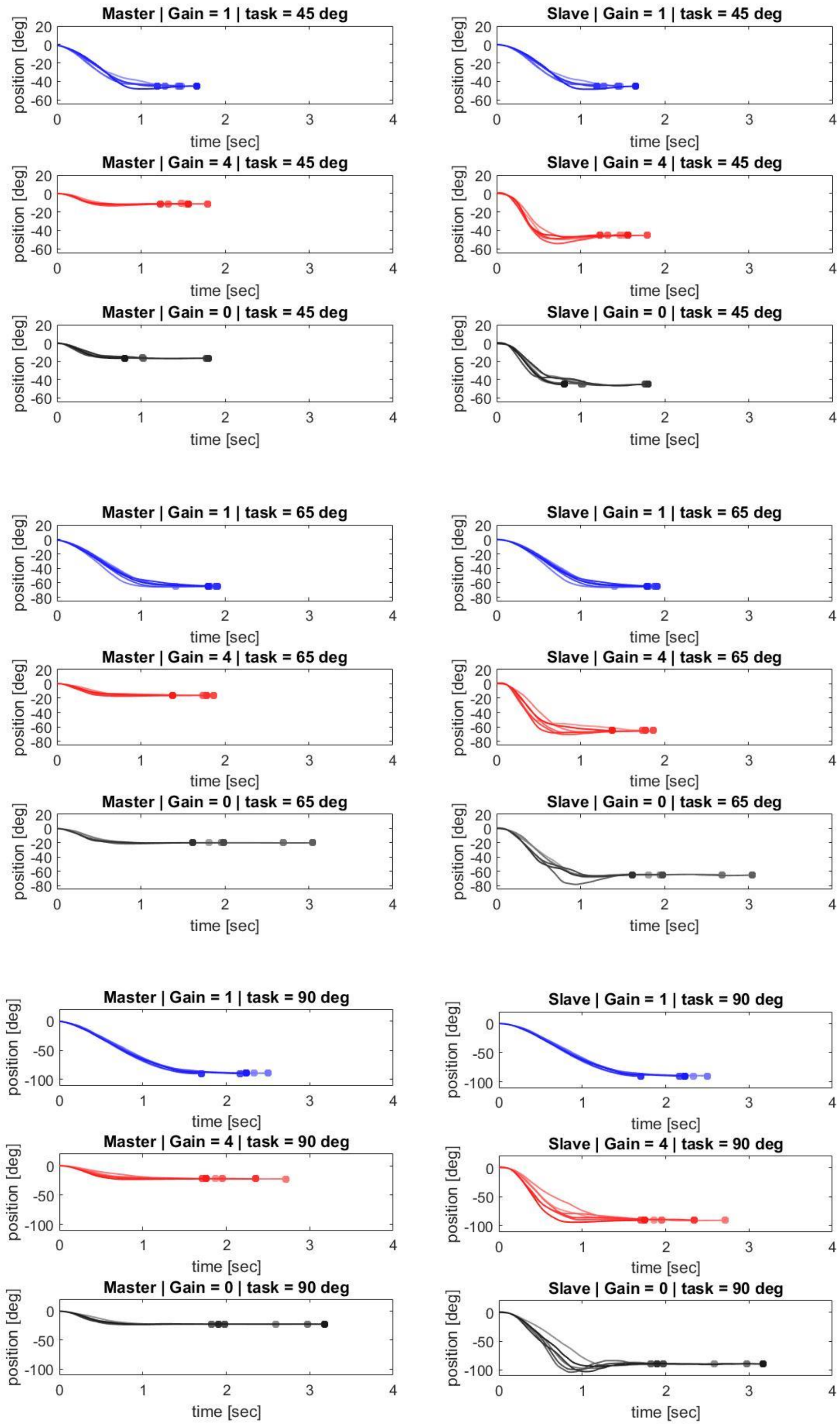

Fig 59: The time traces for all tasks of the orientations of a typical subject. On the left the master input rotations are shown for the three different extension methods (blue = baseline, red = constant scaling, black = variable scaling). The scaling factor can be seen between the master and slave rotations. Further different strategies can be seen, where the constant gain completes the gross positioning tasks faster compared to the baseline. Finally, the it is possible to see that the approach of the variable scaling method changes while the variable gain increases, i.e. larger rotations.

Velocity time traces

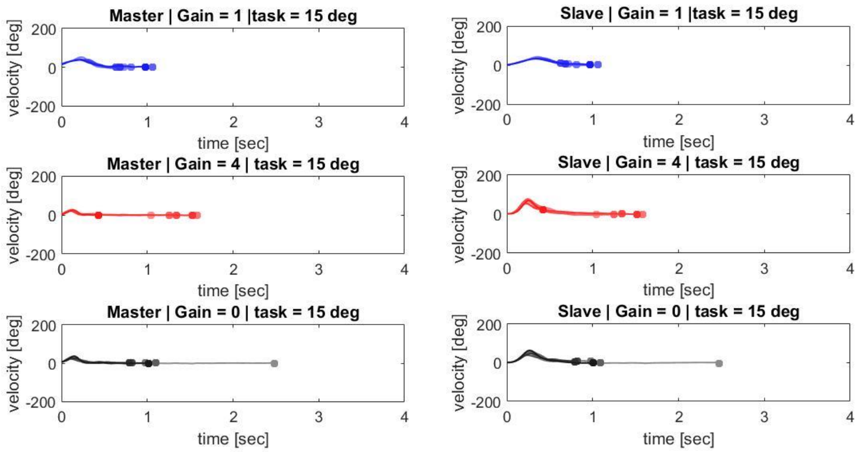

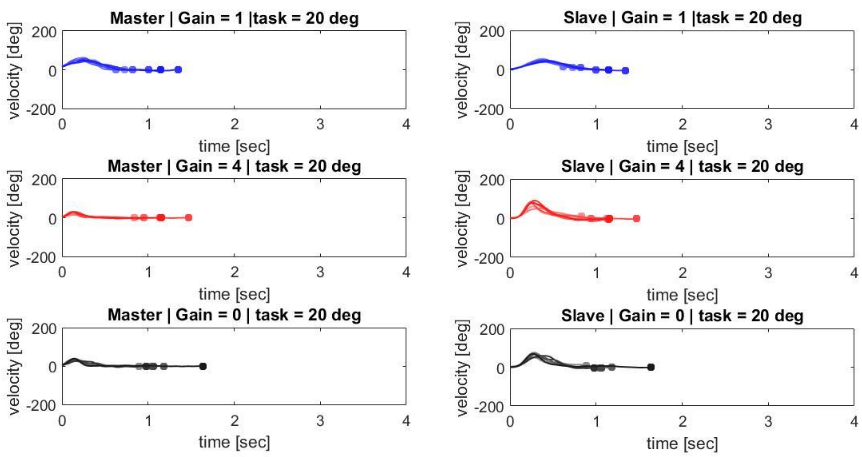

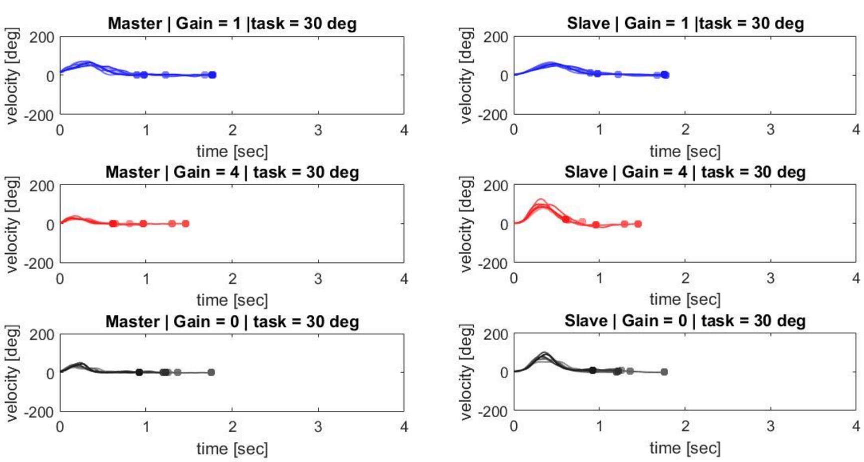

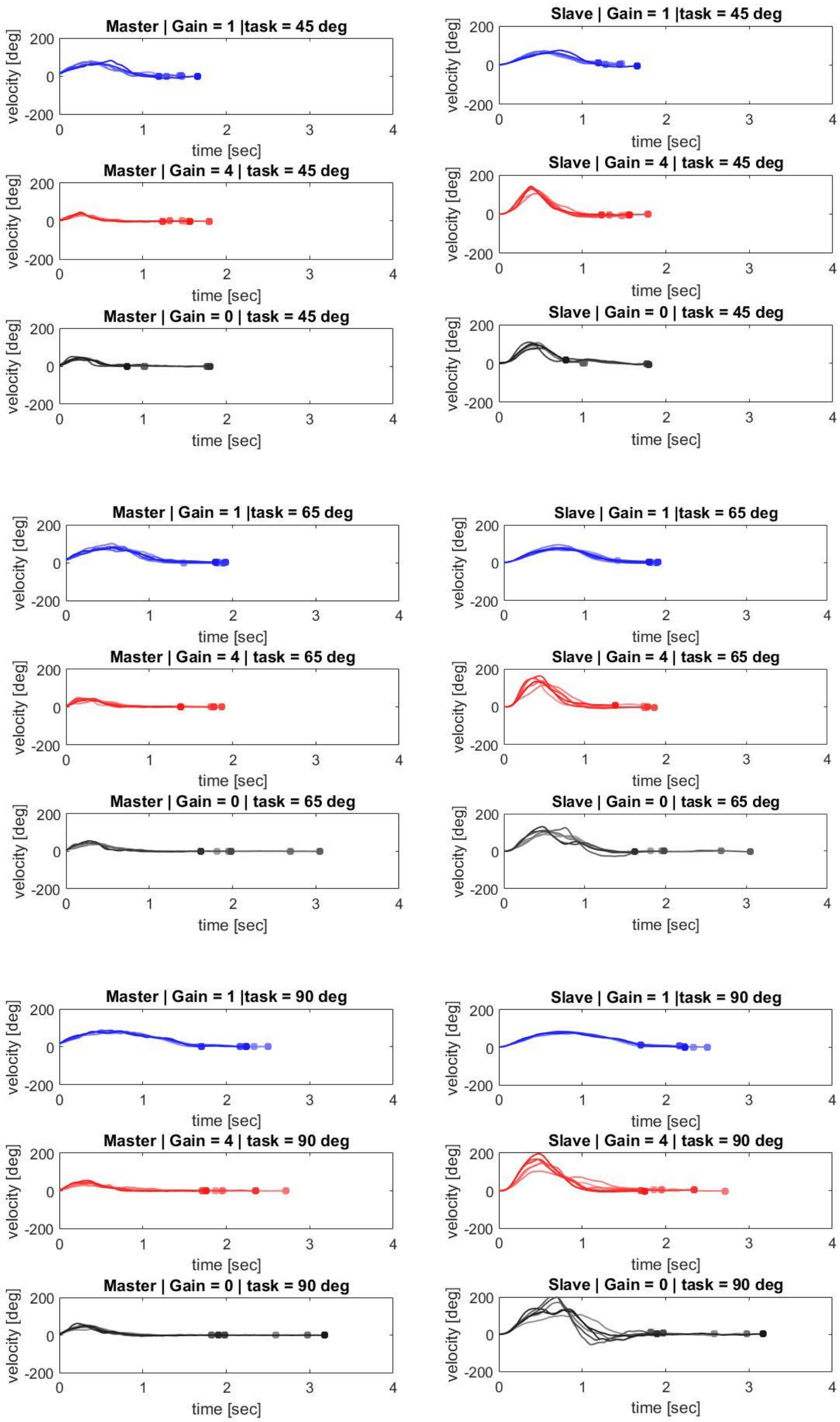

Fig 60: The time traces for all tasks of the velocities of a typical subject. On the left the master input rotations are shown for the three different extension methods (blue = baseline, red = constant scaling, black = variable scaling). The scaling factor can be seen between the master and slave rotations. Further different strategies can be seen, where the constant gain completes the gross positioning tasks faster compared to the baseline. Finally, the it is possible to see that the approach of the variable scaling method changes while the variable gain increases, i.e. larger rotations. Finally, bell-shaped curves are detected, which stand for typical human pointing tasks (Casiez et al., 2007).

Assumptions

The calculated metrics were averaged over the repetitions per participant, for each of the workspace extension methods. To analyze the effect of the different scaling methods a one-way repeated-measures analysis of variance (ANOVA) was performed. No post-hoc corrections were applied, in order to avoid type II errors and to enhance clarity of the results. Further, a linear regression analysis was performed to test the suitability of Fitts' law for the different extension methods versus the index of difficulty. In order to apply these interferential statistics, the data must meet the following assumptions (Laerd, 2013):

- Assumption 1: Dependent variables are measured at the continuous level.
- Assumption 2: Independent variables consist at least two categorical, 'related groups' or 'matched groups'.
- Assumption 3: There are no significant outliers in the related groups.
- Assumption 4: The distribution of the dependent variables in the related groups are approximately normally distributed.
- Assumption 5: The variance of the differences between all combinations of related groups are equal (sphericity).

The first two assumptions are met since all the dependent variable (metrics) were measured at the continuous level. And the independent variables, the workspace extension methods, consisted of related groups. For analyzing the other assumptions statistical test were required. For detecting the significant outliers in data Tukey's method was applied. Further, for determining the normality of the distribution of the data the Lilliefors test was performed. Finally, for testing the sphericity of the data Mauchly's test was performed. The statistical test and the results are described in more detail in the following sections of this appendix.

Outliers

To test the third assumption, that there are no significant outliers in the related groups, Tukey's method was used to detect the major outliers (Tukey, 1997). The outliers were removed, since they were caused by uninteresting reasons. For example; the concentration might have lapsed on that trial, or the participant hesitated because momentarily forgot the target rotation. According to Tukey's method major outliers lie more than 3.0 times the interquartile range below the first quartile or above the third quartile. The major outliers are based on the total positioning time, which means that this can be caused by fine or gross positioning errors. In the Fig 61 a major outlier is shown for the typical subject (subject number 12).

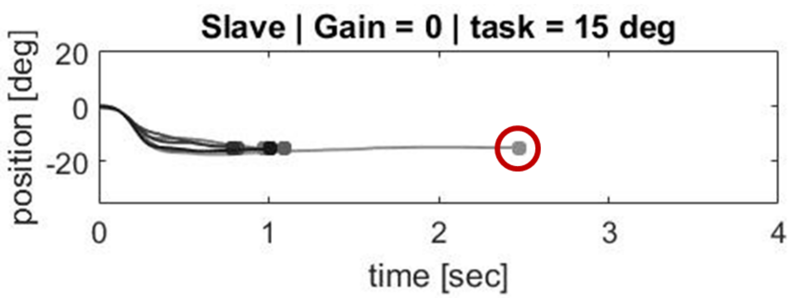

Fig 61: Trials of a typical subject, where a major outlier is detected with the method of Tukey and redly encircled.

After performing Tukey's test 1.4 percent (total of 18) of the trials were removed from all the measurements during the experiment (12 subjects x 3 controllers x 6 tasks x 6 repetitions = 1296). All the outliers lay 3 time above the third quartile and not before the first quartile. In Table 15 the number of the trial is presented whenever it was detected as a major outlier and excluded from further statistical tests.

Table 15: The detected and removed major outliers according to Tukey's test. The number stands for the trial number

Subject	**Baseline gain**						**Constant gain**						**Variable gain**					
	15	**20**	**30**	**45**	**65**	**90**	**15**	**20**	**30**	**45**	**65**	**90**	**15**	**20**	**30**	**45**	**65**	**90**
1	-	-	-	-	-	-	-	-	-	-	-	-	-	-	2	-	-	-
2	-	-	-	-	-	-	-	-	-	-	-	3	-	-	-	-	-	-
3	2	-	-	-	-	-	-	-	-	-	-	-	-	-	-	-	-	-
4	-	-	-	-	-	-	-	-	-	-	-	-	-	-	-	-	2	-
5	-	5	-	-	-	-	-	-	-	-	-	-	-	-	-	-	2	-
6	-	-	-	-	-	-	-	-	-	-	6	-	-	-	-	4, 6	-	-
7	-	-	-	-	-	5	-	-	-	-	-	-	-	-	-	-	-	-
8	1	1	-	-	-	-	-	6	-	-	-	-	-	-	-	-	-	-
9	-	-	-	-	-	-	-	-	-	-	-	-	-	-	-	-	-	5
10	-	-	1	-	-	-	-	-	-	-	-	-	-	-	-	-	-	-
11	-	-	-	-	5	-	-	-	-	-	6	-	-	-	-	-	-	-
12	-	-	-	-	-	-	-	-	-	-	-	-	1	-	-	-	-	-

Normal distribution

The fourth assumption stated that the distribution of the metrics in the related groups should be approximately normally distributed. The normal distribution was measured with the Lilliefors test (Lilliefors, 1969). The Lilliefors test returns a test decision for the null hypothesis that the data in a certain vector comes from a distribution in the normal family. This hypothesis is tested against the alternative hypothesis which stated that the data does not come from a normal distribution. If the p value is smaller than 0.05 the test rejects the null hypothesis, which means that the data for a certain metric for a certain task is not normally distributed. If the normal distribution assumption is violated the p value is stated in bold. Whenever the p value is larger than 0.05 the assumption is met. In the next tables the p values from the Lilliefors test are presented for the different metrics.

Total positioning time

Task	Baseline	Constant	Variable
15	p=0.50	p=0.50	p=0.50
20	p=0.37	p=0.50	p=0.15
30	p=0.18	p=0.50	p=0.50
45	p=0.50	p=0.50	p=0.50
65	p=0.09	p=0.50	p=0.50
90	p=0.36	p=0.50	p=0.21

Gross positioning time

Task	Baseline	Constant	Variable
15	p=0.44	p=0.11	p=0.40
20	**p<0.05**	p=0.50	p=0.33
30	p=0.50	p=0.50	p=0.32
45	p=0.50	p=0.33	p=0.33
65	p=0.27	p=0.37	p=0.39
90	p=0.48	p=0.34	p=0.50

Fine positioning time

Task	Baseline	Constant	Variable
15	**p<0.05**	p=0.50	p=0.25
20	p=0.17	p=0.50	p=0.08
30	p=0.50	**p<0.05**	p=0.50
45	p=0.50	p=0.45	p=0.50
65	p=0.50	p=0.50	p=0.21
90	p=0.48	p=0.50	**p<0.05**

Fitts' law

Value	Baseline	Constant	Variable
A	p=0.31	p=0.50	p=0.16
B	p=0.50	p=0.50	p=0.10
IP	p=0.50	p=0.50	p=0.41

Reversal rate

Task	Baseline	Constant	Variable
15	p=0.36	p=0.50	p=0.09
20	p=0.41	p=0.50	p=0.50
30	p=0.12	p=0.50	p=0.50
45	p=0.35	p=0.16	p=0.50
65	p=0.50	p=0.27	p=0.14
90	p=0.06	**p<0.01**	p=0.21

Mean absolute jerk master

Task	Baseline	Constant	Variable
15	p=0.11	p=0.32	**p<0.05**
20	**p<0.05**	**p<0.01**	**p<0.01**
30	**p<0.01**	p=0.08	p=0.41
45	**p<0.05**	**p<0.05**	p=0.47
65	**p<0.01**	p=0.15	**p<0.05**
90	p=0.07	p=0.21	p=0.11

Mean absolute jerk slave

Task	Baseline	Constant	Variable
15	p=0.50	**p<0.05**	**p<0.01**
20	**p<0.01**	**p<0.01**	**p<0.01**
30	**p<0.01**	p=0.07	p=0.39
45	**p<0.05**	p=0.10	p=0.31
65	**p<0.001**	p=0.47	**p<0.05**
90	**p<0.05**	p=0.50	p=0.05

Van der Laan satisfying

Dimension	Baseline	Constant	Variable
Satisfying	p=0.14	p=0.50	p=0.50
Usefulness	p=0.45	p=0.50	p=0.13

It can be seen that the majority of the metrics are normally distributed. However, a few tasks within the metrics are not normally distributed. According to Larson (2008), the ANOVA is robust to moderate deviations of normality. Therefore, all metrics will be analyzed with a one-way repeated measures ANOVA. Whenever analyzing the results of the non-normal distributed metrics, it will be kept in mind that the assumption of ANOVA was not fulfilled.

Sphericity

The last assumption in order to perform valid interferential statistics was that the variance of the differences between all combinations of related groups are equal (sphericity). The assumption of sphericity was verified with Mauchlys Sphericity Test (Mauchly, 1940). Mauchly's tests the null hypothesis that the variances are equal across the data. If the p value is significant (<.05) the sphericity assumption is violated. Whenever the assumption is violated the Greenhous-Geisser correction will be applied to the ANOVA tests. The Greenhous-Geisser correction decreases the degree of freedom, this results in a more conservative F value from the ANOVA test. In the following tables the p value of the Mauchly's test are presented. If the sphericity assumption is violated the p value is presented in bold and in further statistics the Greenhous-Geisser correction will be applied to the ANOVA tests.

Total positioning time

Task	P value
15	p=0.06
20	p=0.52
30	p=0.08
45	p=0.11
65	**p<0.05**
90	**p<0.01**

Gross positioning time

Task	P value
15	p=0.45
20	p=0.72
30	p=0.24
45	p=0.10
65	**p<0.05**
90	**p<0.05**

Fine positioning time

Task	P value
15	p=0.23
20	p=0.38
30	p=0.34
45	p=0.66
65	**p<0.05**
90	p=0.11

Fitts' law

Value	P value
A	p=0.06
B	p=0.13
IP	p=0.88

Reversal rate

Task	P value
15	p=0.72
20	p=0.70
30	p=0.78
45	p=0.78
65	**p<0.05**
90	**p<0.05**

Mean absolute jerk master

Task	P value
15	**p<0.05**
20	p=0.06
30	**p<0.05**
45	**p<0.05**
65	**p<0.05**
90	p=0.27

Mean absolute jerk slave

Task	P value
15	**p<0.05**
20	p=0.06
30	p=0.21
45	**p<0.05**
65	**p<0.01**
90	**p<0.001**

Van der Laan

Dimension	P value
Usefulness	p=0.75
Satisfying	p=0.50

From the results of Mauchly's test it can be concluded that sometimes the Greenhous-Geisser correction is required for the ANOVA test. Mostly for larger rotations and for the jerk metrics this is the case.

Descriptive and interferential statistics

It can be concluded that it is legit to apply interferential statistics on the data. However, it needs to be kept in mind that the distribution was not always from a normal family. Further, sometimes Greenhous-Geisser correction is required.

In the next sections the descriptive statistics, including the mean value and the 95 percent of the confidence interval, are shown for all the metrics. Further, the interferential statistics, such as ANOVA and Linear regression analysis, are presented, including the post hoc results whenever applicable. Whenever a significant difference was found a post hoc analysis was executed to determine which scaling method differs from the rest. No post-hoc corrections were applied, in order to avoid type II errors and to enhance clarity of the results. Finally, the metrics are shown in graphs presenting all the different tasks of the metrics.

Total positioning time

Total positioning time is the time in seconds required by the operator to complete the whole pointing task. In Table 16 the descriptive statistics of this metric are presented and in Table 17 the results of the one way repeated measures ANOVA is shown. Finally, descriptive and interferential statistics are shown in Fig 62 for the extension methods per rotational task.

Table 16: **Total positioning: Descriptive statistics: Mean (95% CI)**

Task (deg)	**Baseline**	**Constant**	**Variable**
15	0.89 (0.09)	1.02 (0.10)	0.87 (0.11)
20	0.91 (0.10)	1.04 (0.11)	1.00 (0.09)
30	1.22 (0.11)	1.23 (0.13)	1.22 (0.11)
45	1.41 (0.11)	1.42 (0.10)	1.75 (0.18)
65	1.56 (0.09)	1.74 (0.15)	2.25 (0.30)
90	1.99 (0.15)	1.94 (0.14)	3.12 (0.43)

Table 17: **Total positioning: Interferential statistics: One way repeated measures ANOVA**

Main effect			**Post hoc**		
			Variable	**Variable**	**Baseline**
			Baseline	**Constant**	**Constant**
Task (deg)	**F value**	**p value**	**p value**	**p value**	**p value**
15	F(2,22)=4.6	p < 0.05	0.7470	<0.001	0.0715
20	F(2,22)=2.9	p = 0.0766	-	-	-
30	F(2,22)=0.0	p = 0.9975	-	-	-
45	F(2,22)=12.6	p < 0.001	<0.01	<0.01	0.7778
65	F(1.3,14.7)=11.3	p < 0.01	<0.01	<0.05	0.0591
90	F(1.2,13.4)=25.2	p < 0.001	<0.001	<0.001	0.6572

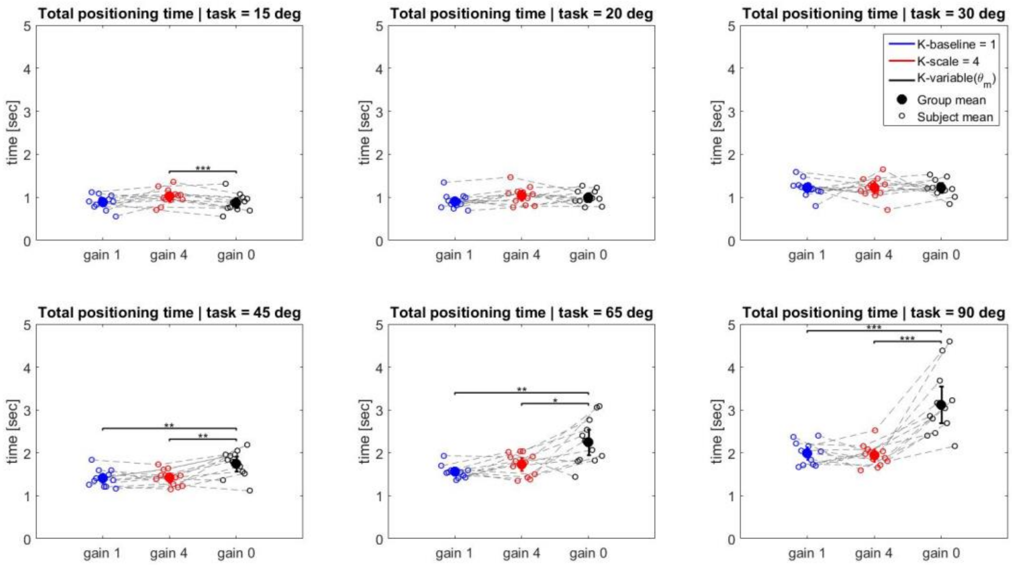

*Fig 62: Total positioning time for the three extension methods and all the rotational tasks. No differences are found between the constant and the baseline controller. Further, an improved performance of the variable scaling is found for the smallest rotation and decreased performances for rotations up to 45 degrees (not designed for this region). Significant differences are shown with *** for $p \leq 0.001$, ** for $p \leq 0.01$ and * for $p \leq 0.05$.*

Gross positioning time

Gross positioning time is the time in seconds required by the operator to complete the task from start to the target rotation minus five degrees. In Table 18 the descriptive statistics of this metric are presented and in Table 19 the results of the one way repeated measures ANOVA is shown. Finally, descriptive and interferential statistics are shown in Fig 63 for the extension methods per rotational task.

Table 18: **Gross positioning: Descriptive statistics: Mean (95% CI)**

Task (deg)	Baseline	Constant	Variable
15	0.42 (0.06)	0.10 (0.02)	0.22 (0.05)
20	0.43 (0.07)	0.21 (0.04)	0.31 (0.06)
30	0.70 (0.09)	0.35 (0.05)	0.54 (0.09)
45	0.87 (0.07)	0.53 (0.07)	0.83 (0.10)
65	1.17 (0.11)	0.71 (0.11)	0.94 (0.10)
90	1.44 (0.16)	0.91 (0.14)	0.89 (0.12)

Table 19: **Gross positioning: Interferential statistics: One way repeated measures ANOVA**

Main effect			Post hoc		
			Variable	**Variable**	**Baseline**
			Baseline	**Constant**	**Constant**
Task (deg)	**F value**	**p value**	**p value**	**p value**	**p value**
15	F(2,22)=144.0	p < 0.001	<0.001	<0.001	<0.001
20	F(2,22)=53.1	p < 0.001	<0.001	<0.001	<0.001
30	F(2,22)=67.9	p < 0.001	<0.001	<0.001	<0.001
45	F(2,22)=35.7	p < 0.001	0.4014	<0.001	<0.001
65	F(1.3,13.9)=34.5	p < 0.001	<0.01	<0.001	<0.001
90	F(1.3,14.3)=26.9	p < 0.001	<0.001	0.6597	<0.001

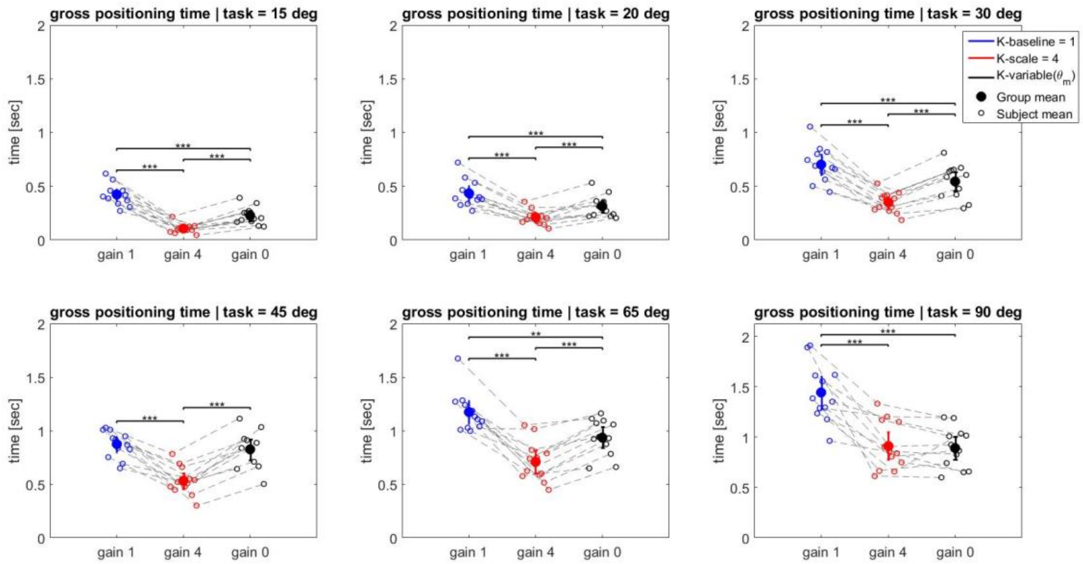

*Fig 63: Gross positioning time for the three extension methods and the different rotational tasks. For all rotations the gross positioning time is less for the constant scaling compared to the baseline. Further, constant scaling is faster compared to the variable gain for all rotations, except for 90 degrees. Finally, the variable rotation is faster compared to the baseline scaling for all rotations, except for 45 degrees. Significant differences are shown with *** for $p \leq 0.001$, ** for $p \leq 0.01$ and * for $p \leq 0.05$.*

Fine positioning time

Fine positioning time is the time in seconds required by the operator to complete the last five degrees of the pointing task. In Table 20 the descriptive statistics of this metric are presented and in Table 21 the results of the one way repeated measures ANOVA is shown. Finally, descriptive and interferential statistics are shown in Fig 64 for the extension methods per rotational task. Finally, in Fig 65 the linear regression analysis is shown for the fine positioning time versus the gain.

Table 20: **Fine positioning: Descriptive statistics: Mean (95% CI)**

Task (deg)	**Baseline**	**Constant**	**Variable**
15	0.47 (0.06)	0.92 (0.09)	0.64 (0.09)
20	0.48 (0.09)	0.83 (0.10)	0.69 (0.08)
30	0.52 (0.09)	0.88 (0.12)	0.68 (0.06)
45	0.53 (0.10)	0.89 (0.07)	0.92 (0.11)
65	0.39 (0.06)	1.02 (0.14)	1.34 (0.28)
90	0.55 (0.12)	1.03 (0.16)	2.23 (0.44)

Table 21: **Fine positioning: Interferential statistics: One way repeated measures ANOVA**

Main effect			**Post hoc**		
			Variable Baseline	**Variable Constant**	**Baseline Constant**
Task (deg)	**F value**	**p value**	**p value**	**p value**	**p value**
15	F(2,22)=48.5	p < 0.001	<0.001	<0.001	<0.001
20	F(2,22)=19.8	p < 0.001	<0.001	<0.05	<0.001
30	F(2,22)=11.8	p < 0.001	<0.05	<0.05	<0.01
45	F(2,22)=18.3	p < 0.001	<0.001	0.6465	<0.001
65	F(1.3,14.7)=26.2	p < 0.001	<0.001	0.0963	<0.001
90	F(2,22)=47.4	p < 0.001	<0.001	<0.001	<0.01

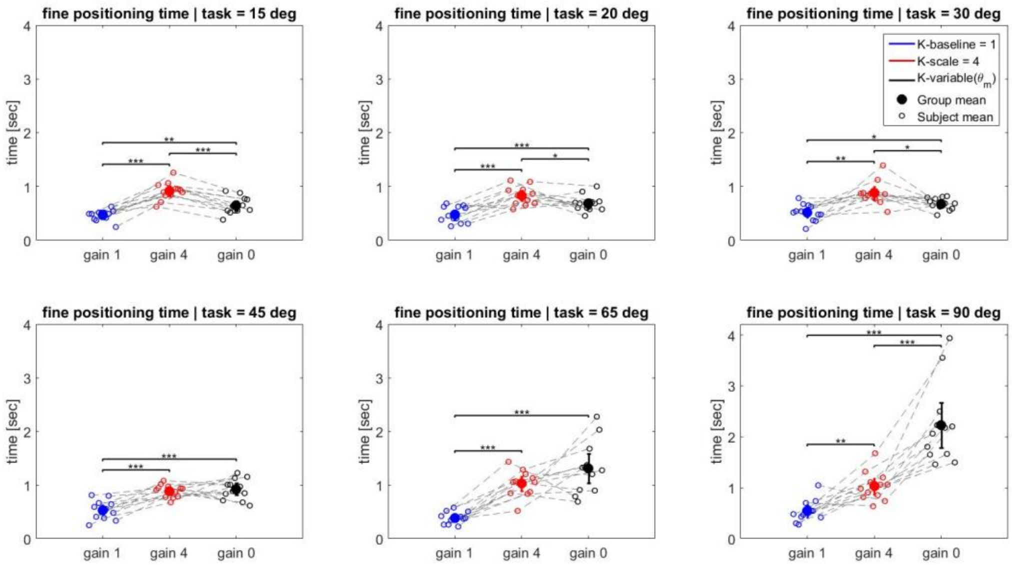

*Fig 64: Fine positioning time for the three extension methods for all the rotation tasks. The baseline scaling shows improved performances compared to the constant scaling for all rotations. Further, the variable scaling shows improved performances compared to the constant scaling for rotations below 45 degrees, for 45 and 65 degrees no differences are detected and for the highest rotation decreased performances are shown for the variable scaling. Finally, the baseline scaling showed improved performances for all rotations compared to the variable scaling method. Significant differences are shown with *** for $p \leq 0.001$, ** for $p \leq 0.01$ and * for $p \leq 0.05$.*

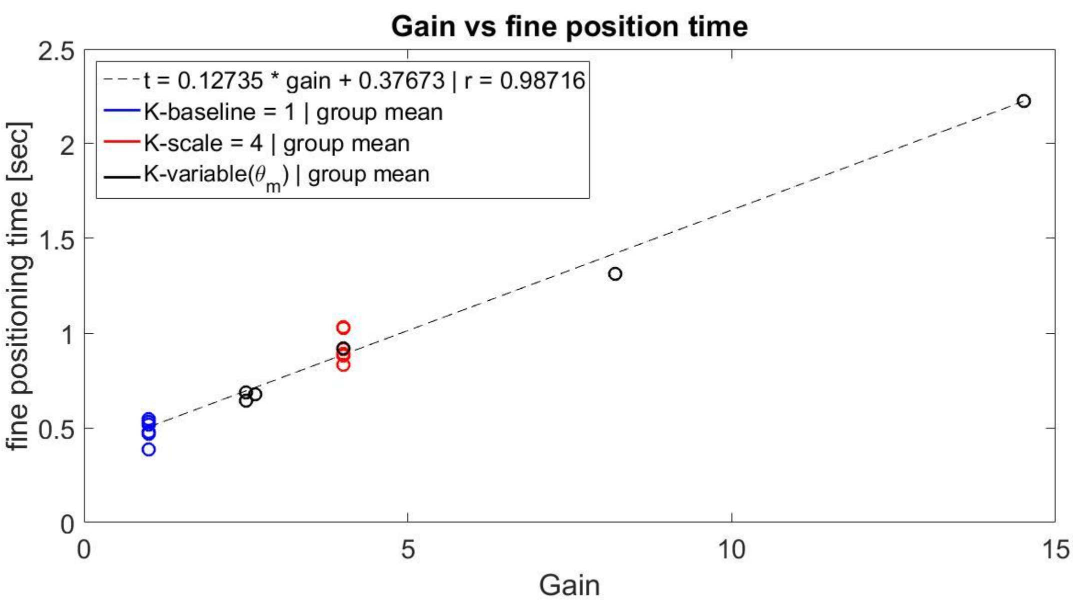

*Fig 65: Fine positioning time versus the gain. According to Pearson' correlation coefficient (0.99) there is a strong linear relation between the gain of the extension method and the fine positioning time. A relationship was found with the following form: fine positioning time = 0.13*gain+0.38. This means that by increasing the gain the fine positioning time increases with 0.13 second.*

Fitts' law

Fitts' law is a predictive model for human telemanipulation movements during rotational scaling, which is based on the Index of Difficulty and total positioning time. The descriptive statistics of a, b and the Index of Performance (IP) (1/b) are shown in Table 22. Linear regression is performed to determine the strength of the relationship between total positioning time and the Index of Difficulty (Table 23 and Fig 66). Finally, the results of the ANOVA are shown in Table 24 and Fig 67 for the index of performance of the different extension methods.

Table 22: **Fitts' law: Descriptive statistics: Mean (95% CI)**

Value	**Baseline**	**Constant**	**Variable**
A	-0.88 (0.27)	-0.61 (0.32)	-2.81 (0.76)
B	0.42 (0.05)	0.38 (0.06)	0.86 (0.17)
IP	2.46 (0.30)	2.79 (0.42)	1.28 (0.22)

Table 23: **Fitts law: Interferential statistics: Linear regression**

Workspace extension method	**F value**	**p value**	**R2**
Baseline	F(1,4)=82,6	<0.001	0,95
Constant	F(1,4)=104,8	<0.001	0,96
Variable	F(1,4)=50,0	<0.01	0,93

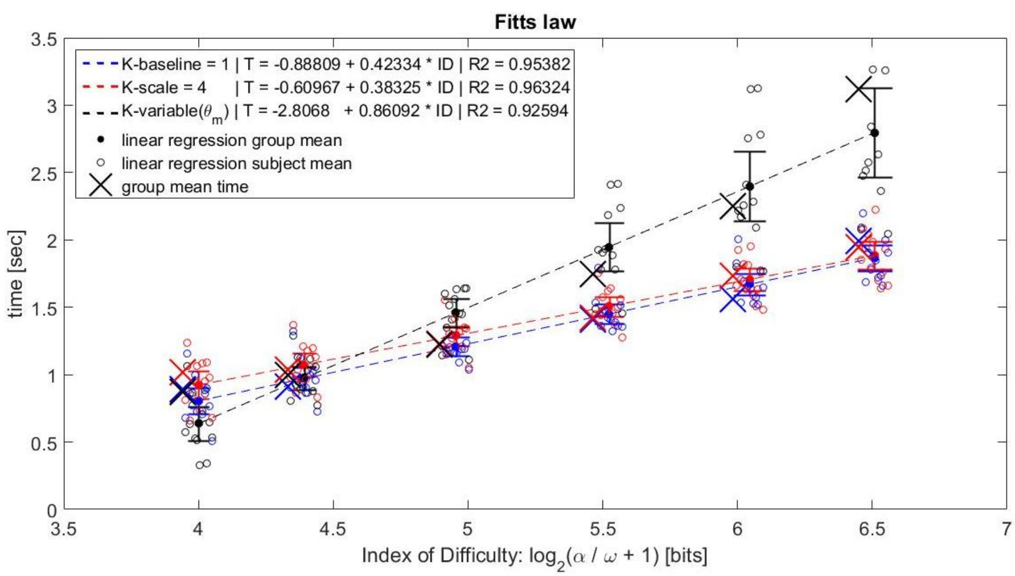

Fig 66: Fitts' law models for the three different extension methods. Significant linear regression equations were found for Fitts' law to predict completion time based on the Index of Difficulty of the task for all extension methods. Whenever extrapolating the linear regression lines of the constant methods a cross point can be detected where the baseline method will perform less compared to the constant method. The variable controller shows overestimation of the mean time at small rotations and underestimation at large rotations.

Table 24: **Index of performance: Interferential statistics: One way repeated measures ANOVA**				
Main effect		**Post hoc**		
		Variable	**Variable**	**Baseline**
		Baseline	**Constant**	**Constant**
F value	**p value**	**p value**	**p value**	**p value**
F(2,22)=26,8	p < 0.001	<0.001	<0.001	0.1402

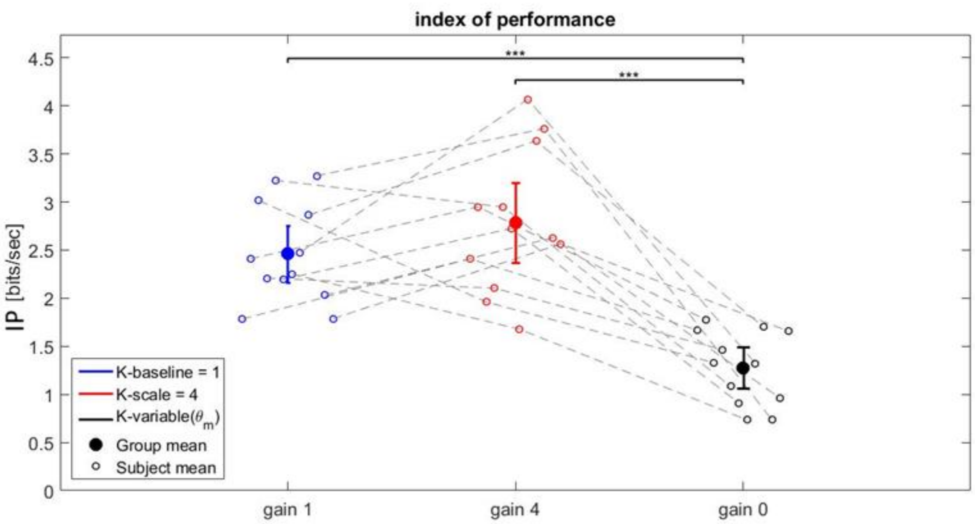

*Fig 67: Index of Performance metric [bits/sec] for the three extension methods. Differences can be seen between the variable method and the other two extension methods. No differences were found between the constant and baseline method. Significant differences are shown with *** for $p \leq 0.001$, ** for $p \leq 0.01$ and * for $p \leq 0.05$.*

Reversal rate

The reversal rate is the amount of reversals of the operator at the master side and is used to measure the operator control effort. This is calculated by counting the amount of zero crossings of the master velocity. In Table 25 the descriptive statistics of this metric are presented and in Table 26 the results of the one way repeated measures ANOVA is shown. Finally, descriptive and interferential statistics are shown in Fig 68 for the extension methods per rotational task.

Table 25: **Reversal rate: Descriptive statistics: Mean (95% CI)**			
Task (deg)	**Baseline**	**Constant**	**Variable**
15	1.52 (0.36)	2.92 (0.54)	2.14 (0.53)
20	1.16 (0.40)	2.53 (0.58)	2.43 (0.81)
30	1.67 (0.78)	3.18 (0.81)	1.54 (0.63)
45	1.31 (0.61)	2.83 (1.03)	3.70 (1.20)
65	0.72 (0.32)	3.72 (1.08)	8.26 (2.93)
90	1.06 (0.65)	4.29 (1.63)	16.45 (4.44)

Table 26: **Reversal rate: Interferential statistics: One way repeated measures ANOVA**					
Main effect			**Post hoc**		
			Variable Baseline	**Variable Constant**	**Baseline Constant**
Task (deg)	**F value**	**p value**	**p value**	**p value**	**p value**
15	F(2,22)=10.2	p<0.001	0.0546	<0.05	p<0.01
20	F(2,22)=7.6	p<0.01	<0.05	0.7889	p<0.01
30	F(2,22)=7.1	p<0.01	0.7823	<0.01	p<0.05
45	F(2,22)=7.3	p<0.01	<0.01	0.1921	p<0.05
65	F(1.2,13.0)=16.1	p<0.01	<0.001	<0.05	p<0.001
90	F(1.3,14.5)=40.9	p<0.001	<0.001	<0.001	p<0.01

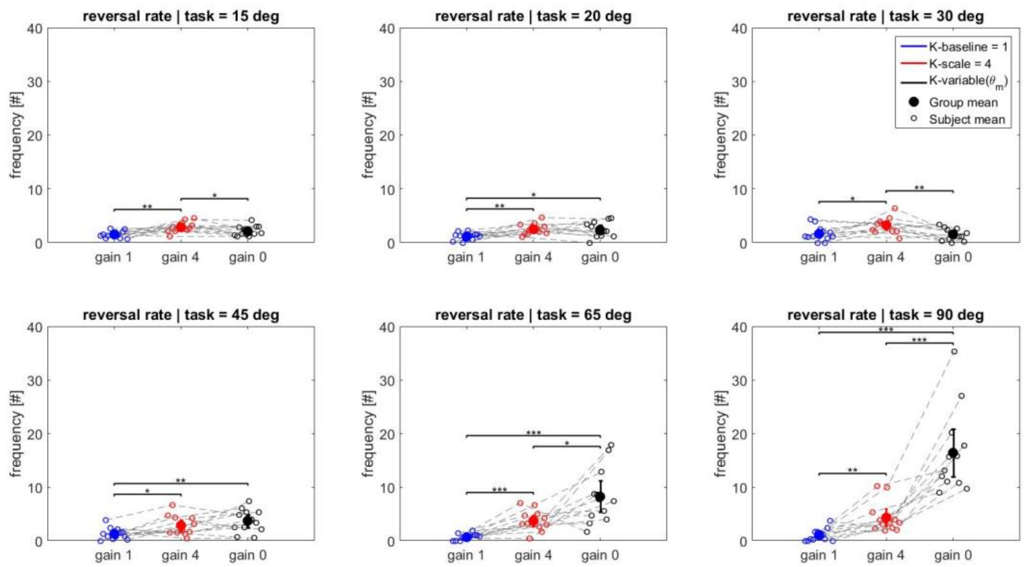

*Fig 68: Reversal rate for the three extension methods for all the rotational tasks. For all rotations the baseline method showed less reversals compared to the variable and constant methods. For the rotations 15 and 30 degrees the variable method showed less reversals compared to the constant method, however, for the rotations 65 and 90 degrees more reversals are shown for the variable method. Significant differences are shown with *** for $p \leq 0.001$, ** for $p \leq 0.01$ and * for $p \leq 0.05$.*

Mean absolute jerk

The jerk is the time derivative of the acceleration and is used to measure the smoothness of the manipulations. Smoothness is a hallmark for skilled and coordinated ballistic movements. A higher jerk means a lower smoothness of the movement. In this study the smoothness of the movement is measured by the absolute minimum jerk, normalized by peak speed, such that the metric is a measure of smoothness only and not confound with changes in overall movement speed: $\frac{1}{\dot{x}_{\mathrm{peak}}} \int |\dddot{x}(\mathrm{t})| \mathrm{dt}$.

Master

In Table 27 the descriptive statistics of this metric are presented and in Table 28 the results of the one way repeated measures ANOVA is shown. Finally, descriptive and interferential statistics are shown in Fig 69 for the extension methods per rotational task.

Table 27: **Jerk master: Descriptive statistics: Mean (95% CI)**			
Task (deg)	**Baseline**	**Constant**	**Variable**
15	0.39 (0.14) e+16	0.47 (0.22) e+16	0.47 (0.34) e+16
20	0.17 (0.13) e+16	0.42 (0.27) e+16	0.54 (0.34) e+16
30	0.46 (0.26) e+16	0.56 (0.22) e+16	1.07 (0.45) e+16
45	0.71 (0.23) e+16	1.03 (0.41) e+16	2.14 (0.88) e+16
65	1.15 (0.43) e+16	1.82 (0.67) e+16	2.32 (1.30) e+16
90	2.69 (1.05) e+16	3.30 (1.28) e+16	2.32 (1.56) e+16

Table 28: **Jerk master: Interferential statistics: One way repeated measures ANOVA**					
Main effect			**Post hoc**		
			Variable	**Variable**	**Baseline**
			Baseline	**Constant**	**Constant**
Task (deg)	**F value**	**p value**	**p value**	**p value**	**p value**
15	F(1.4,15.1)=0.2	p = 0.7188	-	-	-
20	F(2,22)=2.6	p = 0.0955	-	-	-
30	F(1.3,14.4)=7.6	p < 0.05	<0.05	<0.05	0.2722
45	F(1.4,15.1)=10.6	p < 0.01	<0.01	<0.01	0.1284
65	F(1.3,14.2)=2.0	p = 0.1803	-	-	-
90	F(2,22)=0.7	p = 0.5230	-	-	-

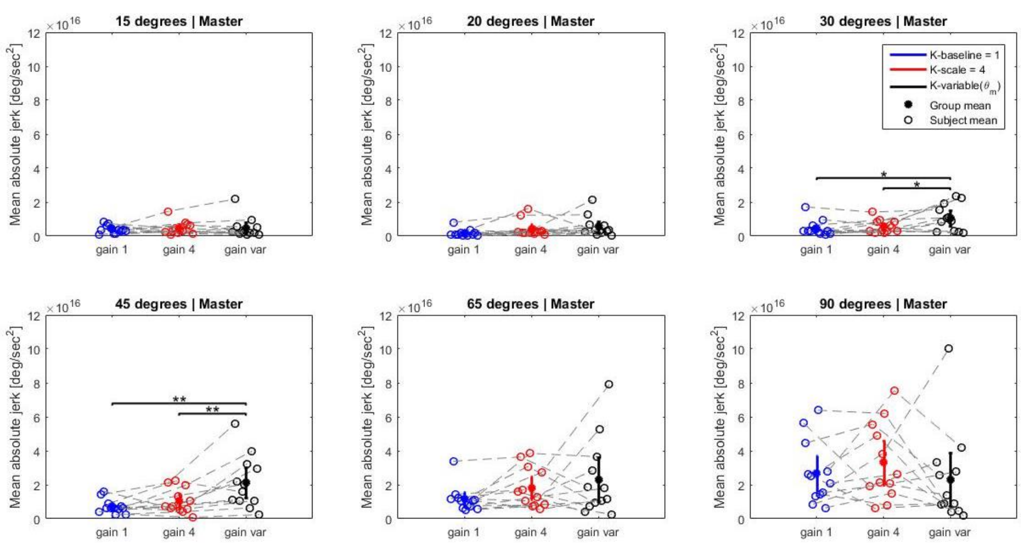

*Fig 69: mean absolute jerk normalized by peak speed at the master side for the extension methods for the different tasks. Differences are detected at 30° and 45°, for the other rotations no differences were detected. This higher jerk suggests that the movements with the variable scaling method are less smooth and therefore less skilled and coordinated. A possible explanation for this phenomenon could be the highest changes in gain, i.e. highest non-linearity's, took place at those rotations. Significant differences are shown with *** for $p \leq 0.001$, ** for $p \leq 0.01$ and * for $p \leq 0.05$.*

Slave

In Table 29 the descriptive statistics of this metric are presented and in Table 30 the results of the one way repeated measures ANOVA is shown. Finally, descriptive and interferential statistics are shown in Fig 70 for the extension methods per rotational task.

Table 29: **Jerk slave: Descriptive statistics: Mean (95% CI)**			
Task (deg)	**Baseline**	**Constant**	**Variable**
15	0.24 (0.08) e+16	0.21 (0.09) e+16	0.22 (0.14) e+16
20	0.10 (0.07) e+16	0.20 (0.12) e+16	0.26 (0.14) e+16
30	0.26 (0.16) e+16	0.27 (0.09) e+16	0.48 (0.17) e+16
45	0.38 (0.12) e+16	0.46 (0.17) e+16	1.13 (0.42) e+16
65	0.54 (0.20) e+16	0.78 (0.25) e+16	1.43 (0.73) e+16
90	1.26 (0.48) e+16	1.34 (0.45) e+16	1.61 (1.14) e+16

Table 30: **Jerk slave: Interferential statistics: One way repeated measures ANOVA**					
Main effect			**Post hoc**		
			Variable Baseline	**Variable Constant**	**Baseline Constant**
Task (deg)	**F value**	**p value**	**p value**	**p value**	**p value**
15	F(1.3,13.9)=0.1	p = 0.8497	-	-	-
20	F(2,22)=2.6	p = 0.0969	-	-	-
30	F(2,22)=5.4	p < 0.05	<0.05	<0.01	0.9526
45	F(1.3,14.4)=14.7	p < 0.001	<0.05	<0.01	0.3815
65	F(1.1,12.3)=4.3	p = 0.0552	-	-	-
90	F(1.1,12.5)=0.2	p = 0.6581	-	-	-

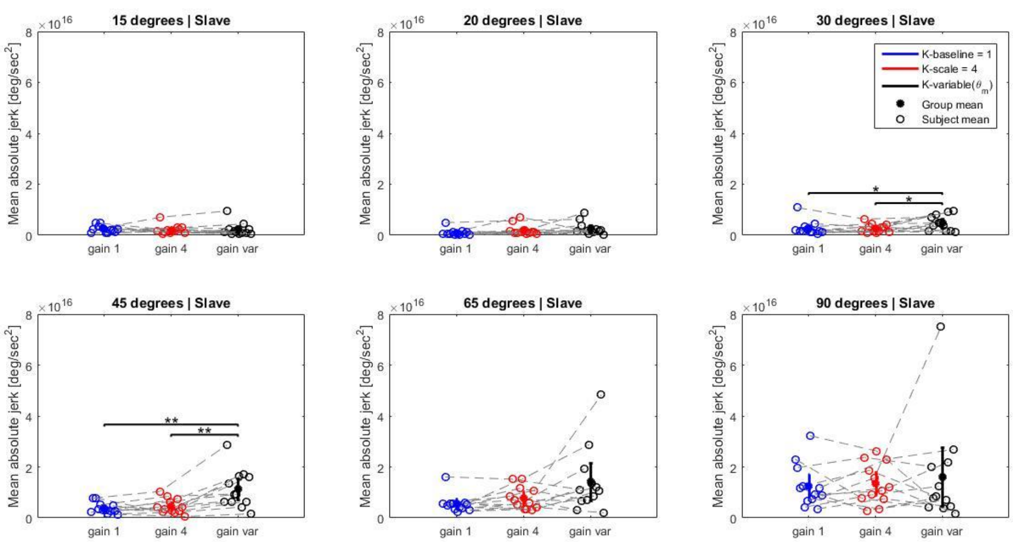

*Fig 70: mean absolute jerk normalized by peak speed at the slave side for the extension methods for the different tasks. Differences are detected at 30° and 45°, for the other rotations no differences were detected. This higher jerk suggests that the movements with the variable scaling method are less smooth and therefore less skilled and coordinated. A possible explanation for this phenomenon could be the highest changes in gain, i.e. highest non-linearity's, took place at those rotations. Significant differences are shown with *** for p ≤ 0.001, ** for p ≤ 0.01 and * for p ≤ 0.05.*

Van der Laan acceptance scale

The van der Laan questionnaire (appendix 6) is used as a subjective measurement to test the acceptance of the participants for the three different extension methods. The questionnaire consists of nine questions and measures the acceptance in two dimensions; usefulness and satisfying. In Table 31 the descriptive statistics of this metric are presented and in Table 32 the results of the one-way ANOVA are shown. Finally, descriptive and interferential statistics are shown in Fig 71 for the extension methods.

Table 31: **Van der Laan: Descriptive statistics: Mean (95% CI)**			
	Baseline	**Constant**	**Variable**
Usefulness	0.40 (0.26)	0.77 (0.40)	0.65 (0.24)
Satisfying	0.73 (0.19)	0.42 (0.43)	0.04 (0.36)

Table 32: **Van der Laan: Interferential statistics: One way ANOVA**					
Main effect			**Post hoc**		
			Variable	**Variable**	**Baseline**
			Baseline	**Constant**	**Constant**
Dimension	**F value**	**p value**	**p value**	**p value**	**p value**
Usefulness	F(2,22)=1.9	P=0.1803	-	-	-
Satisfying	F(2,22)=3.8	p<0.05	<0.01	0.2118	0.2410

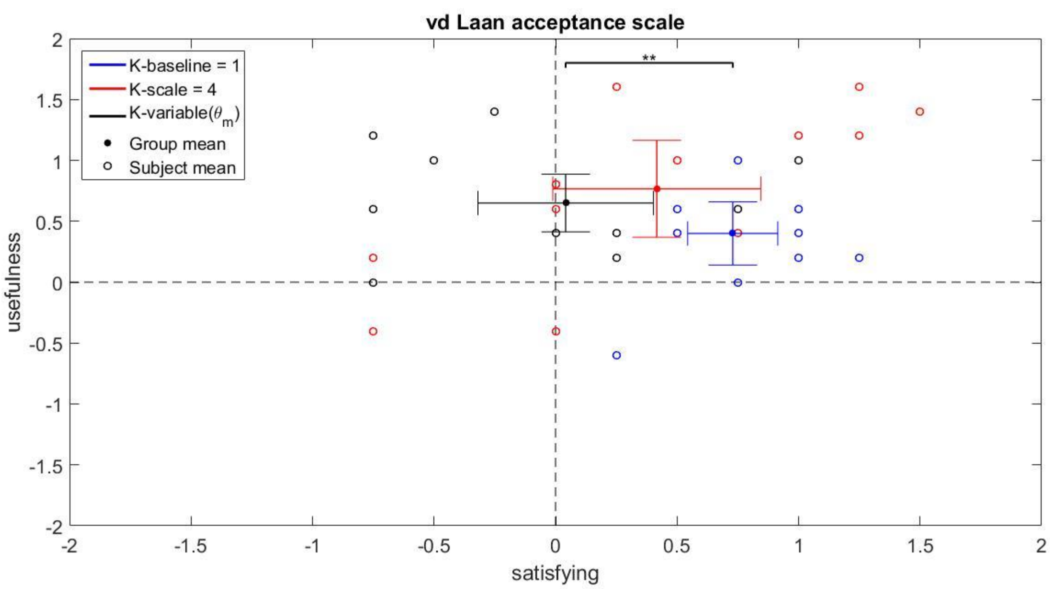

*Fig 71: Van der Laan acceptance scale; on the horizontal axis the satisfying dimension and on the vertical axis the usefulness dimension. No differences between the methods on the usefulness dimension. On the satisfying dimension differences between variable and baseline method. Further, all mean values are at the top right plan, i.e. positive scores on both dimensions. Significant differences are shown with *** for $p \leq 0.001$, ** for $p \leq 0.01$ and * for $p \leq 0.05$.*

Appendix 5: Informed consent

Dear participant,

Introduction

You have been asked to participate in this research. In this informed consent, the essential information about this research is provided to you. I am Roel van der Klauw, performing my graduation for the master Biomedical Engineering in collaboration with the company Heemskerk Innovative Technology (HIT) and the technical university of Delft.

Purpose

Tele-operations allow humans to complete tasks in a remote environment. This is done by a master-slave system, consisting of a joystick (master) and a robot-arm (slave). Movements executed by the human operator on the master device are translated via the controller to the slave device, which interacts with the remote environment. A big unsolved issue in teleoperations is the limited rotational workspace of the master with respect to the slave. To overcome the lack of rotational workspace at the master side rotational workspace extension methods are required. The purpose of the research is to evaluate different rotational workspace extension methods.

Experimental procedure

The setup of the experiment consists of a master and a slave. The Geomagic touch will be used as a master device. And the Ulna arm will be used as the slave. The participant (operator) will be located without direct visuals on the slave, the operator has contact with the slave and the remote environment via video feedback (Fig 72).

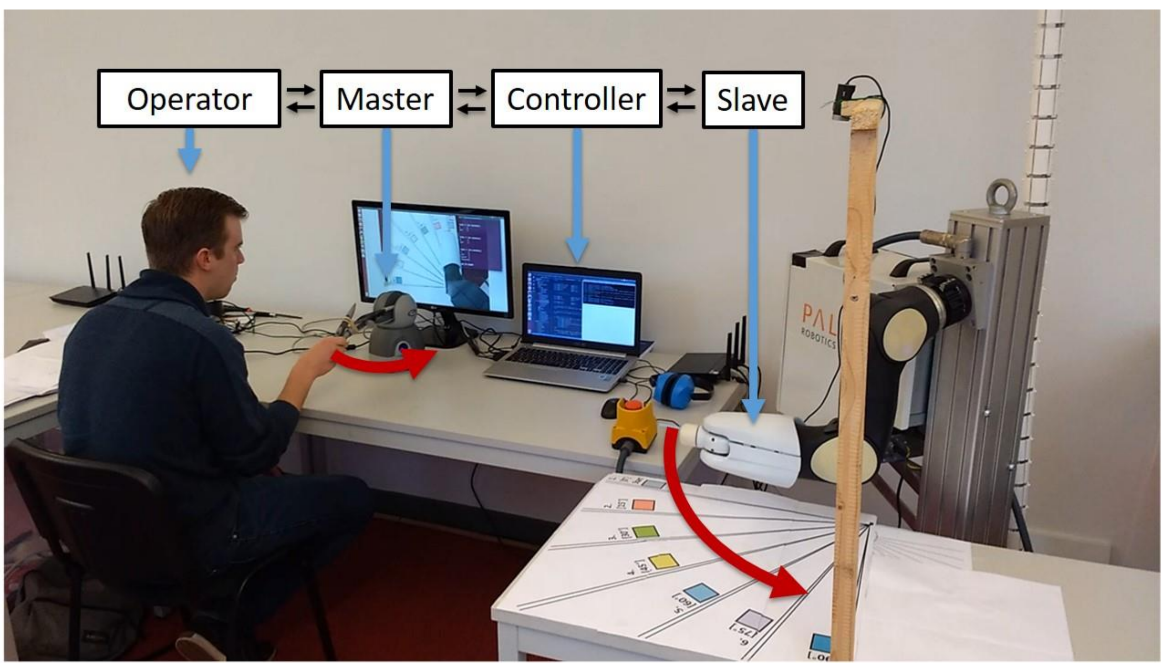

Fig 72: Experimental setup. The operator rotates the slave in the remote environment by rotating the master joint. The controller manages the information flow between master and slave. The operator receives visual feedback from the remote environment on the cockpit screen.

The experiment starts with the informed consent and a short introduction and explanation about the experimental system. This is followed by a training session to practice with the system to get familiar with the tele-operation concept followed by the real experiment. During the experiment, different workspace extension methods are applied to the participant in a random order. This experimental conditions start with five training trails directly followed with five trials recorded for the real experiment (i.e. without a break in between). During the experiment, a Vd Laan questionnaire will be taken. The whole protocol is graphically shown in Fig 73.

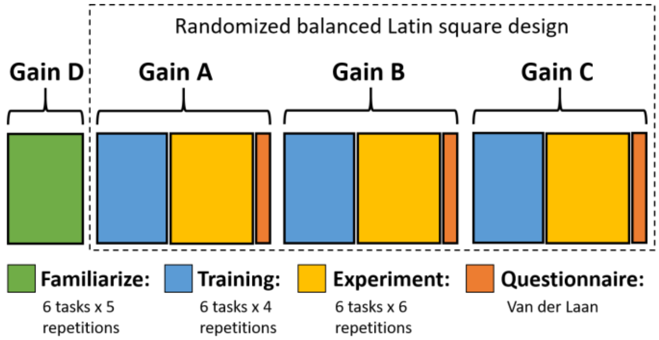

Fig 73: Protocol of the experiment for one participant. Starting with familiarization of the setup with Gain D. Followed by the experiment with the three-experimental condition (randomized). Each condition started with a training of 4 repetitions, followed by 6 measured repetitions and the Van der Laan questionnaire.

The goal of this experiment is to rotate the robotic arm towards six different targets. The participant receives instructions about the desired task via cockpit screen (Fig 74). The time starts whenever the participant moves the arm from the start position and stops whenever the reference point is within the boundaries of the target for 0.5 seconds, this is shown by a progress bar. After this the participant is guided back with forces by the master device towards the start position. Whenever the operator is for 0.5 seconds at the start position the next target is presented at the screen. This continues till all the repetitions are performed.

<u>The goal of the task is to perform the task as **fast** as possible, while emphasizing **accuracy** rather than speed.</u>

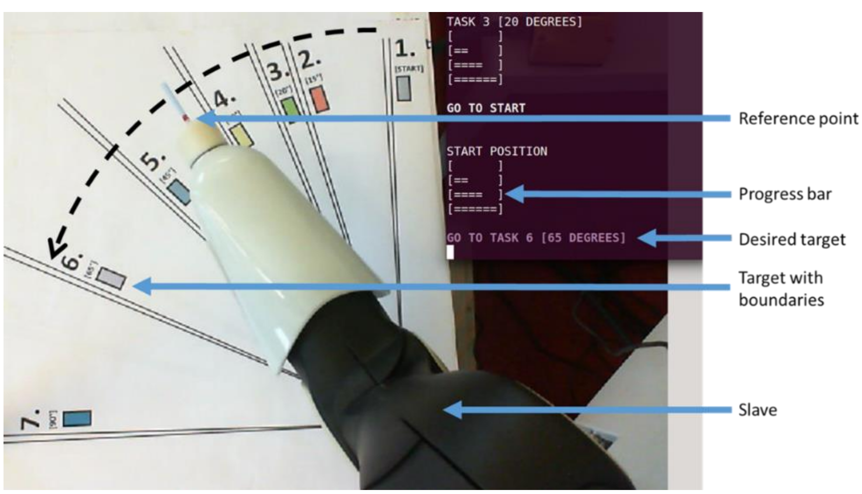

Fig 74: Visual feedback presented on the cockpit screen to the operator while performing the rotational pointing task. With the slave arm, rotating above the map with rotational tasks. The goal is to rotate the reference point within the boundaries of a desired target rotation. On the right the progress bar is shown, where it is possible to see the progress bar filling and the desired task is indicated (task 6 at 65 degrees).

The recordings and questionnaires are used anonymously. Personal data is not available to persons other than the researcher. The only directly identifiable data that is kept longer than 6 months is the information on this informed consent form.

Participation in this study is voluntary. If you feel any form of discomfort during the experiment, please inform the experimental leader. You are free to quit the experiment at any time. For questions after the study, please contact Roel van der Klauw.

I, the undersigned, declare to have read and understood the information about the project, the use of data and to consent to the experiment.

Name participant: _______________

Gender: _______________

Age: _______________

Date: _______________

Signature: _______________

Appendix 6: Van der Laan questionnaire

I find the controller during condition 1 (please tick a box on every line)

1 Useful |__|__|__|__|__| Useless

2 Pleasant |__|__|__|__|__| Unpleasent

3 Bad |__|__|__|__|__| Good

4 Nice |__|__|__|__|__| Annoying

5 Effective |__|__|__|__|__| Superfluous

6 Irritating |__|__|__|__|__| Likeable

7 Assisting |__|__|__|__|__| Worthless

8 Undesirable |__|__|__|__|__| Desirable

9 Raising Alertness |__|__|__|__|__| Sleep-inducing

I find the controller during condition 2 (please tick a box on every line)

1 Useful |__|__|__|__|__| Useless

2 Pleasant |__|__|__|__|__| Unpleasent

3 Bad |__|__|__|__|__| Good

4 Nice |__|__|__|__|__| Annoying

5 Effective |__|__|__|__|__| Superfluous

6 Irritating |__|__|__|__|__| Likeable

7 Assisting |__|__|__|__|__| Worthless

8 Undesirable |__|__|__|__|__| Desirable

9 Raising Alertness |__|__|__|__|__| Sleep-inducing

I find the controller during condition 3 (please tick a box on every line)

1 Useful |__|__|__|__|__| Useless

2 Pleasant |__|__|__|__|__| Unpleasent

3 Bad |__|__|__|__|__| Good

4 Nice |__|__|__|__|__| Annoying

5 Effective |__|__|__|__|__| Superfluous

6 Irritating |__|__|__|__|__| Likeable

7 Assisting |__|__|__|__|__| Worthless

8 Undesirable |__|__|__|__|__| Desirable

9 Raising Alertness |__|__|__|__|__| Sleep-inducing

Adapted from Van der Laan et al. (1997).

References

3D Systems. (2013). *Geomagic touch device guide.* Morrisville.

Astrom, K. (2002). Simple Control Systems. In *Control system design* (pp. 144-176).

Brooks, T. (1990). Telerobotic Response Requirements. *IEEE international conference sysetms, man and cybernetics*, 113-120.

Buxton, W. (1986). In *There's More to Interaction than Meets the Eye: Some Issues in Manual Input* (pp. 319-337). Hillsdale, New Jersey: Lawrence Erlbaum Associates.

Casiez, G., Vogel, D., Pan, Q., & Chailou, C. (2007). RubberEdge Reducing Clutching by Combining position and rate control with elastic feedback. *Proceedings of the 20th annual ACM symposium on User interface software and technology*, 129-138.

DeJong, B., Colgate, E., & Peshkin, M. (2004). Improving teleoperation: reducing mental rotations and translations. *International conference on robotics and automation*, 3708-3714.

Dominjon, L., Lecuyer, A., Brukhardt, J., & Richir, S. (2006). Haptic hybrid rotations: Overcoming hardware angular limitations of force feedback devices. *Virtual reality conference*, 167-174.

Fitts, P. (1954). The information capacity of the human motor system in controlling the amplitude of movment. *Journal of experimental psychology, 47*, 381-391.

Giang, H. (2017, March 31). *Ros*. (Robot operating system) Retrieved May 29, 2017, from http://wiki.ros.org/

Hannaford, B., Wood, L., McAffee, D., & Zak, H. (1991). Performance evaluation of a six-axis generalized force-reflecting teleoperator. *IEEE trans. systems, man and cybernetics, 3*(21), 620-633.

Hee, K., Osch, M., & Veerdonk, E. (2015). Meerwaarde van robotica in de zorg. *Rose robots for care*.

Heemskerk Innovative Technology (HIT). (n.d.). *Semi Autonomous Care Robot (SACRO)*. Retrieved March 28, 2017, from http://www.heemskerk-innovative.nl/?project=semi-autonomous-care-robot-sacro

Jellinek, H., & Card, S. (1990). Powermice and user performance. *ACM Conference on Human Factors in Computing Systems.*

Laerd statistics. (2013). *ANOVA with repeated measures using SPSS statistics*. (Laerd statistics) Retrieved May 29, 2017, from https://statistics.laerd.com/spss-tutorials/one-way-anova-repeated-measures-using-spss-statistics.php

Lambert, P. (2013). *Parallel robots with configurable platforms; Precision and microsystems engineering.* Delft: TU Delft.

Larson, M. (2008). Analysis of variance. *Circulation, 117*(1), 115-121.

Lilliefors, H. (1969). On the Kolmogorov-Smirnov test for the exponential distribution with mean unknown. *Journal of the American Statistical Association, 64*, 387-389.

MacDonald, W., & Hoffmann, E. (1980). Review of relationships between steering wheel reversal rate and drive task demand. *Human factors, 22*(6), 733-739.

MacKenzie, I. (1995). Input devices and interaction techniques for advanced computing. *Virtual environment and advanced interface design*, 437-470.

Mamdouh, M., Ramadan, A., & Abo-Ismael, A. (2012). Evaluation of a proposed workspace spanning technique for small haptic device based manipulator teleoperation. *Intelligent robotics and applications*, 161-170.

Mauchly, J. (1940). Significance Test for Sphericity of a Normal n-Variate Distribution. *The Annals of Mathematical Statistics*(11), 204-209.

McRuer, D., & Jex, H. (1967). A Review of Quasi-Linear Pilot Models. *Transactions on human factors in electronics, 8*(3).

Menchaca-Brandan, M., Liu, A., Oman, C., & Natapoff, A. (2007). Influence of perspective taking and mental rotation abilities in space teleoperation. *international conference on Human-robot interaction , 12*, 271-278.

Meyer, D., Smith, J., Kornblum, S. A., & Wright, C. (1988). Optimality in human motor performance: ideal control of rapid aimed movements. . *Psychological Review*, 340-370.

PAL robotics. (2014). *ULNA handbook.* Barcelona.

Perez, A., & Rosell, J. (2011). An assisted re-synchronization method for robotic teleoperated tasks. *IEEE International Conference on Robotics and Automation*, 886-891.

Poupyrev, I., Weghorst, S., & Fels, S. (2000). Non-Isomorphic 3D Rotational Techniques. *Human factors in computing systems*, 240-547.

Rohrer, B., Fasoli, S., Krebs, H., Hughes, R., Volpe, B., Frontera, W., . . . Hogan, N. (2002). Movement smoothness changes during stroke recovery. *The journal of neuroscience, 22*(18), 8297-8304.

Ryu, D., Kang, S., Kim, M., & Song, J. (2004). Multi-modal user interface for teleoperation of ROBHAZ-DT2 field robot system. *Intelligent robots and systems*, 168-173.

Samur, E. (2012). *Performance metrics of haptic interfaces.* London Heidelberg New York Dordrecht: Springer.

Sprickerhof, J. (2015, June 16). *Rosbag*. (Robot Operating System) Retrieved May 29, 2017, from http://wiki.ros.org/rosbag

Stoelen, M., & Akin, D. (2010). Assessment of Fitts' Law for Quantifying Combined Rotational and Translational Movements. *Human factors, 52*(1), 63-77.

Tukey, J. (1997). *Exploratory data analysis.*

van der Klauw, R. (2016). *Workspace extension method for parallel haptic master devices: Application teleoperation with a care robot.* Delft: TU Delft.

van der Laan, J., Heino, A., & Waard, D. (1997). A simple procedure for the assessment of acceptance of advanced transport telematics. *Transportation research, 5*(1), 1-10.

Versteeg, E. (2016). *Requirements analysis of 7-DOF parallel haptic master device and experimental comparison of two workspace extension techniques for teleoperation in a real life task.* Twente: TU Twente.

Wildenbeest, J., Abbink, A., Heemskerk, C., van der Helm, F., & Boessenkool, H. (2013). The impact of haptic feedback quality on the performance of teleoperated assembly tasks. *IEEE transactions on haptics, 6*(2), 242-252.

Zhai, S. (1995). *Human Performance in Six Degree of Freedom Input Control.* Toronto: University of Toronto.